

1 **Field Intercomparison of Ice Nucleation Measurements: The** 2 **Fifth International Workshop on Ice Nucleation Phase 3** 3 **(FIN-03)**

4
5 Paul J. DeMott¹, Jessica A. Mirrielees^{2,a}, Sarah Suda Petters^{3,b}, Daniel J. Cziczo^{4,c}, Markus D.
6 Petters^{3,b}, Heinz G. Bingemer⁵, Thomas C. J. Hill¹, Karl Froyd^{6,7,d}, Sarvesh Garimella^{4,e}, A.
7 Gannet Hallar^{8,9}, Ezra J.T. Levin^{1,f}, Ian B. McCubbin^{8,9}, Anne E. Perring^{6,7,g}, Christopher N.
8 Rapp^c, Thea Schiebel^{10,h}, Jann Schrod⁵, Kaitlyn J. Suski^{1,i}, Daniel Weber^{5,j}, Martin J. Wolf^{4,k},
9 Maria Zawadowicz^{4,l}, Jake Zenker^{2,m}, Ottmar Möhler¹⁰ and Sarah D. Brooks²

10
11 ¹Department of Atmospheric Science, Colorado State University, Fort Collins, CO, USA

12 ²Department of Atmospheric Sciences, Texas A&M University, College Station, TX, USA

13 ³Department of Marine, Earth and Atmospheric Sciences, North Carolina State University,
14 Raleigh, NC, USA

15 ⁴Department of Earth, Atmospheric and Planetary Sciences, Massachusetts Institute of
16 Technology, Cambridge, MA, USA

17 ⁵Institute for Atmospheric and Environmental Sciences, Goethe University Frankfurt, 60438
18 Frankfurt am Main, Germany

19 ⁶NOAA Earth System Research Laboratory, Boulder, CO, USA

20 ⁷CIRES, University of Colorado, Boulder, CO, USA

21 ⁸Storm Peak Laboratory, Department of Atmospheric Sciences, University of Utah, Salt Lake
22 City, Utah, USA

23 ⁹Department of Atmospheric Sciences, University of Utah, Salt Lake City, Utah, USA

24 ¹⁰Institute of Meteorology and Climate Research (IMK-AAF), Karlsruhe Institute of Technology
25 (KIT), Eggenstein-Leopoldshafen, Germany

26 ^anow at: Chemistry Department, University of Michigan, Ann Arbor, MI

27 ^bnow at: College of Engineering Center for Environmental Research and Technology (CE-
28 CERT); Department of Chemical and Environmental Engineering, University of California
29 Riverside, Riverside, CA

30 ^cnow at: Department of Earth, Atmospheric, and Planetary Sciences, Purdue University, West
31 Lafayette, IN, USA

32 ^dnow at: Air Innova, Boulder, CO, USA

33 ^enow at: ACME AtronOmatic, LLC, Portland, OR, USA

34 ^fnow at: Colorado Department of Public Health and Environment, Denver CO, USA

35 ^gnow at: Department of Chemistry, Colgate University, Hamilton, NY, USA

36 ^hnow at: Faculty 8- Mathematics and Physics, University of Stuttgart, Stuttgart, Germany

37 ⁱnow at: Rainmaker Technology Corporation, El Segundo, CA, USA

38 ^jnow at: Federal Waterways Engineering and Research Institute, Karlsruhe, Germany

39 ^know at: Yale Center for Law and Policy, New Haven, CT, USA

40 ^lnow at: Brookhaven National Laboratory, Richland, WA, USA

41 ^mnow at: Sandia National Laboratories, Albuquerque, NM, USA

42 Correspondence: Paul J. DeMott (Paul.Demott@colostate.edu)

43

44 **Abstract**

45 The third phase of the Fifth International Ice Nucleation Workshop (FIN-03) was
46 conducted at Storm Peak Laboratory in Steamboat Springs, Colorado in September 2015 to
47 facilitate the intercomparison of instruments measuring ice nucleating particles (INPs) in the field.
48 Instruments included two online and four offline measurement systems for INPs, a subset of those
49 utilized in the laboratory study that comprised the second phase of FIN (FIN-02). Composition of
50 the total aerosols was characterized using the Particle Ablation by Laser Mass Spectrometry
51 (PALMS) and Wideband Integrated Bioaerosol Sensor (WIBS) instruments, and aerosol size
52 distributions were measured by a Laser Aerosol Spectrometer (LAS). The dominant total particle
53 compositions present during FIN-03 were composed of sulfates, organic compounds, and nitrates,
54 as well as particles derived from biomass burning. Mineral dust containing particles were
55 ubiquitous throughout and represented 67% of supermicron particles. Total WIBS fluorescing
56 particle concentrations for particles with diameters $> 0.5 \mu\text{m}$ were $0.04 \pm 0.02 \text{ cm}^{-3}$ (0.1 cm^{-3}
57 highest, 0.02 cm^{-3} lowest), typical for the warm season in this region and representing $\approx 9\%$ of all
58 particles in this size range as a campaign average.

59 The primary focus of FIN-03 was the measurement of INP concentration via immersion
60 freezing at temperatures $> -33 \text{ }^\circ\text{C}$. Additionally, some measurements were made in the deposition
61 nucleation regime at these same temperatures, representing one of the first efforts to include both
62 mechanisms within a field campaign. INP concentrations via immersion freezing agreed within
63 factors ranging from nearly 1 to 5 times on average between matched (time and temperature)
64 measurements and disagreements only rarely exceeded one order of magnitude for sampling times
65 coordinated to within three hours. Comparisons were restricted to temperatures lower than $-15 \text{ }^\circ\text{C}$
66 due to limits of detection related to sample volumes and very low INP concentrations. Outliers of

67 up to two orders of magnitude occurred between $-25\text{ }^{\circ}\text{C}$ and $-18\text{ }^{\circ}\text{C}$; better agreement was seen at
68 higher and lower temperatures. Although the 5-10 factor agreement of INP measurements found
69 in FIN-03 aligned with the results of the FIN-02 laboratory comparison phase, giving confidence
70 in progress of this measurement field, this level of agreement still equates to temperature
71 uncertainties of 3.5 to 5 $^{\circ}\text{C}$ that may not be sufficient for numerical cloud modeling applications
72 that utilize INP information.

73 INP activity in the immersion freezing mode was generally found to be an order of
74 magnitude or more, more efficient than in the deposition regime at 95-99% water relative
75 humidity, although this limited data set should be augmented in future efforts.

76 To contextualize the study results an assessment was made of the composition of INPs
77 during the late Summer to early Fall period of this study, inferred through comparison to existing
78 ice nucleation parameterizations and through measurement of the influence of thermal and organic
79 carbon digestion treatments on immersion freezing ice nucleation activity. Consistent with other
80 studies in continental regions, biological INPs dominated at temperatures $> -20\text{ }^{\circ}\text{C}$ and sometimes
81 colder, while arable dust-like or other organic-influenced INPs were inferred to dominate below –
82 $20\text{ }^{\circ}\text{C}$.

83 **1 Introduction**

84 Atmospheric ice nucleation is one of the least certain aerosol-cloud interactions influencing
85 climate (Kanji et al., 2017). Particles that physically catalyze freezing, known as ice-nucleating
86 particles (INPs) (Vali et al., 2015), are found in the atmosphere in concentrations that span many
87 orders of magnitude, ranging from 10^{-3} L^{-1} or fewer at $-5 \text{ }^\circ\text{C}$ to 1000 L^{-1} or greater at $-35 \text{ }^\circ\text{C}$
88 (Petters and Wright, 2015). INP number concentrations typically increase exponentially with
89 degree of supercooling below $0 \text{ }^\circ\text{C}$. However, chemical composition plays an important role in
90 determining if, and at what temperature, individual particles may serve as INPs (Murray et al.,
91 2012). INPs initiate the formation of ice in cold and mixed-phase clouds and in turn influence
92 their physical and optical properties. An increase in INP concentration over a geographic area
93 may increase the frequency of glaciated clouds at constant temperature, which in turn increases
94 precipitation and decreases cloud lifetime (Lohmann and Feichter, 2005). Nevertheless, INP
95 impacts on clouds simulated in global climate models are highly sensitive to how aerosol's ability
96 to nucleate ice is parameterized (Boucher et al., 2013). Parameterizations can only be as accurate
97 as the measurements on which they are based (e.g., Knopf et al., 2021).

98 Measurements of atmospheric INPs remain challenging due to the difficulty representing
99 the physical processes involved in ice nucleation instruments. At temperatures below $\approx -38 \text{ }^\circ\text{C}$,
100 micrometer-sized, dilute water droplets spontaneously freeze due to homogeneous freezing
101 nucleation. Homogeneous freezing nucleation is well understood and included in most cloud
102 formation models. However, at temperatures between 0 and $-38 \text{ }^\circ\text{C}$, freezing requires INPs to
103 facilitate nucleation through a heterogeneous nucleation mechanism (Kanji et al., 2017; Murray et
104 al., 2012; Vali, 1985). Nucleation is hypothesized to proceed through (1) immersion freezing,
105 which occurs when an INP embedded within a water droplet enters a cooler environment, and
106 nucleates an ice crystal, (2) condensation freezing, which occurs when freezing ensues as an

107 aqueous droplet condenses on the surface of an aerosol particle, (3) contact freezing, which occurs
108 when an aerosol in contact with a water droplet surface initiates freezing (Durant and Shaw, 2005;
109 Fornea et al., 2009), and (4) deposition nucleation, which is thought to occur through the direct
110 deposition of water vapor on an INP surface. Of these mechanisms, immersion freezing nucleation
111 is thought to be the most active heterogeneous nucleation process in the atmosphere, though there
112 is considerable disagreement in the literature about the relative importance of other mechanisms
113 (Kanji et al., 2017; Ullrich et al., 2017). When the ambient humidity is below water saturation,
114 nucleation can occur via deposition of water from the vapor phase. In some cases, this behavior
115 may be ascribable instead to water condensation in pores and cavities in aerosols facilitating
116 freezing through a non-deposition mechanism (Marcolli, 2014; Wagner et al., 2016). However,
117 this process is unlikely to be of importance at temperatures > -38 °C (David et al., 2020), which
118 are the focus of this study. We will thus refer to ice nucleation at > -38 °C and below water
119 saturation as happening within the “deposition regime”. Study of the efficiency of the deposition
120 nucleation process in comparison to immersion freezing has been limited for natural INPs.

121 Ice nucleation measurements have been made with instruments designed and built by
122 individual scientists, and more recently with commercial instruments. The ice nucleation
123 community has a history of collaborating to address instrument performance and inconsistencies
124 through participating in instrument intercomparisons, in which the custom-built instruments were
125 operated side-by-side to evaluate instrument response to the same aerosol populations. Ice
126 nucleation workshops have a history to 1967, with repetitions occurring in 1970, 1976, and 2007
127 (DeMott et al., 2011). These exercises were repeated not due to a difference in goals but due to the
128 development and improvement of new ice nucleation instrumentation and a focus on better
129 characterization of heterogeneous ice nucleation processes. An additional factor that has motivated

130 formal and informal instrument intercomparisons is growing recognition of the importance of
131 having coordinated detailed aerosol characterizations and better instruments to provide that
132 information (e.g., Coluzza et al., 2017; DeMott et al., 2011, DeMott et. al, 2018; Knopf et al, 2021;
133 Brasseur et al., 2022; Lacher et al., 2024). To compare concentrations and compositions of INPs,
134 a three-part workshop series, the Fifth International Ice Nucleation Workshop, or “FIN” was held
135 in 2014-2015. The first two phases were held at the Karlsruhe Institute of Technology’s Aerosol
136 Interactions and Dynamics in the Atmosphere (AIDA) facility. FIN-01 focused on determination
137 of composition of INPs by mass spectroscopy (Shen et al., 2024), while FIN-02 entailed a
138 laboratory ice nucleation instrument comparison (DeMott et al., 2018). FIN-03, the mountaintop
139 field intercomparison of ice nucleation instruments is the focus of this manuscript. While
140 laboratory experiments can easily provide broad concentration ranges of particles of specific types
141 for testing, measurements in the ambient atmosphere are the ultimate application of INP measuring
142 systems, and the ambient atmosphere presents the most challenging measurement scenario due to
143 sometimes very low INP concentrations and a host of potential INP source compositions.

144 Ice nucleation measurements have experienced a renaissance in the past decade, resulting
145 in a proliferation in both the number of custom-built instruments and a diversification of
146 measurement techniques employed (Zenker, 2017; DeMott, 2018; Möhler, 2021). Participation in
147 FIN-02 was twice that of the previous formal international workshop intercomparison in 2007 (the
148 International Workshop on Comparing Ice Nucleation Measuring Systems, or ICS-2007 held at
149 the (AIDA) facility (Jones et al., 2011; Kanji et al., 2011). During FIN-02, online and offline
150 instruments sampling the same population of aerosolized particles reported INP concentrations
151 that generally agreed within one order of magnitude across a broad temperature range. Agreement
152 was best in tests of immersion freezing on soils, dusts and bacteria but spanned up to 2 orders of

153 magnitude (or 3 °C in temperature for the same active site density) for illite NX and K-feldspar
154 (DeMott et al., 2018). While relatively good agreement in the laboratory between different
155 measurement methods during FIN-02 represented significant progress for the atmospheric ice
156 nucleation community, intercomparisons in ambient atmospheric settings are more difficult due to
157 lower typical INP concentrations (Lacher et al., 2018) and variations in the chemistry and size of
158 source aerosol and INPs (DeMott et al., 2017; Knopf, 2021; Lacher et al., 2024; Brasseur et al.,
159 2022).

160 To evaluate how a suite of instruments operating collectively perform under the greater
161 measurement challenges of the field setting, FIN-03 was conducted from September 12 to 28, 2015
162 at Storm Peak Laboratory (SPL) in Steamboat Springs, CO, USA (Elevation: 3220 m MSL).
163 Unlike the closure studies of Knopf et al. (2021) and the similar comparative sampling studies of
164 Lacher et al. (2024), both of which occurred in regions surrounded by agricultural activities and
165 possible nearby urban influences, or the study of Brasseur et al. (2022) that was focused within a
166 boreal forest, this remote continental mountaintop site at an elevation of 3220 m provided the
167 opportunity to sample both regional and long-range INP sources within both the boundary layer
168 and free troposphere. The site is typically in the free troposphere during the nighttime and early
169 morning, and in the boundary layer from the late morning to early evening, although topography
170 and wind direction influence this timing (Collaud Coen et al., 2018). When in the free troposphere,
171 the site is more likely to reflect influences by regional or long-range transport of aerosols. For
172 example, during FIN-03, the variety of air masses that were sampled and sensed by aerosol
173 instruments included ones passing over phosphate mines in Idaho (on September 18 and 20) and
174 mined deposits of rare earth metals at Mountain Pass, CA (on September 27) (Zawadowicz et al.,
175 2017). When the convective boundary layer height reaches the elevation of the laboratory, the site

176 is likely more impacted by local/regional aerosol sources. Additionally, meteorological transitions
177 can occur (e.g., frontal boundary passage, wind direction shifts), driving changes in aerosol sources
178 that may indirectly occur in response to those changes (e.g., biological aerosols, carbonaceous
179 particles from biomass burning, and mineral/soil dust). While the constantly fluctuating
180 environmental conditions during FIN-03 added an additional challenge to the intercomparison,
181 they also provided a realistic setting for atmospheric INP measurements. In addition to adding
182 challenges, conducting the intercomparison in the presence of complex aerosols in the field
183 provided the opportunity to survey instrument response to varied particle sources.

184 Participation in FIN-03 included online continuous flow diffusion chambers (CFDCs) and
185 aerosol collections for offline INP measurements, representing a subset of the instruments that
186 operated in FIN-02 (DeMott et al., 2018). Online instruments have the advantage that the aerosol
187 being evaluated as INPs remain free-floating and unaltered, never touching a substrate nor
188 requiring shipment of samples to a laboratory. Online techniques can also monitor INP
189 concentration changes occurring over short time scales. Nevertheless, they are limited in the
190 thermodynamic conditions that can be represented over a given time frame, and they are limited
191 by volume sampling rates in assessing the low concentrations of INPs at modest supercooling.
192 Offline techniques, i.e., those in which samples are collected in the field and subsequently
193 processed in laboratory, provide the opportunity to capture large sample volumes (albeit over
194 longer time scales) and consequently assess a wider temperature range of INP activation
195 properties.

196 Since aerosol physical and chemical properties strongly influence their ability to activate
197 as INPs (Hoose and Möhler, 2012; Kanji et al., 2017; Murray et al., 2012), measurements of
198 particle sizes and composition (see Section 2) were included to lend context to the variable

199 composition of aerosols and evaluate their potential role in ice nucleation activity. Rather than use
200 these data for attempting closure, FIN-03 focused on using data to constrain existing
201 parameterizations to diagnose INP compositions during the study period. Also, in contrast to other
202 recent studies, special effort was made to characterize deposition nucleation activity in addition to
203 immersion freezing.

204 **2 Methods**

205 **2.1 Aerosol property measurements**

206 Measurements of aerosol physical, chemical, and biological particle properties were made
207 during FIN-03 to provide context to INP measurements. Sampling manifolds, which draw air into
208 SPL from outdoors at high flow, are as follows: Inlets were located in each of the two wings of
209 SPL that frame the living area, referred to as the “instrument” laboratory (facing north) and the
210 “chemistry” laboratory (facing south). The “original” inlet system in the instrument laboratory
211 (Hallar et al. 2011; Petersen et al. 2019) feeds a nephelometer (see below) and a standard suite of
212 aerosol instruments (not operational for FIN-03). This 15 cm diameter aluminum inlet rises 4 m
213 above the roofline. At ≈ 1 m inside the laboratory, it transitions to a 15 cm horizontal manifold.
214 With a flow of ≈ 500 L min^{-1} , aerosol transmission calculations have characterized the system to
215 have a 50% upper particle size cut-off at an aerodynamic diameter of 5 μm (Hallar et al., 2011).
216 The “new” inlet system consists of two identical stainless steel, turbulent-flow, ground-based inlets
217 described by Petersen et al. (2019), which are straight and enter the laboratory vertically. One is
218 in the SPL instrument laboratory, and one is in the chemistry laboratory. These inlets that extend
219 10 m above the laboratory roof have been demonstrated to have 50% upper particle size cut-offs
220 at an aerodynamic diameter of approximately 13 μm for a wind speed of 0.5 m s^{-1} . Additional

221 computational fluid dynamics simulations suggest that this size cut-off remains above 5 μm even
222 for exterior wind speeds up to 15 m s^{-1} (Petersen et al., 2019), higher than achieved at any time
223 during FIN-03 sampling. Little bias was seen in ambient aerosol sampling between the original
224 inlet system and the new, turbulent flow-based inlets based on the metric of total aerosol scattering
225 (Petersen et al., 2019). Flow rates and transfer lines to individual instruments are described after
226 the aerosol property measurements are introduced, at the conclusion of this section.

227 A Laser Aerosol Spectrometer (LAS, model 3340, TSI Inc., St. Paul, Minnesota, USA)
228 was used to measure the aerosol size distribution over the diameter range 0.089-10 μm . Aerosols
229 were assumed dry based on relative humidity always remaining below 30% when measured from
230 its sample line. Sample was drawn at 0.1 L min^{-1} and sampling was done from the turbulent flow
231 inlet system located in the SPL chemistry laboratory, as described further below. Size calibrations
232 were performed using polystyrene latex spheres (PSL, Duke Scientific). PSL diameters were
233 converted to ammonium sulfate equivalent diameters using Mie theory (Froyd et al., 2019).
234 Particle concentrations are reported as a function of equivalent ammonium sulfate diameter.
235 Volume and surface area distributions are derived assuming spherical particles. Number
236 concentrations and surface areas, further informed by aerosol composition measurements, allows
237 for connection to INP concentration predictions, and this information is used herein to
238 diagnostically infer mineral and soil dust influences on INPs during the study. We will particularly
239 reference the parameterizations of Niemand et al. (2012) that links mineral surface area to INP
240 concentrations and DeMott et al. (2015) that links dust number concentrations at sizes larger than
241 0.5 μm to INP concentrations.

242 Measurements using a three-wavelength integrating nephelometer (TSI Model-3563,
243 Shoreview, MN) also provided information on aerosol distributions via their optical properties.

244 This nephelometer is part of the National Oceanic and Atmospheric Administration Federated
245 Aerosol Network (Andrews et al., 2019). The nephelometer splits scattered light into red (700 nm),
246 green (550 nm), and blue (450 nm) wavelengths. Impactors to cut aerosols at aerodynamic sizes
247 below 1 and 10 μm are alternately used upstream of air flowing into the instrument. The
248 nephelometer sampled within the original inlet in the SPL instrument laboratory. A blunt tap from
249 this original SPL inlet manifold provided air samples to the nephelometer system via 1" i.d.
250 conductive tubing.

251 The Particle Analysis by Laser Mass Spectrometry (PALMS) instrument performed
252 measurements of the composition of 0.2 to 3.0 μm aerosol particles. The PALMS was designed
253 and operated by the National Oceanic and Atmospheric Administration (NOAA) as described in
254 Thomson et al. (2000). Particles are sampled, focused, and accelerated via an aerodynamic lens
255 inlet (Schreiner et al., 2002) before passing into a vacuum chamber where they successively pass
256 through two continuous-wave detection laser beams (532 nm Nd:YAG) and scatter light. Vacuum
257 aerodynamic diameter is determined based on the transit time. The detection signal triggers an ArF
258 excimer laser that emits a 193 nm pulse to simultaneously ablate and ionize single particles. The
259 resulting ions are analyzed with a unipolar time-of-flight mass spectrometer, which allows polarity
260 switching during the particle flight, thereby producing positive or negative ion mass spectra for
261 individual particles. PALMS spectra are classified into compositional categories, and fractions are
262 averaged over 5 min sample periods. Number, surface area, and mass concentration products for
263 the different particle types are generated by combining PALMS size-dependent fractional
264 composition data with absolute particle concentrations measured by the LAS instrument (Froyd,
265 et al. 2019; Froyd et al., 2022). When PALMS compositional concentrations are referenced in the

266 results of FIN-03 aerosol compositions in Section 3.2, they have been determined by these
267 methods.

268 The NOAA Wideband Integrated Bioaerosol Sensor, Model 4A (WIBS-4A; Droplet
269 Measurement Technologies, Longmont, CO) was used to detect fluorescent properties of
270 individual particles and assess the presence of biological particles. Measurements are presumed
271 to characterize dry particles. The WIBS-4A is described in detail elsewhere (Gabey et al., 2010;
272 Kaye et al., 2005; Perring et al., 2015) and is only briefly summarized here. As described in
273 Zawadowicz et al. (2019), the gain for the WIBS-4A used at SPL was set to detect and classify
274 particles between 0.4 and 10 μm . First, the optical diameter of particles entering the detection
275 cavity is determined by light scattered during transit through a 635 nm laser beam. This signal
276 triggers the sequential firing of two xenon flash lamps filtered to produce narrow excitation
277 wavebands centered at 280 and 370 nm. The resulting fluorescence is detected by two wideband
278 photomultiplier detectors observing 310-400 nm and 420-650 nm. Fluorescing particles were
279 categorized according to the intensity of the signal in each of three channels (channel A excitation
280 280 nm/emission 310-400 nm, channel B excitation 280 nm/emission 420-650 nm, channel C
281 excitation 370 nm/emission 420-650 nm). Particles for which the measured emission intensity in
282 only one channel met the threshold (such that the signal intensity exceeded the value equal to three
283 standard deviations above the mean) were assigned Type A, B, or C, and particles for which the
284 measured emission intensity in two or more channels met the threshold were assigned Type AB,
285 BC, BC, or ABC (Perring et al., 2015). The interpretation of particle composition according to
286 the seven WIBS-4A channels is not straightforward, as many fluorophores are active in each
287 channel, including non-biological components (Perring et al., 2015; Pöhlker et al., 2012). Channel
288 A fluorophores include biological components such as tryptophan, phenylalanine as well as

289 nonbiological components which interfere with the determination of biological content, including
290 polycyclic aromatic hydrocarbons (PAHs) (pyrene, naphthalene, phenanthrene). Biological
291 fluorophores, which produce a signal in channel C, include the reduced form of nicotinamide
292 adenine dinucleotide (NADH), nicotinamide adenine dinucleotide phosphate (NADPH), and
293 riboflavin, and potential non-biological interference in channel C may result from the presence of
294 humic acid in aerosol particles. Channel B fluorophores are not generally considered to be
295 biological in nature, though riboflavin and dry cellulose both produce signals in this channel.

296 We report WIBS-4A channel data herein under these noted caveats and further utilize these
297 data to explore links to immersion freezing biological INP concentrations, as has been done in
298 some previous efforts. Tobo (2013) previously reported relations of biological INPs acting in the
299 immersion freezing mode (measured by the Colorado State University (CSU) CFDC) to
300 fluorescent biological aerosol particles (FBAP) at sizes $> 0.5 \mu\text{m}$ measured in the understory of a
301 Ponderosa pine forest in Colorado. In that work, an ultraviolet aerodynamic particle sizer (UV-
302 APS) with excitation wavelength at 355 nm and emission wavelengths 420-575 nm was used as a
303 reference for FBAP concentrations. Due to differences between the excitation and emission
304 wavelengths, UV-APS measurements correspond most closely with Type C particles detected by
305 the WIBS-4A (Healy et al., 2014). Consequently, a conservative or “low” estimate of FBAP for
306 use in the parameterization of Tobo et al. (2013) we employ herein uses the sum of C, AC, BC and
307 ABC particles. A “high” FBAP for this parameterization has also been used by Twohy et al.
308 (2016), considering all non-B-only particles (A, AB, ABC, AC, BC, C). We will use both
309 definitions in our presented results and partly justify the higher estimate because the CSU-CFDC
310 assuredly does not capture all biological INPs due to the use of the upstream impactor (see below).
311 A final class of particles defined by WIBS-4A data for relation to immersion freezing INPs are

312 denoted as FP3 particles (Wright et al., 2014). FP3 particles are particles that show strong emission
313 in the 310 to 400 nm spectral band when excited by 280 nm light (A type) but are only weakly
314 represented as B and C types. A threshold of 1900 arbitrary fluorescence units in the 310 to 400
315 nm band is used to denote FP3 particles (Wright et al., 2014). FP3 particles have been connected
316 to immersion freezing INP concentrations in multiple environments (Wright et al., 2014; Suski et
317 al., 2018; Cornwell et al., 2023).

318 Flow rates and transfer lines to each instrument are summarized as follows. The PALMS,
319 LAS, and WIBS-4A sampled from the SPL turbulent flow inlet stack at 0.75, 0.1, and 0.3 vlp_m,
320 respectively, via a common 0.19" i.d. aluminum tube. The total flow was held at 1.2 vlp_m using a
321 variable dump flow, and the line was split into multiple 0.115" o.d. stainless steel tubing sections
322 connecting to each instrument. All tubing junctions employed Y-splitters, and all reducing fittings
323 were internally beveled to prevent impaction losses. Sample lines were not actively dried, but
324 relative humidity was < 30% in LAS and WIBS-4A. For the LAS instrument, the theoretical
325 transmission of the inlet system was 98%, 84%, and 57% for 1, 3, and 5 μm aerodynamic diameter
326 particles, respectively, with gravitational settling being the dominant loss process. Transmission
327 to WIBS-4A for the same sizes was 99%, 90%, and 76%. Size distributions were not corrected for
328 transmission losses. The nephelometer sampled from the original inlet in the SPL instrument
329 laboratory via a blunt tap manifold and 1" i.d. conductive tubing.

330 **2.2 INP measurement methods**

331 All specific instruments used in FIN-03 were also used in the FIN-02 laboratory campaign.
332 A summary listing of all ice nucleation instruments utilized in FIN-03 is provided in Table 1.
333 Detailed operating principles, siting of samplers (rooftop versus within SPL), and experimental
334 methods for each instrument follow below. In this work, we will refer to the FIN-03

335 “intercomparison period” to define the times that all INP instruments co-sampled air with
 336 substantial temporal overlap for direct comparison. This means that on a given day a sample was
 337 fully collected within the comparison time unit of 3 hours (informed by aerosol data, as discussed
 338 later) or overlapped the comparison period if the collection time was somewhat longer. Other times
 339 of sampling by the different instrument groups were devoted to special science investigations only
 340 partly covered herein.

341

342 **Table 1** Descriptions of INP instruments.

	Instrument	Type	Institute	References
Online/direct	Continuous flow diffusion chamber (CSU-CFDC)	Continuous flow diffusion chamber (cylindrical)	Colorado State University	(Eidhammer et al., 2010; Rogers, 1988; Rogers et al., 2001)
	Spectrometer for ice nuclei (MIT-SPIN)	Continuous flow diffusion chamber (parallel)	Massachusetts Institute of Technology	(Garimella et al., 2016; Garimella et al., 2017; Kulkarni & Kok, 2012)
Offline/post-processing	Frankfurt Ice Nuclei Deposition Freezing Experiment deposition mode (FRIDGE-DC)	Low pressure diffusion chamber (on wafers)	Goethe University Frankfurt	(Schrod et al., 2016)
	Frankfurt Ice Nuclei Deposition Freezing Experiment immersion freezing mode (FRIDGE-CS)	Cold stage droplet freezing array (on wafers)	Goethe University Frankfurt	(Schrod et al. 2020; DeMott et al. 2018)
	Ice spectrometer (CSU-IS)	Aliquot freezing array	Colorado State University	(Hill et al., 2016; Hiranuma et al., 2015)
	Cold stage (NCSU-CS)	Cold stage droplet freezing array (on hydrophobic glass slides)	North Carolina State University	(Wright & Petters, 2013; Yadav et al., 2019)

343

344 *2.2.1 Online INP measurements*

345 Two online instruments participated in intercomparison experiments in FIN-03. We
346 describe the basic design and operating principles and procedures, sampling inlets, measurement
347 uncertainties and correction for false counting issues, and any special studies reported herein for
348 the CFDC instruments from CSU and the Massachusetts Institute of Technology (MIT). A third
349 CFDC from Texas A&M University was used primarily for special studies to develop
350 depolarization detection of ice, already reported (Zenker et al., 2017).

351 The CSU-CFDC

352 This online INP instrument has the most established history as an online technique for
353 activating and counting INPs. The CSU-CFDC operating principles are described in prior works
354 (Rogers, 1988; Rogers et al., 2001; Eidhammer et al., 2010). Application and considerations for
355 interpreting data have been described by DeMott et al. (2018). The CSU-CFDC is composed of
356 nested cylindrical copper walls that are chemically ebonized to be hydrophilic so they can be
357 evenly coated with ice. The chamber is divided into two sections vertically. For FIN-03, the CSU-
358 CFDC was operated to establish a temperature gradient between the colder (inner) and warmer
359 (outer) ice walls in the upper ≈ 50 cm “growth” section to produce either water subsaturated or
360 water supersaturated conditions at various temperatures within a central lamina. Aerosol particles
361 were directed into that central lamina. For the flow rates used (10 v_lpm total flow, 1.5 v_lpm sample
362 flow) the residence time was ≈ 5 s in the growth region. Ice crystals forming on INPs in the growth
363 section continued to grow for ≈ 2 s in the lower ≈ 35 cm “evaporation” section of the chamber where
364 the outer wall temperature was adjusted to be at an equivalent temperature to the inner (cold) wall
365 to promote evaporation of liquid drops. When operating in the water supersaturated regime, water

366 relative humidity was controlled to be nominally at 105% during FIN-03 to stimulate droplet
367 growth and subsequent freezing, for best comparison to offline immersion freezing methods. For
368 probing ice nucleation in the deposition nucleation regime, relative humidity (RH) was controlled
369 to $\approx 95\%$. Temperature uncertainty is ± 0.5 °C at the reported CSU-CFDC lamina processing
370 temperature and relative humidity uncertainty depends inversely on temperature, as discussed by
371 DeMott et al., (2018), estimated for example as 2.4 % for a lamina RH of 105% at -25 °C.
372 Processing temperatures spanned -15 to -32 °C during FIN-03.

373 The CSU-CFDC sampled from one of the turbulent aerosol inlet ports, located in the SPL
374 instrument laboratory. Connection was via 0.19” inner diameter conductive tubing. Prior to
375 entering the CFDC, aerosol was further dried using two inline diffusion driers and then size-limited
376 using dual single-jet impactors that achieve a 50% upper particle size cut-off at an aerodynamic
377 diameter of 2.5 μm . This limitation on aerosol sizes helps to remove ambiguity when
378 distinguishing ice crystals at ≈ 4 μm sizes from aerosol particles using an optical particle counter
379 at the CSU-CFDC outlet. Counts greater than this size divided by sample volume define INP
380 concentrations.

381 Uncertainty in calculation of INP concentrations must account for background counts that
382 can occur due to ejection of frost emanating from interior surfaces of the CSU-CFDC over
383 operational periods. We follow Levin et al. (2019) in this regard. Frost corrections are defined via
384 use of time intervals sampling ambient air through a HEPA filter. A typical daily cycle at each
385 temperature point was to bookend 10-min ambient air sampling with 5-min filter periods. Sample
386 data were background corrected by subtracting the interpolated filter period concentration before
387 and after each sampling period. Background corrected data were then averaged to ≈ 5 -min sampling
388 times to increase statistical confidence. Poisson counting errors during filtered and ambient

389 sampling periods were added in quadrature, and INP concentrations were judged statistically
390 significant at the 95% confidence level if they were greater than 1.64 times this combined INP
391 error (one-tailed z test). Interior inlet tubing losses are not considered in the reported INP data
392 because they have been estimated at 10% or less in the past. INP concentration correction
393 underestimates inferred (by a factor of 3) to be due to aerosols spreading outside of the lamina
394 during measurements specifically of mineral dust INPs (DeMott et al., 2015) are not generally
395 applied to the data herein, though this is discussed regarding the intercomparison results and INP
396 parameterizations in this paper.

397 An aerosol concentrator (MSP Model 4240) was used at selected times during FIN-03 to
398 improve sampling statistics, in the same manner as in previously published studies (Tobo et al.
399 2013; Suski et al., 2018; Cornwell et al., 2019). The aerosol concentrator was positioned open to
400 the air on the roof of the instrument laboratory room (covered and not used during rainfall), with
401 a short 0.19” inner diameter copper line containing the concentrated aerosol entering the laboratory
402 vertically from about 3 m above the CFDC. Concentration factors for INPs can vary depending on
403 the ambient INPs present in a given environment. These were evaluated in the same manner as
404 Tobo et al. (2013), leading to an average increase of INPs by 90 times (± 45) during operation of
405 the aerosol concentrator compared to ambient inlet periods during this study (not shown here
406 because analysis repeats the efforts referenced above). A three-way manual stainless-steel valve
407 was used to direct sample air to the CSU-CFDC from either the turbulent flow inlet or the aerosol
408 concentrator.

409 Supplemental studies with the CSU-CFDC reported herein used a high temperature heating
410 tube (Suski et al., 2018) placed in-line following the three-way valve for removing aerosol organics
411 prior to INP measurements. The use of a tube heater upstream of the CSU CFDC to expose single

412 particles to 300°C is intended to isolate the action of total organic versus inorganic INPs via
413 comparison of ambient versus heat-treated particle streams. Simultaneous measurements of heated
414 and unheated aerosol streams are not possible with a single CFDC, so sampling was conducted by
415 alternating the channel chosen following a flow splitter during subsequent 10-minute periods, and
416 ignoring aerosol changes that rarely occurred over such times.

417 The MIT Spectrometer for Ice Nuclei (SPIN)

418 The MIT-SPIN (Droplet Measurement Technologies, Boulder, CO), a commercially
419 produced, parallel-plate CFDC, also sampled during FIN-03. Measurements were focused on ice
420 nucleation below water saturation for FIN-03. Operating principles are described in Garimella et
421 al. (2016) and Garimella et al. (2017). SPIN consists of two flat walls separated by 1.0 cm and
422 coated in approximately 1.0 mm of ice. Aerosol particles are fed into the chamber in a lamina flow
423 of about 1.0 liters per minute and are constrained to the centerline with a sheath flow of about 9.0
424 liters per minute. The temperature and relative humidity that the aerosol lamina experiences were
425 controlled by varying the temperature gradient between the two iced walls (Kulkarni & Kok,
426 2012). After exiting the nucleation chamber, the particles enter SPIN's optical particle counter,
427 which sizes aerosol on a particle-by-particle basis for diameters between 0.2 and 15 μm .
428 Temperature uncertainty was 0.5 °C. For the lamina RH conditions below 100% used in FIN-03,
429 the RH uncertainties were 0.7, 1.3 and 1.7% at -20, -25, and -30 C, respectively.

430 The MIT-SPIN sampled from one of the turbulent flow inlet systems, located within the
431 SPL aerosol chemistry laboratory. It was connected to the inlet system port with a short section of
432 0.19" inner diameter conductive tubing.

433 Data processing for SPIN, including definition of uncertainties, was performed following
434 similar procedures as used for the CSU-CFDC instrument, with a few distinctions. A cut-size for

435 potential ice particles was set to 5 μm diameter. A low-pass filter was applied next to remove all
436 1 Hz data that exceeded a total of three counts s^{-1} , as recommended by Richardson et al. (2007) to
437 reduce frost background noise that equated to INP concentrations larger than about 200 L^{-1} (>2
438 standard deviations above mean values discussed later) for the SPIN sampling flow rate. A
439 depolarization filter was next applied to isolate particle data specific to ice using 1 Hz averaged
440 backscattering data from the SPIN's OPC, with instrument specific values of 3.5 and -0.25 for the
441 $\log_{10}(\text{Size})$ and $\log_{10}(\text{S1/P1})$ measurements respectively (Garimella et al., 2016). Ice particle data
442 was then converted from counts per second to number density per volume of sample flow (L^{-1}).
443 Frost ejected from the plates of the SPIN chamber beyond that removed by the low-pass filter was
444 characterized using particle-free sampling periods when the sample flow was diverted through a
445 HEPA filter by an automated three-way valve. Linear interpolation of filter period INP
446 concentrations was used to approximate background frost concentrations throughout the
447 measurement period (a minimum of 4, 5-min filter periods for each set-point temperature within a
448 2–3-hour period) and smoothed using a five-minute moving average. Sample data was background
449 frost corrected by subtracting this smoothed background frost density from total number density
450 in each 5-min sample period. Finally, a SPIN specific particle concentration correction factor of
451 1.4 is applied to account for non-ideal instrument behavior (e.g., out of lamina particles) resulting
452 in underestimation of INPs as described by Garimella et al. (2017). As the field measurements
453 from this study predate the laboratory experiments performed to determine SPIN uncertainties, the
454 minimum reported correction factor was selected to remain conservative in reported
455 measurements.

456 As for the CSU-CFDC, estimation of INP concentration measurement error for the MIT-
457 SPIN assumed the background corrected INP concentration follows a Poisson distribution. Then,

458 the Poisson error for both INP and background frost concentrations were defined as the square root
459 of the sample mean. The significance test statistic was defined by the quadrature sum of counting
460 errors multiplied by the z-score for a one-tailed z-test at the 95% confidence interval. INP
461 measurements were deemed statistically significant if the mean INP concentration was greater than
462 this test statistic.

463 *2.2.2 Offline INP measurements*

464 Offline methods have undergone many improvements in recent years and have been
465 successfully used in a complementary manner for comparison to online methods in other recent
466 intercomparisons (DeMott et al., 2017; DeMott et al., 2018; Hiranuma et al., 2015; Wex et al.,
467 2015; Knopf et al., 2021; Brasseur et al., 2022; Lacher et al., 2024). In FIN-03 particles were
468 collected from the air using liquid impingers and filter samplers. Impinger liquid and water
469 suspensions created from immersed filters were analyzed for immersion freezing of distributed
470 droplet volumes using the North Carolina State University Cold Stage (Wright et al., 2013), the
471 CSU Ice Spectrometer (Hiranuma et al., 2015; DeMott et al., 2018), and the FRankfurt Ice Nuclei
472 Deposition FreezinG Experiment (FRIDGE) instrument (Schrod et al., 2016). All measurements
473 were made offsite after the return of impinger liquid and filters to the participant institutions, as
474 done in most intercomparisons of this type. The handling of samples is mentioned regarding each
475 instrument below.

476 The North Carolina State University Cold Stage (NCSU-CS)

477 The North Carolina State University cold stage (NCSU-CS) has been previously described
478 by Wright and Petters (2013) and Hader et al. (2014). Procedures used for collecting immersion
479 freezing spectra are described below and by Yadav et al. (2019). During FIN-03, filter samples,
480 impinger samples and precipitation samples were collected for analysis using the NCSU-CS. For

481 the intercomparison, the filter and impinger results are considered. Filter samples were collected
482 from the roof of Storm Peak Lab for 3–4 hours twice daily using 47 mm Nuclepore polycarbonate
483 filters (0.2 μm pore size) housed in an open-faced stainless-steel filter holder operated at 14 L
484 min^{-1} (at altitude) or $\approx 9 \text{ L min}^{-1}$ at standard temperature and pressure conditions (STP) of 1013 mb
485 and 0 $^{\circ}\text{C}$. Filter holders were directed downward and sheltered from precipitation by a large,
486 inverted metal bowl. Images are shown in supplemental Section S1. Each filter was resuspended
487 in 6 ml prefiltered HPLC grade ultrapure water. Impinger samples were collected directly into
488 ultrapure water using a glass bioaerosol impinger (SKC, Inc.) as described by Hader et al. (2014)
489 and DeMott et al. (2018). The impinger jets air at 10.6 L min^{-1} ($\approx 7 \text{ L min}^{-1}$ STP) into a 20 mL
490 water reservoir, impacting 80% of particles $\geq 200 \text{ nm}$ in diameter and $\approx 100\%$ of particles $\geq 1 \mu\text{m}$
491 (Willeke et al., 1998). Impinger samples were collected in the same manner as was done for all
492 shared liquid samples for the FIN-02 intercomparison (DeMott et al., 2018) except that Teflon tape
493 replaced stopcock grease to seal the impinger glass lid to prevent jamming. Water evaporating
494 from the reservoir was replaced hourly; the impinger was in a rooftop shelter with its inlet
495 extending horizontally through a hole in the shelter wall, into the open air at a height of ≈ 6 feet
496 below the position of filter sampling units that were mounted on an outside railing. Water used
497 onsite was filtered (0.2 μm) Milli-Q water. All samples were stored at $-20 \text{ }^{\circ}\text{C}$ onsite, shipped on
498 dry ice, then stored at $-80 \text{ }^{\circ}\text{C}$ until analysis at NCSU.

499 Freezing statistics for each liquid sample were acquired by pipetting an array of
500 approximately 256 droplets of $1 \mu\text{L} \pm 0.88\%$ volume on four hydrophobic glass slides under dry
501 N_2 gas. Temperature was ramped at a rate of $-2 \text{ }^{\circ}\text{C min}^{-1}$ and freezing was detected at a temperature
502 resolution of 0.17 $^{\circ}\text{C}$ (every 5 s) using CCD camera images collected from an optical microscope.
503 Temperature uncertainty based on repeatability of homogeneous freezing tests is 0.1 $^{\circ}\text{C}$ (Hiranuma

504 et al., 2015). Except for pure dust samples, the dependence of the population median freezing
 505 temperature on cooling temperature is less than 1°C per decade in cooling rate, including
 506 measurements of ambient INPs (Wright et al., 2013). A decade in cooling rate is much larger than
 507 the variations in cooling rate used by instruments in FIN-03 (-0.33 to 2 °C min⁻¹). The expected
 508 shift in INP spectra due to variability in cooling rate is much less than the total uncertainty and
 509 thus corrections for cooling rate are not further considered here. The concentration of ice nuclei at
 510 temperature T per unit volume of liquid is given by Vali (1971):

$$511 \quad c_{IN}(T) = \frac{-\ln(f_{unfrozen}(T))}{V_{drop}\Delta T} \quad (1)$$

512 where $f_{unfrozen}$ is the fraction of unfrozen droplets at T and V_{drop} is the population-median droplet
 513 volume. The concentration of ice nucleating particles (INP) in the atmosphere is given by:

$$514 \quad c_{INP}(T) = \frac{c_{IN}(T) \cdot f \cdot V_{liquid}}{V_{air}} \quad (2)$$

515 where f accounts for any serial sample dilutions with pure water used to focus measurements within
 516 different temperature ranges, V_{liquid} is the liquid suspension sample volume, and V_{air} is the volume
 517 of air sampled (flow rate at STP \times duration). The high temperature resolution freezing data were
 518 collected 3 \times per sample and $f_{unfrozen}$ was binned into 1 °C intervals for spectral calculations.
 519 Confidence intervals reported in archived data were given as ± 2 standard deviations of the mean
 520 temperature uncertainty of measurements (typically 0.5 to 1 °C). We will refer to the processed
 521 filter samples as NCSU-CS (F) and processed impinger samples as NCSU-CS (I). Note that filter
 522 samples were more concentrated by a factor ≈ 5 due to the greater V_{liquid} used in the impinger for
 523 the stated air collection volumes. Thus, the filter technique is more sensitive and has a lower limit
 524 of detection (LOD). The precise ratio for a specific experimental period depended on the exact
 525 sampling times of filter and impinger, and the exact number of droplets analyzed for the filter,

526 impinger sampling, averaging across repeats, and binning into 1-degree intervals. For this reason,
527 the ratio of LOD for the averaged samples may differ slightly from this estimate.

528 As for all INP samples in FIN-03, “blanks” were collected for each of the NCSU-CS
529 sample types. The normal procedure for most blank filter assessments in the field is to momentarily
530 expose a clean filter to flow in a collection unit. In the spirit of procedural testing that typifies
531 workshops like FIN-03, a different method was trialed by the NCSU group., Ten filter “blanks”
532 were specially collected on days during FIN-03 by placing a 0.2 μm pore size filter as a backing
533 filter to an 0.05 μm pore size filter in a secondary filter unit that was exposed to the same total
534 ambient flow conditions as the primary INP filter unit. This 0.2 μm filter was processed the same
535 as the primary INP filter (rinsed in 6 ml ultrapure water) and freezing results were presumed to
536 provide a quite conservative estimate of filter background INPs. It was indeed found that the
537 number of INPs per blank filter in these collections were much higher than for standard blank filter
538 method used by the other groups. The results from the 10 blank filters were averaged across the
539 processed temperature range, and an upper confidence limit of 1 $^{\circ}\text{C}$ was defined. All INP
540 concentration results for each ambient filter were rejected if in any given temperature bin they fell
541 below this upper confidence bound. In sum, 20% of the original measurement points based on
542 filter collections were removed from measurement intercomparisons by this blanking operation.
543 Impinger blanks were collected via separation of some water from the pure water storage container
544 each time the impinger unit was filled with pure water to begin an air sampling period. Thus,
545 blanks were specific to each ambient impinger sample. The same 1 $^{\circ}\text{C}$ upper confidence bound
546 that characterizes NCSU-CS measurements was applied in each case to identify sample
547 temperature points where the liquid suspension INPs fell below the upper confidence limit of the
548 impinger blanks. These were removed from intercomparisons.

549 CSU Ice Spectrometer (CSU-IS)

550 The CSU-IS also post-processed particles sampled onto filters during FIN-03. This
551 instrument has been described in Hiranuma et al. (2015) and Suski et al. (2018). Samples were
552 collected for approximate periods of 4 hours for intercomparison periods (longer for overnight
553 samples – not part of the intercomparison) using pre-cleaned 0.2 μm pore diameter, 47 mm
554 polycarbonate Nuclepore filters (Suski et al., 2018) mounted in disposable, sterile open-faced and
555 face-up holders (Nalgene), with a typical sample flow rate of 14.9 L min^{-1} (ambient) and 9.5 L
556 min^{-1} (STP). Filters were collected on the same exterior laboratory roof railing as the NCSU filters,
557 approximately 2 m distant. All filter samples were frozen following collection and stored at $-20\text{ }^{\circ}\text{C}$
558 before transit on dry ice and storage again at $-20\text{ }^{\circ}\text{C}$ until processing at the CSU laboratory. Pre-
559 sterilization procedures and overall clean protocols for preparation and handling of filters are
560 detailed in Suski et al. (2018) and Barry et al. (2021b). Particle re-suspension was done through
561 20 minutes of shaking filters in sterile 50 mL Falcon polypropylene tubes (Corning Life Sciences)
562 with 6-10 mL of 0.02 μm pore diameter filtered deionized water. Further 20-fold dilutions using
563 filtered water were made as needed to permit measurement of freezing spectra to the low
564 temperature limit of operation of the CSU-IS.

565 Immersion freezing INP temperature spectra were obtained by distributing 24 - 32 aliquots
566 of 50 μL particle suspensions into the sterile 96-well PCR trays that mount in the CSU-IS. Other
567 wells were filled with serial dilution samples and pure water. The cooling rate was $-0.33\text{ }^{\circ}\text{C min}^{-1}$.
568 Frozen wells were counted at 0.2 - 1 $^{\circ}\text{C}$ degree intervals to a limit of about $-28\text{ }^{\circ}\text{C}$, and
569 cumulative numbers of INP mL^{-1} of suspension estimated using Eq. 1. Conversion to ambient air
570 concentrations std L^{-1} were made based on distributed suspension volume and the total air volumes
571 collected (Eq. 2). Several filter blanks were collected during FIN-03, and one was tested and used

572 to obtain background INP numbers per filter. Blank INPs were found to account for <5% of INPs
573 at -20 and -25 °C, and thus corrections were ignored. Binomial sampling confidence intervals
574 (95%) were derived for INP concentrations following Agresti & Coull (1998). The temperature
575 uncertainty of INP measurements is ± 0.2 °C (Hiranuma et al., 2015).

576 As a supplemental contribution to FIN-03, portions of IS aerosol suspensions were set aside
577 (e.g., suspensions of 6 to 8 ml can serve up to three or more IS aliquot fills) for treatments to
578 proximally isolate total biological, other organic and inorganic contributions to measured
579 immersion freezing INP concentrations. To assess removal of heat labile INP entities, a 2 mL
580 aliquot of suspension was re-tested in the IS after heating to 95 °C for 20 min (McCluskey et al.
581 2018). To attempt to remove all organic INPs, 1 mL of 30% H₂O₂ was added to a 2 mL aliquot of
582 suspension and the mixture heated to 95 °C for 20 min while illuminated with UVB fluorescent
583 bulbs to generate hydroxyl radicals (residual H₂O₂ is then removed using catalase) (Suski et al.
584 2018), and the INPs were again assessed for freezing spectra in the IS. Herein we describe a subset
585 of samples collected on September 15, September 23, and September 25 that were subjected as IS
586 suspensions to the two treatments. The interpretation of data from exposure of particle suspensions
587 to 95 °C is that the reduction of INP concentrations under thermal treatment is a proxy for the
588 concentration of biological (proteinaceous and microbial) INPs which have been eliminated or
589 deactivated through treatment. A strong reduction in INP activity observed after peroxide
590 treatment indicates dominant organic INP populations, whereas a lack of response to this treatment
591 is assumed to indicate that inorganic INPs such as mineral dusts dominate non-heat labile INPs.
592 This assessment for bulk suspensions of particles could be directly compared to measurements of
593 300 °C heat treated single particles in the online CSU CFDC measurements on these same days,
594 providing a more insightful investigation of INP compositions.

595 Taken together, such treatment studies show general utility for estimating biological
596 contributions to INP, overall organic contributions and the importance of inorganic contributions,
597 as done for a variety of locations (McCluskey et al., 2018; Suski et al., 2018; Barry et al., 2021a;
598 Knopf et al., 2021; Testa et al., 2021). However, we note that not all biological materials may be
599 completely denatured or removed by heat (Testa et al., 2021; Daily et al., 2022; Alsante et al.,
600 2023) and not all organics may be removed by peroxide. For example, denaturation is the
601 disruption of higher order (secondary, tertiary, and quaternary structure) in a protein which leads
602 to a loss or lessening of function. Simpler proteins or peptides, such as glutathione, have no higher
603 order structure, and thus cannot be denatured (Alsante et al., 2023). Consequently, estimates of
604 biological contributions to INP based on these treatments may be considered as lower limits for
605 the FIN-03 samples analyzed.

606 FRIDGE Cold Stage and Deposition Nucleation Measurements

607 The FRIDGE instrument can operate as a low temperature cold chamber or low
608 temperature and pressure diffusion chamber device for measuring the concentration of INPs by
609 two independent methods: a) a droplet freezing assay on a cold stage, hereafter FRIDGE-CS
610 (Schrod et al., 2020; DeMott et al. 2018; Hiranuma et al. 2015), which addresses immersion
611 freezing similarly to the NCSU-CS and the CSU-IS and b) the diffusion chamber method, hereafter
612 FRIDGE-DC, that addresses the deposition nucleation and condensation freezing modes
613 introduced in Schrod et al. (2016) and is the standard method for operating the FRIDGE device
614 (e.g., DeMott et al, 2018). The ice nucleation analysis is performed inside the FRIDGE instrument
615 for both methods, yet the sampling process, addressed nucleation modes and the specific analytical
616 procedures differ as described below.

617 For the FRIDGE-CS method, aerosol particles were sampled via a short ¼” conductive
618 tube from the shared turbulent flow aerosol inlet in the SPL instrument laboratory on Teflon
619 membrane filters (Fluoropore PTFE, 47 mm, 0.2 µm, Merck Millipore Ltd.). The sampling
620 duration ranged from 50 to 240 minutes, resulting in air volumes between 250 and 1000 std. L.
621 The particles were extracted in 10 ml deionized water by shaking. Approximately 150, 0.5 µL
622 droplets from that solution were pipetted onto a clean, silanized silicon wafer on the cold stage of
623 the FRIDGE instrument and cooled by $-1^{\circ}\text{C min}^{-1}$ at ambient pressure. A CCD camera detects
624 freezing events and counts the number of frozen droplets as a function of temperature. This process
625 is repeated with fresh droplets and fresh substrates until approx. 1000 droplets are attained. The
626 INP number concentration is derived using Eqs. 1 and 2, as for the NCSU-CS and CSU-IS. An
627 upper bound on temperature uncertainty is estimated as $\pm 0.5^{\circ}\text{C}$. Binomial sampling confidence
628 intervals (95%) were derived for INP concentrations as done for the CSU-IS, following Agresti &
629 Coull (1998). Pure water and suspensions of blank filters in pure water showed no freezing at
630 temperatures $> -20^{\circ}\text{C}$ and a contribution of no more than 15% toward total INPs at -29°C , the
631 lowest temperature for which data are reported herein. Consequently, corrections were ignored for
632 this intercomparison.

633 For the FRIDGE-DC measurements, particles were collected using an electrostatic aerosol
634 collector (EAC) (Schrod et al., 2016) was connected to the same aerosol flow inlet via a short ¼”
635 conductive tube. Within the EAC aerosol particles are electrostatically precipitated onto silicon
636 wafers, which are used as sample substrates. After sampling is completed, the analysis at select
637 pairs of temperature and relative humidity set points follows in a separate step. For that, the wafer
638 was placed on the cold stage inside the diffusion chamber. The chamber was evacuated, the
639 temperature is set to the first analysis temperature. In a second, much larger volume, pure water

640 vapor is regulated by pressure control to the desired supersaturation. Once the water vapor diffuses
641 into the chamber, ice forms on the activated INPs and a CCD camera is used to record and count
642 the emerging ice crystals, which appear as bright objects. It is assumed that one ice crystal
643 represents one INP. The water vapor atmosphere and thus the growth of ice crystals is maintained
644 for up to 100 seconds until the valve to the water vapor source is closed and the chamber is
645 evacuated again. The process is repeated at increasing humidity first, and then at progressively
646 lower temperatures. At SPL samples were taken with the EAC for 50, 75 and 120 minutes,
647 resulting in volumes of approximately 64-150 sL. The samples were analyzed by default at -20
648 $^{\circ}\text{C}$, -25 $^{\circ}\text{C}$ and -30 $^{\circ}\text{C}$ and 95 %, 99% and 102% water saturation. In addition, a few samples were
649 analyzed at -15 $^{\circ}\text{C}$. This was a supplemental contribution by the FRIDGE group for
650 comprehensive analysis of INP activation in the deposition regime, and for comparison to online
651 data in this regime collected for some days. Temperature uncertainty is the same as for the
652 FRIDGE-CS method. RH uncertainty is $\pm 2\%$ based on observing visible condensation on
653 particles at 100% RH. INP concentration uncertainties are given as binomial confidence limits, the
654 same as for the CSU-IS.

655

656 **2.3 INP processing and sampling strategies**

657 As a campaign strategy, samples were collected over different time periods in the day to
658 reflect both varied weather conditions and aerosol populations arriving at the mountain laboratory.
659 For intercomparison, a select number of 3 to 4-hour sampling periods were allocated in which
660 online instruments nominally operated at a few predesignated temperature and relative humidity
661 ranges, while samples were collected continuously for off-line analysis. While aerosol conditions
662 can change within a 4-hour time frame, this was agreed upon as a minimal reasonable period for
663 comparability to obtain statistically reliable results. Similar sampling strategies have been

664 employed in the past intercomparisons (DeMott et al., 2017; Knopf et al., 2021). Overall,
665 measurements were conducted over a wide range of temperatures (-7 to -34 °C) in the
666 heterogeneous ice nucleation regime.

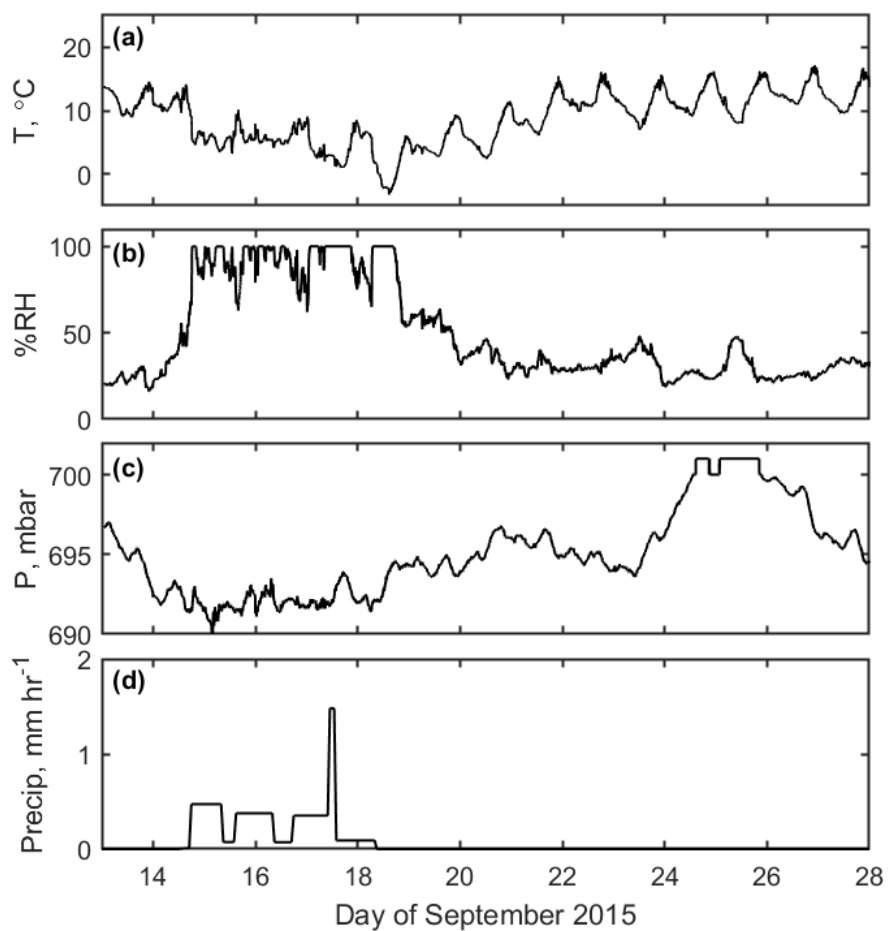
667 **3 Results and discussion**

668 **3.1 Meteorological context**

669 Weather conditions during FIN-03 were characterized using auxiliary measurements.
670 Weather data (temperature, humidity, winds and pressure) were obtained for Storm Peak
671 Laboratory through the MesoWest ([https://mesowest.utah.edu/cgi-](https://mesowest.utah.edu/cgi-bin/droman/meso_base_dyn.cgi?stn=STORM)
672 [bin/droman/meso_base_dyn.cgi?stn=STORM](https://mesowest.utah.edu/cgi-bin/droman/meso_base_dyn.cgi?stn=STORM)) mesonet (STORM site), supplemented with
673 measurements from instruments operated at SPL through the Western Regional Climate Center
674 (WRCC) (<https://wrcc.dri.edu/weather/strm.html>) for the two days that were absent in the
675 MesoWest record. Air temperature, relative humidity, and barometric pressure time series are
676 shown in Figure 1(a), 1(b) and 1(c), respectively. Precipitation was measured via a rain gauge at
677 Storm Peak Laboratory provided by NCSU. Precipitation rate was calculated from the quotient of
678 precipitation (in mm) and time collected (in hours), as shown in Figure 1(d). Back trajectories for
679 all the sampling days in FIN-03 are reported by Zawadowicz et al. (2017), showing 72-hr air mass
680 transits from regions that included Southern California, Washington State and Eastern Nebraska.

681 Relatively warm, dry conditions were observed initially at the Storm Peak Laboratory.
682 Clear skies on September 11 and 12, 2015 gave way to clouds and haze on September 13. Cooler
683 temperatures, lower barometric pressure, and higher relative humidity (generally above $> 70\%$)
684 accompanied rainfall on September 14. This was followed by continued rain on September 15,
685 intermittent rain and short periods of hail on September 16, a mixture of rain, snow, and sleet on
686 September 17, and snow on September 18. The next and longest period in the study, September

687 19 to 28, was marked by an increase in temperature, an increase in barometric pressure, lower
688 relative humidity, and a lack of precipitation. More detailed weather records including daily
689 photographs and a summary of human-produced daily observations are summarized in
690 supplemental Section S1. Daily wind rose plots are provided in Figure S1.



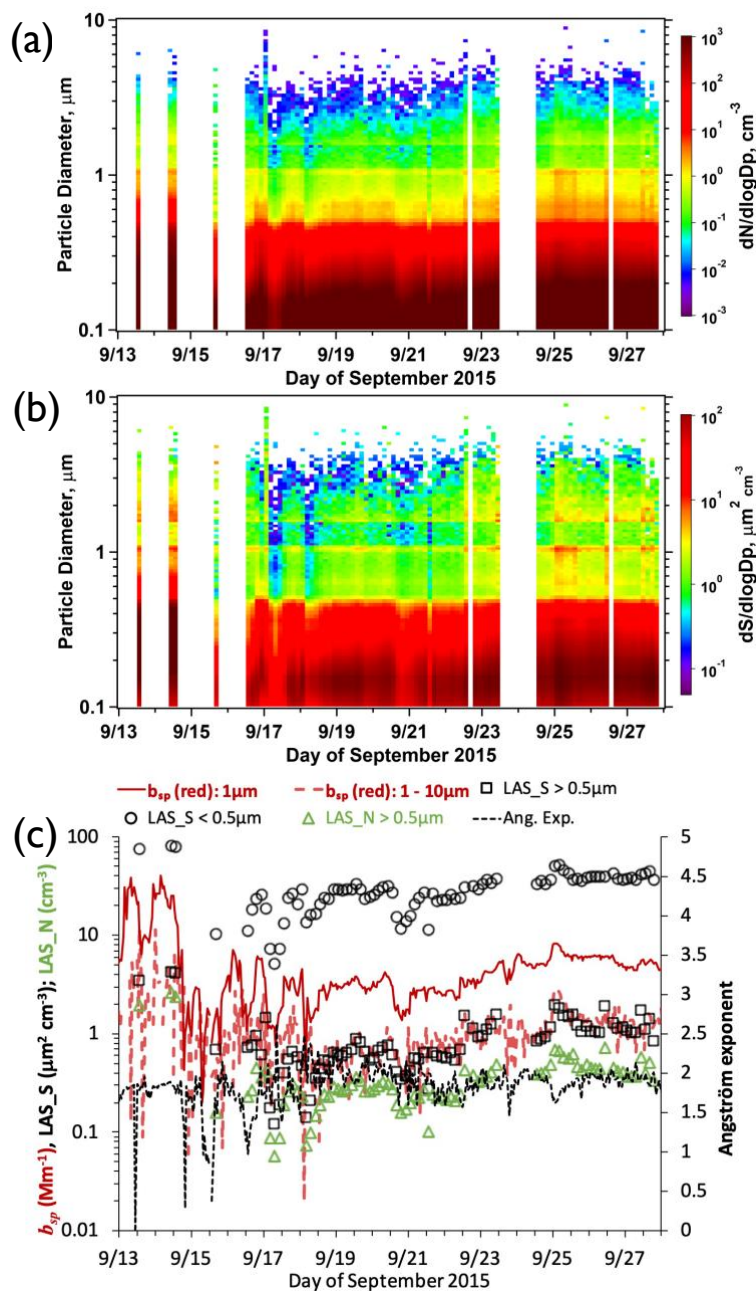
691
692 **Figure 1.** Weather conditions over the course of FIN-03, including (a) air temperature, (b) relative
693 humidity, (c) barometric pressure, and (d) precipitation rate.

694 **3.2 Aerosol context**

695 **3.2.1 Aerosol size distribution and surface area**

696 The time series of aerosol size distribution measured by the LAS (in three hour means) is
697 shown in Figure 2a. The maximum and minimum total LAS concentrations were 706 cm^{-3} and 74
698 cm^{-3} respectively, and the mean and standard deviation of the total LAS concentration throughout
699 FIN-03 were 410 cm^{-3} and 138 cm^{-3} , respectively. The highest total LAS concentration recorded
700 during FIN-03 (706 cm^{-3}) occurred in the early hours on September 25. Elevated aerosol
701 concentration (at least one standard deviation above the mean) was also observed during midday
702 on September 13, before and during midday on September 14, before midday on September 25, in
703 the afternoon on September 26, and around midday on September 27.

704 The timeline of LAS aerosol surface area in Figure 2b emphasizes that surface area was
705 predominately submicron throughout the study, with a mode at about $0.16 \mu\text{m}$. This is important
706 to note, in combination with chemical composition information discussed in the next section,
707 because it is relevant to understanding the likely sizes and surface areas of INPs. We will revisit
708 the surface area of INPs for use in parameterizations in a later section. Quantitative timelines of
709 LAS surface area above and below $0.5 \mu\text{m}$ are shown in Figure 2c. Surface area at above $0.5 \mu\text{m}$
710 is about a factor of 30 lower than at below this size over most of the study period. Also shown in
711 Figure 2c is nephelometer scattering (b_{sp}) in the red channel (700 nm) showing a dominant
712 contribution when the upstream impactor was set to $1 \mu\text{m}$ (aerodynamic) and a much lower level
713 of $1 - 10 \mu\text{m}$ scattering. This scattering from coarse mode particles is consistent with and trends
714 with the LAS surface area in the supermicron regime, while the Angström exponent (calculated
715 using red and blue channels) being close to 2 (small particle dominance) throughout the study is
716 consistent with the dominance of submicron contributions to total surface area. Figure 2 also
717 emphasizes that the lowest aerosol concentrations and surface areas occurred during varied time
718 in the wet period of the study from midday on the 14th through the 17th of September. Finally,



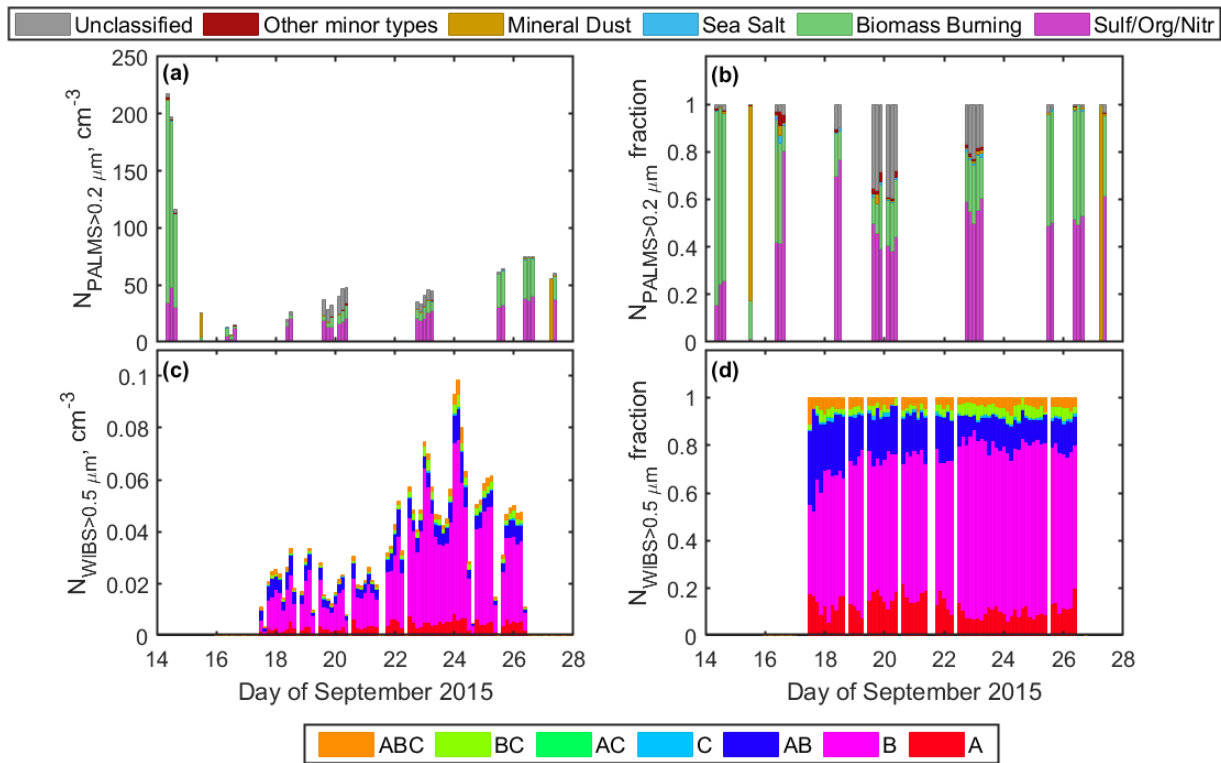
719
 720 **Figure 2.** Time series of dry particle number concentration distribution (ambient conditions, not STP)
 721 measured by the laser aerosol spectrometer (LAS) in a), shown as three-hour means at ambient pressure.
 722 Time series of particle surface area distribution is in b). c) Timeline of nephelometer scattering (1-hr data)
 723 in the red channel for $< 1 \mu\text{m}$ and $1 - 10 \mu\text{m}$ size ranges, 3-hr LAS number concentration $> 0.5 \mu\text{m}$, 3-hr
 724 LAS surface area at sizes below and above $0.5 \mu\text{m}$, and Angström exponent (dashed, right axis).
 725

726 adjacent 3-hr periods rarely represented surface area changes of more than a factor of 2 in the size
727 range $> 0.5 \mu\text{m}$ and was usually within 10-20%. Large differences across 3-hour periods were less
728 frequent for surface area at smaller sizes. These factors confirm the validity of the selected
729 intercomparison time periods.

730 **3.2.2 Aerosol composition**

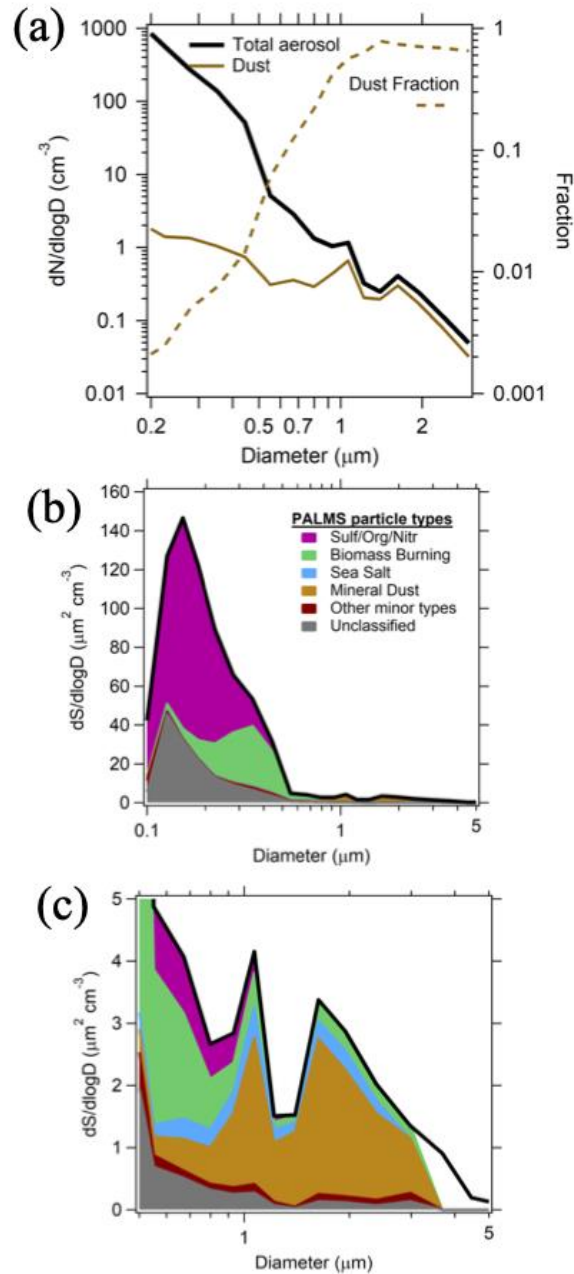
731 The number concentration of aerosol particles from 0.2 to 3 μm with characteristic spectra
732 belonging to eight composition categories (sulfate/organic/nitrate, biomass burning, elemental
733 carbon, sea salt, mineral dust, meteoric, alkali salt, and fuel oil combustion), and the number
734 concentration of unclassified aerosol particles by the PALMS, were assessed for three-hour
735 averages through the FIN-03 period. For simplicity, four of these categories (elemental carbon,
736 meteoric, alkali salt, and fuel oil combustion) were combined into a category called “other” due to
737 the low concentration of particles in each of these categories resulting in 6 total classifications
738 (SulfOrgNit = sulfates/organics/nitrates, BioBurn = products of biomass burning, Sea salt, Mineral
739 dust, and Unclassified), as shown in Figure 3a. The three-hour averages of the number fractions of
740 each particle type were also calculated as the fraction of the total aerosol number concentration
741 measured by the PALMS in each of the six classifications, as shown in Figure 3b. The dominant
742 categories throughout the FIN-03 campaign were BioBurn (mean $26 \pm 43 \text{ cm}^{-3}$, maximum 177 cm^{-3}),
743 SulfOrgNit (mean $22 \pm 13 \text{ cm}^{-3}$, maximum 48 cm^{-3}), and mineral dust (mean $3 \pm 11 \text{ cm}^{-3}$,
744 maximum 55 cm^{-3}). The mineral dust type also includes soil particles (crustal species mixed with
745 organic material) (Zawadowicz et al., 2019). The highest total particle number concentration
746 measured by the PALMS (218 cm^{-3}) occurred on September 14 (of which 177 cm^{-3} consisted of
747 biomass burning and 34 cm^{-3} consisted of sulfates/organics/nitrates). This biomass burning plume
748 impacted the site for several hours. Mineral/soil dust particles were ubiquitous throughout the

749 study, with a concentration of $0.128 \pm 0.446 \text{ cm}^{-3}$ (median and interquartile range). Anomalous
 750 concentrations $>10 \text{ cm}^{-3}$ observed for a few 5-min sample periods on September 15 are likely due
 751 to road dust emitted from site. Dust concentrations were $<1 \text{ cm}^{-3}$ for 90% of the PALMS samples.
 752 Mineral/soil dust represented a median of 0.3% of particles in the $>0.2 \mu\text{m}$ size range, increasing
 753



754
 755 **Figure 3.** Subplots (a) and (b) show the aerosol particle number (ambient conditions, not STP) and relative
 756 fractions (by cumulative count at all sizes) of each of the six PALMS compositional particle types for the
 757 three-hour periods during which the PALMS was used to sample ambient air. Subplots (c) and (d) show
 758 the aerosol particle number concentration and relative fractions (by count) of particles with diameter >0.5
 759 μm in each of the channels (A, B, AB, C, AC, BC, and ABC, which are described in Perring et al., 2015)
 760 over the course of the FIN-03 field campaign.

761



762
 763 **Figure 4.** a) Total aerosol versus mineral/soil dust (ambient) number size distribution and dust fraction
 764 interpreted from PALMS and LAS data for all times that the PALMS was sampling during FIN-03. b)
 765 Surface area distribution differentiated for PALMS compositional types during the same sampling times.
 766 c) Expanded plot from b) for the coarse mode size range to emphasize progressive dominance of dust
 767 components at diameters $> 0.5 \mu\text{m}$.

768

769 to 23% and 67% for >0.5 and >1.0 μm particles (Figure 4a). Similarly, mineral dust contributions
770 to total surface area are inconsequential for total aerosol surface area (Figure 4b) but dominate in
771 the coarse mode regime for the study (Figure 4c). We revisit this result in discussions of
772 parameterization of INPs in Section 3.5.

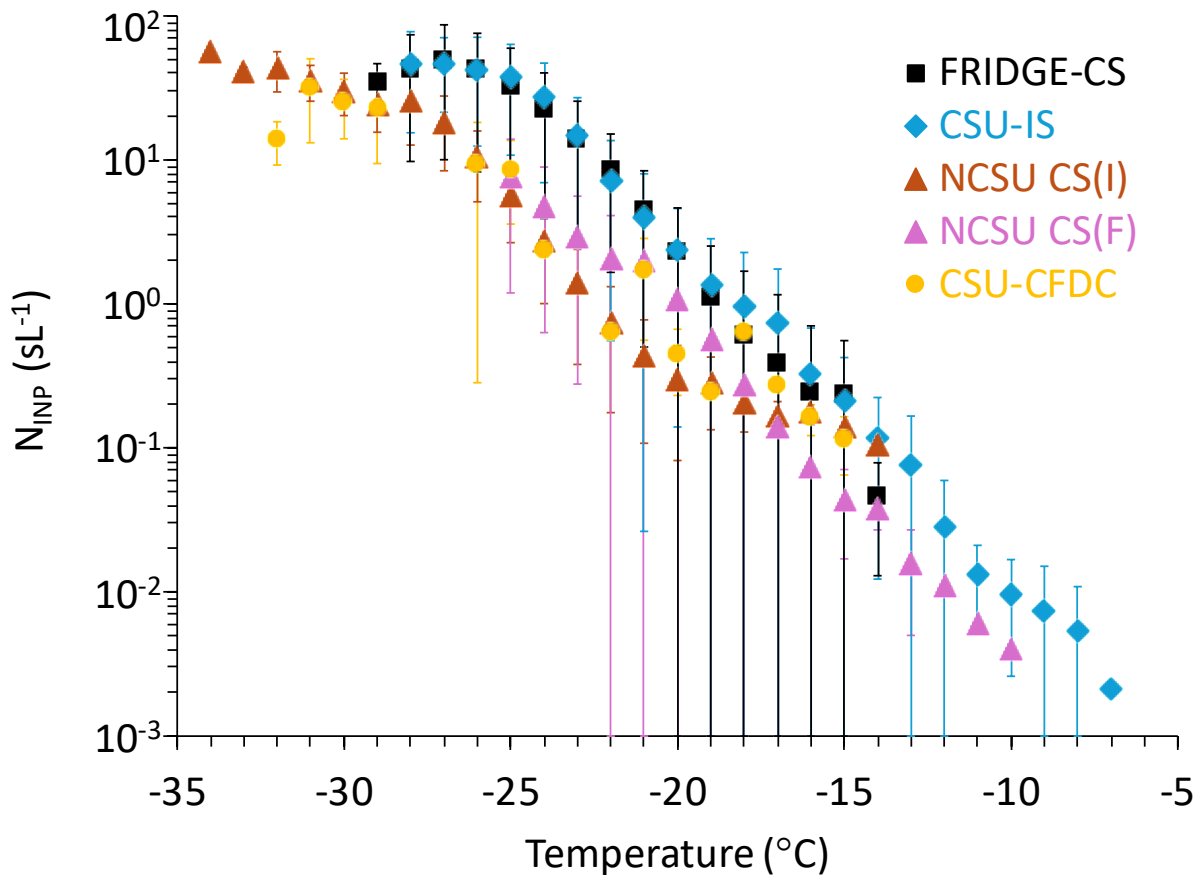
773 The daily average number concentration of fluorescing aerosol particles corresponding
774 with each of the seven WIBS-4A types with diameter > 0.5 μm is shown in Figure 3(c), and the
775 daily average number fraction of each WIBS-4A type is shown in Figure 3(d). The dominant types
776 of fluorescent aerosol particles throughout the FIN-03 field campaign were types B, AB, and A,
777 which on average accounted for $63.2\% \pm 8.7\%$, $16.0\% \pm 6.3\%$, and $12.5\% \pm 3.9\%$ of the particles
778 detected by the WIBS respectively.

779 In contrast with the daily average number fraction in each PALMS category, the relative
780 contributions of each of the seven WIBS-4A particle types did not vary much over the course of
781 the study when the WIBS-4A was operational, with perhaps the exception that Type AB decreased
782 in prevalence from September 18 (42.9%) to September 21 (10.1%). A modest trend occurred from
783 lower total fluorescing particle concentrations (0.02 to 0.04 cm^{-3} at STP) from September 17
784 through the 21st to higher concentrations (0.07 to 0.15 cm^{-3} at STP) from September 22 through
785 the 26th. WIBS-4A data was not collected on September 13-16, nor on September 27. The first
786 period was somewhat critical to evaluating INP relations to bioaerosols, so we note here in advance
787 this caveat. Time-resolved size distributions for each WIBS-4A channel, as well as the total
788 particle concentration measured across these seven channels, are shown in supplemental Figure
789 S2. FBAP assignments related to INP predictions will be discussed in Section 3.5.

790 3.3 Immersion freezing measurements

791 A summary of the number concentrations of immersion freezing INPs (N_{INP}) over the
792 course of the field campaign, for all measurements averaged at one degree temperature intervals
793 for each instrument, is shown in Figure 5. The concentration of INPs detected over this range
794 ranged over five orders of magnitude (0.01 to 160 L⁻¹). Only two sets of instruments were able to
795 explore the temperature regimes of -30 °C and colder due their design to permit operation there,
796 or warmer than -15 °C due to detection limits (controlled by sample volume and drop size used
797 for immersion freezing). At any one temperature, differences up to a little more than one order of
798 magnitude are apparent in comparing average data from individual methods, mirroring results
799 presented in previous laboratory and field studies (Hiranuma et al., 2015; DeMott et al., 2017,
800 2018; Knopf et al., 2021; Brasseur et al., 2022; Lacher et al., 2024).

801 As expected, a trend of increasing N_{INP} with decreasing temperature was observed for the
802 FRIDGE-CS, CSU-IS, NCSU-CS (I and F), and CSU-CFDC. Incremental changes in N_{INP} with
803 decreasing temperature was similar for all measurements that spanned a broad temperature range.
804 The dependence of N_{INP} on temperature is nearly log-linear from -10 to -27 °C, excepting perhaps
805 a steepening of slope from -20 to -25 °C and some lowering of slope below this temperature. This
806 comparability of dN_{INP}/dT contrasts with an apparent increasing high bias of drop suspension
807 freezing measurements versus CFDC measurements



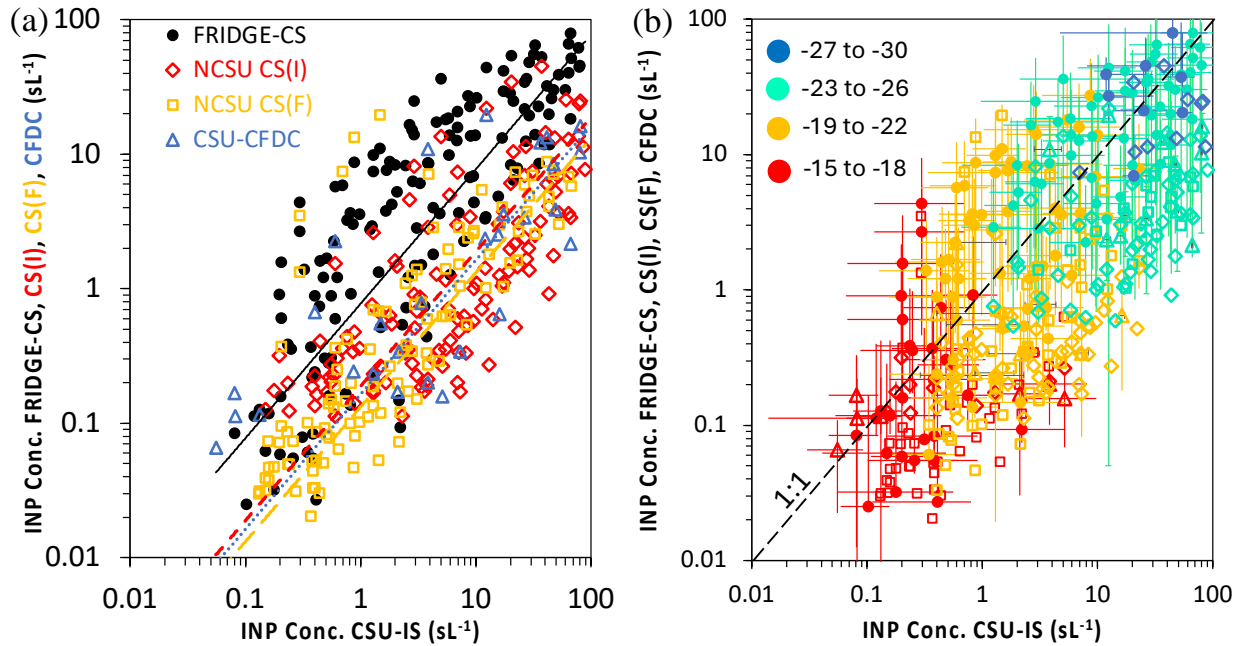
808
 809 **Figure 5.** Campaign average immersion freezing INP concentrations (sL^{-1}) in $1\text{ }^{\circ}\text{C}$ bins for instruments
 810 participating in intercomparison studies. Error bars represent one standard deviation in the measurement
 811 means collected at the specified temperature and not measurement uncertainties. The error bars strike the
 812 lower axis when the standard deviation exceeded the means. The times over which the INP concentration
 813 has been averaged for each instrument is explained in the text.

814
 815 during comparable sampling at various surface sites (non-mountaintop or free troposphere) found
 816 in DeMott et al. (2017) but agrees with FIN-02 laboratory studies (DeMott et al., 2018) and recent
 817 atmospheric studies at Puy de Dome (Lacher et al., 2024). INP concentration variability at single
 818 temperatures, reflected in Figure 5 as a standard deviation of bin means, is likely due to variations
 819 in aerosol properties affecting INPs in response to production and scavenging processes upstream

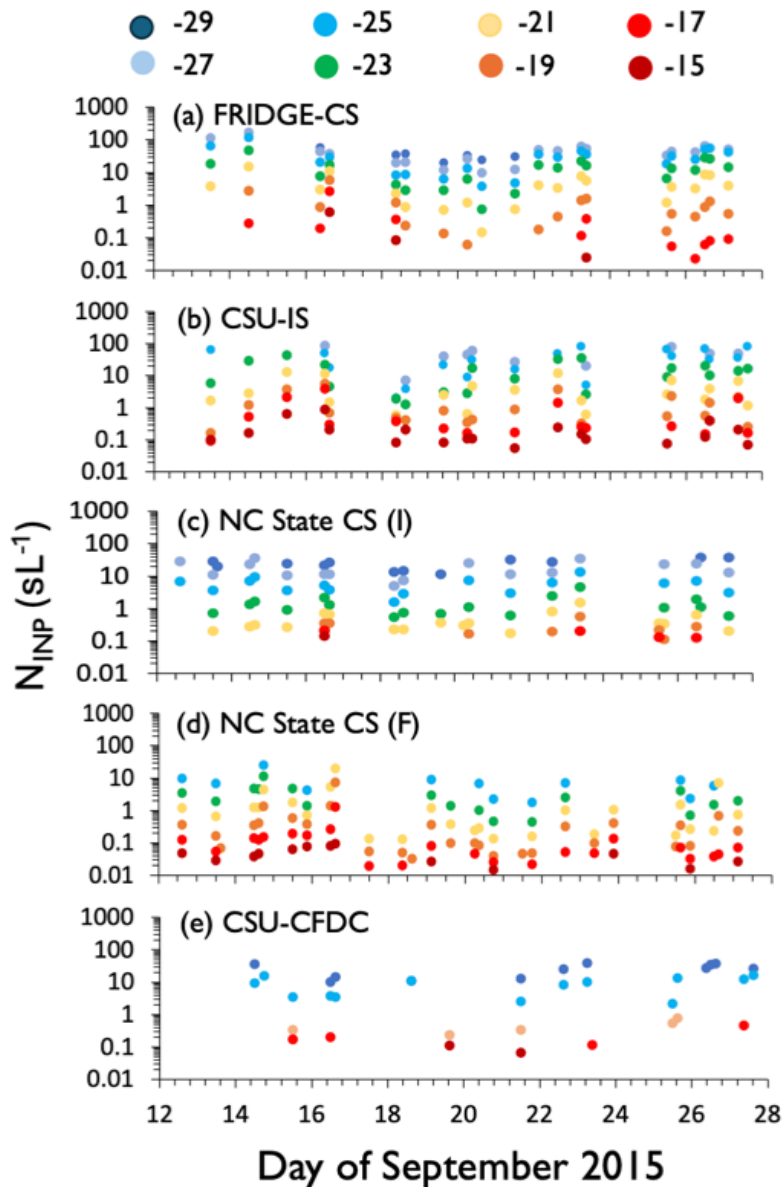
820 of the site. Nevertheless, generally higher N_{INP} measurements were obtained with the FRIDGE-
821 CS and the CSU-IS than the CSU-CFDC and NCSU-CS (F) and NCSU-CS (I) analyses. Such
822 biases in other studies have been attributed to different efficiencies in sampling of largest particles
823 (e.g., Lacher et al., 2024; Cornwell et al., 2023), but the collection methods for offline
824 measurements in this study were substantially similar, as discussed further below. Hence, we
825 cannot attribute measurement differences to a systematic source. Comparability of impinger versus
826 filter sampling methods for immersion freezing measurements via the NCSU-CS mirrors the
827 findings in DeMott et al. (2017), suggesting that particle removal from filters can be highly
828 effective for immersion freezing measurements of ambient particles.

829 To view the data in a more complete manner over the entire project, we explore direct
830 comparisons of different instrument as scatterplots and measurement ratios on temporal bases.
831 First, in Figure 6, we show a commonly used representation of large INP project data as INP
832 concentrations for four instruments versus one other and segregate the data into broad 4-degree
833 temperature ranges. The data used for normalization were from the CSU-IS, though we might have
834 used any other. Linear regressions were plotted in Figure 6 to show the overall average differences
835 between measurements that are already evident in Figure 5. Figure 6a thereby demonstrates the
836 generally good correspondence between the NCSU-CS data of both types and the CSU-CFDC data
837 that measure factors of 5 to 8 lower INP concentrations on average compared to the CSU-IS, as
838 well as the closer correspondence of the FRIDGE-CS (22% lower) and CSU-IS data. Greatest
839 variations in INP concentrations over the course of the project were focused in the -20 to -25 °C
840 temperature regime (Figure 6b), where variations reached nearly two orders of magnitude. This is
841 not an uncommon observation, also seen in Lacher et al. (2024). Surprising, but not easily

842 understood yet, is the fact that all measurement methods could at times measure equivalently to or
 843 more than the CSU-IS.



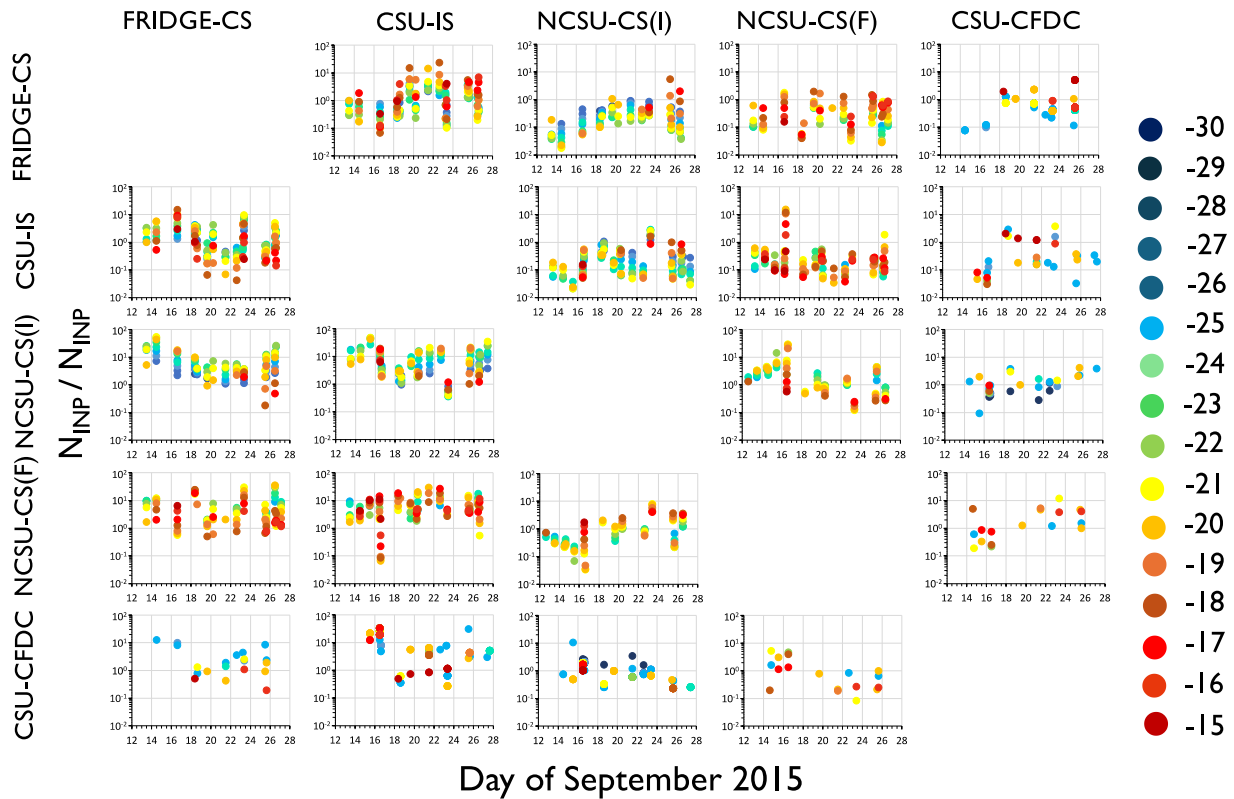
844
 845 **Figure 6.** (a) INP concentrations for all intercomparison measurement points of FIN-03 from the FRIDGE-
 846 CS, NCSU-CS (I), NCSU-CS (F) and CSU-CFDC compared to the INP concentrations from the CSU-IS
 847 measurements. Linear regressions with zero intercepts are color coded for each, having slopes of 0.78, 0.19,
 848 0.13 and 0.16 for the FRIDGE-CS, NCSU-CS (I) and CSU-CFDC, respectively. (b) The same data are
 849 color coded for different temperature ranges in $^{\circ}\text{C}$ and the 1:1 relation is shown. Errors are confidence
 850 intervals for FRIDGE-CS, CSU-CFDC, and CSU-IS data. These are not shown for the NCSU-CS data since
 851 these are given as temperature errors and would need interpolation to plot as N_{INP} errors.



852
 853 **Figure 7.** Time series of immersion-freezing mode INP concentrations (sL^{-1}) measured during
 854 intercomparison periods by (a) the FRIDGE-CS, (b) the CSU-IS, (c) the NC State CS (I), (d) the NC State
 855 CS (F), and (e) the CSU-CFDC. An additional data point from the MIT-SPIN is shown as a square data
 856 point in the CSU-CFDC panel. Note that data for the CFDC is plotted only for the most common
 857 temperatures of -30, -25, -20 and -15 °C. INP concentrations shown in this figure are those measured within
 858 three-hour blocks of time but may capture longer or shorter time periods depending on the specific
 859 instrument sampling time that overlapped these periods.

860 Temporal data provided further descriptions of instrument comparability. Immersion
861 freezing N_{INP} in 1 °C bins were compared for periods of the day broken into three-hour intervals
862 in the time series of Figure 7. While absolute INP concentration magnitudes differ, it is not difficult
863 to see comparability of general trends amongst the data sets, albeit with episodic discrepancies that
864 will be discussed further below. For example, all methods measure higher INP concentrations early
865 in the study, a low point around the 18th of September and a build up again toward the end of the
866 study. For example, INP concentrations at temperatures > -20 °C were at a maximum during the
867 precipitation period, as might be expected for rainfall production of biological INPs (Huffman et
868 al., 2013; Mignani et al., 2021; Testa et al., 2021; Cornwell et al., 2023), while the strongest
869 differences between the concentrations of INPs active at higher and lower temperatures occurred
870 for all instrumental measurements during the period of warming under high pressure later in the
871 study. The latter observation might be expected for a strong contribution of dust-like INPs, with a
872 steeper dN_{INP}/dT . These positive points suggesting that the instruments were measuring the same
873 INP cycles was also seen in the study of Lacher et al. (2024), c.f., their Figure 4.

874 Periods of agreement and discrepancy are clearer in examining the ratios of time-matched
875 and temperature-matched three-hour immersion N_{INP} values that were calculated for each pair of
876 instruments, as shown in Figure 8. Numbers of overlapping measurement periods, their geometric
877 means, standard deviations and normal 95% confidence intervals of all ratios (all times and
878 temperatures) plotted in each panel of Figure 8 are documented in Table 2. Reiterating what is
879 apparent from campaign-wide results in Figure 5 and 6, Figure 8 indicates the best agreement for
880 short-term periods throughout the study was observed between the FRIDGE-CS and the CSU-IS,
881 in which only 4 out of 146 3-hour, time- and temperature-matched N_{INP} (3%) did not agree within
882 an order of magnitude. Nevertheless, discrepancies of a few to several times did occur from



884

885 **Figure 8.** Ratios of the immersion freezing INP concentrations measured by each instrument, to the
 886 immersion INP concentrations measured by each other instrument (three-hour averages). Each instrument
 887 (FRIDGE, CSU-IS, NC State-CS (I), NC State-CS (F), and CSU-CFDC) is represented by one of the five
 888 columns as well as one of the five rows.

889

890 September 16th onward, focused most often at $>-22^{\circ}\text{C}$. These biases flipped in both directions,
 891 with the CSU-IS measuring higher from the 19th to the 22nd and the FRIDGE-CS higher at some
 892 other times, notably the 16th, 23rd and 26th of September. None of these periods were distinguished
 893 in any discernible manner by weather or aerosol properties. For example, LAS and PALMS
 894 concentrations were no more than 20% different from the FIN-03 campaign means during any of
 895 these periods. Aerosol surface areas were about a factor of two lower overall during the 19th to

896 22nd period than for the period after the 23rd (Figure 2), which does not imply a special sampling
897 bias for larger particles for the IS filter that was open to the air, a point we will discuss further
898 below.

899 Both the FRIDGE-CS and CSU-IS showed high bias from a few to more than 10 times
900 versus NCSU-CS(I) or CS(F), primarily at processing temperatures below $-20\text{ }^{\circ}\text{C}$, whereas ratios
901 closer to 1 indicated much better agreement at $>-20\text{ }^{\circ}\text{C}$ later in the study. The poorest agreement
902 overall was observed for the CSU-IS compared to the NCSU-CS(I), a combination for which 26
903 out of 128 (20%) immersion N_{INP} means did not agree within an order of magnitude. Agreement
904 between the FRIDGE-CS and the NCSU-CS(I) was only slightly better, as 15 out of 107 (14%)
905 time-matched N_{INP} means did not agree within an order of magnitude. Higher than order of
906 magnitude such discrepancies at lower temperatures were markedly present on September 13, 14,
907 23 and 26. Based on PALMS data, the 14th was richer in compounds from biomass burning, poorer
908 in sulfates, organics, and nitrates, and slightly poorer in mineral dust than average, as discussed in
909 Section 3.2. The concentration of $> 0.5\text{ }\mu\text{m}$ particles measured by the LAS during this time was
910 also relatively high (2.5 cm^{-3} compared to the campaign mean $0.45\pm 0.62\text{ cm}^{-3}$). However, the 14th
911 is not markedly distinguished overall in the timeline of all INP measurements in Figure 7, so
912 perturbations to composition and concentrations of all particle sizes due to the biomass burning
913 event did not appear to specially perturb the INP populations. We have already noted that the 23rd
914 and 26th of September had aerosol populations that were not much different than the project mean
915 on those days.

916

917

918 **Table 2.** Count number, geometric mean, standard deviation (St. dev.), and 95% normal confidence
 919 intervals (CI) for the N_{INP} ratio data of Figure 8 in the main manuscript, including all temperature points.
 920 As for that figure, numerator instrument is on the upper horizontal scale and denominator instrument is
 921 listed on the vertical scale.

		FRIDGE- CS	CSU- IS	NCSU- CS(I)	NCSU- CS(F)	CSU- CFDC
FRIDGE-CS	N Mean St. dev. CI		146 0.93 2.86 0.46	107 0.20 0.57 0.10	90 0.26 0.43 0.09	20 0.52 1.12 0.49
CSU-IS	N Mean St. dev. CI	146 1.07 2.41 0.39		128 0.19 0.52 0.09	112 0.21 2.39 0.44	29 0.26 0.92 0.34
NCSU-CS(I)	N Mean St. dev. CI	107 4.99 9.85 1.87	128 5.40 9.41 1.63		83 1.49 5.03 1.08	28 0.97 1.11 0.41
NCSU-CS(F)	N Mean St. dev. CI	94 3.81 7.78 1.60	112 4.80 5.47 1.01	83 0.66 1.51 0.32		18 1.37 2.88 1.33
CSU-CFDC	N Mean St. dev. CI	20 1.91 3.54 1.55	29 3.79 8.98 3.26	28 1.02 1.91 0.71	18 0.73 1.61 0.74	

922

923

924

925

926

927 **Table 3.** Percent agreement within one order of magnitude of N_{INP} for all times and temperatures

	N_{INP} (FRIDGE-CS)	N_{INP} (CSU-IS)	N_{INP} (NCSU CS(I))	N_{INP} (NCSU CS(F))	N_{INP} (CSU-CFDC)
N_{INP} (FRIDGE-CS)	100.0				
N_{INP} (CSU-IS)	97.3	100.0			
N_{INP} (NCSU CS(I))	85.9	68.6	100.0		
N_{INP} (NCSU CS(F))	75.0	59.2	96.2	100.0	
N_{INP} (CSU-CFDC)	100.0	87.5	100.0	84.6	100.0

928

929 The CSU-CFDC INP measurements generally agreed with the other measurements within

930 an order of magnitude for data collected on the same day and temperature, excepting a particularly

931 low bias versus the CSU-IS at higher temperatures on the 16th of September (rain and hail day)

932 and at lower temperatures on the 25th of the month. Nevertheless, its measurements of INP

933 concentration were in best agreement with all methods overall for temperatures > -20 °C, albeit

934 for the most limited number of matches (18 to 29). CSU-CFDC INP concentrations also tended to

935 be lower than those from the FRIDGE-CS and CSU-IS at temperatures below -20 °C. A similar

936 divergence in online versus offline N_{INP} measurements in this temperature range was reported by

937 DeMott et al (2017) for ground-based sampling, with online measurements tending to measure

938 progressively lower INPs than offline integrated filter or impinger collections at below -20 °C,

939 approaching one order of magnitude below -25 °C. At the Puy de Dome Mountain station (Lacher

940 et al. 2024), only modest and insignificant underestimates were made by the CSU-CFDC (also

941 using a 2.5 μm using impactor) versus offline INP concentrations when all were measured from a

942 PM10 inlet. CSU-CFDC INP measurements were comparable on average with measurements from

943 the NCSU-CS(I) and NCSU-CS(F), consistent with the mean results shown in Figure 5.

944 Comparing the timeline of ratios of NCSU-CS(I) to NCSU-CS(F), only 3 out of 83 (3.6%)
945 of the INP concentrations obtained through analysis by the identical off-line apparatus differed by
946 more than an order of magnitude.

947 Despite the discrepancies noted in the time- and temperature-matched data, a more positive
948 message from the intercomparison is that the mean N_{INP} reported by different instruments for all
949 temperature conditions taken together generally fell well within a span of one order of magnitude.
950 Figure S3 (values provided in Table 3) shows the percent of immersion INP measurements in
951 which all instrument pairs agreed within one order of magnitude. This is also consistent with the
952 representation shown in Figure 6 for which linear regressions imply that the CSU-IS measured
953 N_{INP} a factor of 1.4 to 8 times higher than other methods. Similarly, and importantly, the geometric
954 mean ratios for Figure 8 listed Table 2 were below a factor of about 5 in all cases. This level of
955 agreement compares well with the findings from FIN-02, for which the immersion N_{INP} measured
956 by several online and offline instruments agreed within an order of magnitude. This is encouraging
957 given that FIN-02 was a laboratory intercomparison on single composition aerosol samples
958 consisting of particles with diameter $< 2 \mu\text{m}$ whereas FIN-03 was a field campaign in which
959 temporal changes in the concentration, size distribution, and composition of INPs at Storm Peak
960 Laboratory were all potential factors. This level of correspondence shows that field data can be
961 collected with nearly the same level of accuracy as laboratory experiments. While also mimicking
962 the results of DeMott et al. (2017) for a smaller instrument comparison exercise, agreement was
963 quite similar to that found in another recent intercomparison where INP concentrations measured
964 by multiple systems were found to match within a factor of 5 (Lacher et al., 2024).

965 A possible explanation for N_{INP} measurement discrepancies that has been tendered in other
966 intercomparison campaigns sampling ambient air is that INPs are highly sensitive to the size range

967 of collected aerosol, and systematic size-dependent differences in collection efficiencies vary for
968 different collection types (DeMott et al., 2017; Knopf et al., 2021; Lacher et al., 2024). For
969 example, Lacher et al. (2024) found significant underestimates of INPs by both online and offline
970 methods measuring from the PM10 inlet versus offline measurements from filter collections made
971 on the laboratory rooftop. In this study, as we have noted above, a similarly consistent difference
972 between rooftop versus laboratory or between online and offline measurements is not found.
973 FRIDGE-CS INP concentration measurements from the turbulent-flow inlet and CSU-IS INP
974 concentration measurements from the rooftop filter agreed within an average of about 30% over
975 the course of the study. The CSU-CFDC INP measurements that were limited and thus biased by
976 its upstream total particle impactor (at 2.5 μm) agreed well on average with the NCSU (F) and (I)
977 measurements, although we may note that if the CSU-CFDC data had been corrected for
978 instrumental loss of particles “out-of-lamina” as found for measurements on mineral dust (DeMott
979 et al., 2015), INP concentration results would have been within a factor of two of the CSU-IS and
980 FRIDGE-CS data. Larger particles do tend to have higher likelihood of containing ice nucleation
981 sites, so biases in their collection can lead to sometimes large differences in assessed INP
982 concentrations (Mason et al., 2016). Disaggregation of the very largest collected particles when
983 placed in water suspensions has also been implicated for discrepancies between different substrate
984 collections (DeMott et al., 2017; Lacher et al., 2024). For example, if very large aggregates that
985 are preferentially collected by one substrate versus another, disaggregation in water could lead to
986 a high bias in ice nucleation sites effective at lower temperatures. There may have been additional
987 line losses for the online instruments sampling from an inlet and using tubing to transfer particles,
988 though these tend to be of minor influence at below the impactor size cut (Knopf et al., 2021). The
989 impinger is known to be less efficient for small (<200 nm) and large (>10 μm) particle capture,

990 but unless the relatively light to moderate wind conditions at the inlet during FIN-03 conferred
991 some special bias, Hader et al. (2014) predict a 50% capture efficiency at near 10 μm . The filter
992 samplers on the rooftop should have been equivalent, with the only difference being the orientation
993 of filters for the NCSU samples (mounted face-down). The size bias in this configuration is
994 unknown. The FRIDGE filter should have captured particles with the same efficiency as the
995 turbulent flow inlet, since only a very short line connected the filter to the interior inlet structure
996 in the laboratory. Only if very large INPs $> 13 \mu\text{m}$ were dominant by number amongst total INPs,
997 which is unexpected, would the FRIDGE filter collection have been expected to differ from the
998 rooftop CSU-IS filter collections.

999 Besides size-dependent sampling biases, the fact that measurements of immersion freezing
1000 INP concentrations from ambient air can be uncertain by up to one order of magnitude may result
1001 from unquantifiable random or non-random factors, or more likely from quantifiable factors that
1002 were not fully controlled in this field study nor easily controlled across investigating teams in
1003 general. Examples of known issues that were only documented after FIN-03 relate to inconsistency
1004 in sample materials or sample handling and storage (e.g., Barry et al., 2021b; Beall et al., 2021).

1005 **3.4 Relation of immersion freezing INPs to aerosol properties**

1006 While establishing correlations between INPs and aerosol properties were not a focus of
1007 the intercomparison, the ancillary aerosol data did allow for inspecting some simple linear
1008 correlation analysis. This provides insight into the size range of greatest relevance for the INP
1009 intercomparison period. Throughout the campaign, a positive and significant trend between total
1010 LAS particle concentration (i.e., $> 0.1 \mu\text{m}$) and N_{INP} was observed for FRIDGE-CS ($R = 0.55\text{-}0.74$
1011 and $p < 0.05$ for measurements at $-28 \text{ }^\circ\text{C} < T < -15 \text{ }^\circ\text{C}$), but no clear statistically significant trend
1012 was observed between total LAS particle concentration and N_{INP} for the other four instruments

1013 (Figure S4a). A greater number of significant positive trends were found between the concentration
1014 of particles with diameter $> 0.5 \mu\text{m}$ and N_{INP} . This was the case for the FRIDGE-CS ($R = 0.54-$
1015 0.94 and $p < 0.05$ for measurements at $-28 \text{ }^\circ\text{C} < T < -19 \text{ }^\circ\text{C}$), CSU IS ($R = 0.46-0.72$ and $p < 0.05$
1016 for measurements at -21 to $-25 \text{ }^\circ\text{C}$), NCSU CS(I) ($R = 0.46-0.61$ and $p < 0.05$ for measurements
1017 at $-29^\circ\text{C} < T < -24 \text{ }^\circ\text{C}$), and the NCSU CS(F) ($R = 0.51-0.64$ and $p < 0.05$ for measurements at $-$
1018 $26 \text{ }^\circ\text{C} < T < -22 \text{ }^\circ\text{C}$).

1019 No consistent, significant ($p < 0.05$) correlation was found between changes in composition
1020 (from the PALMS categories and WIBS-4A types) and immersion freezing N_{INP} across the range
1021 of setpoint temperatures employed during FIN-03 (Figure S4b).

1022 **3.5 Inferences to INP compositions during FIN-03**

1023 To provide context for the discussed intercomparisons and because this study provides data
1024 needed for testing the relevance of existing parameterizations of ice nucleation in regional and
1025 global climate models (Andreae & Rosenfeld, 2008; Morris et al., 2011; Seifert et al., 2011), we
1026 utilize some previously-developed ice nucleation parameterizations for specific compositions to
1027 diagnose consistency or not with INP compositions in the high altitude environment of FIN-03.
1028 We examine parameterizations for mineral dust INPs that have different links to larger size particle
1029 concentrations (DeMott et al., 2015) versus mineral dust surface area (Niemand et al., 2012), and
1030 biological INPs as linked to fluorescent particle concentrations (Tobo et al., 2013; Twohy et al.,
1031 2016). Hereafter we will refer to these parameterizations as DeMott 2015, Niemand 2012, and
1032 Tobo 2013. We also utilize a more direct method of probing INP compositions using the CSU-IS
1033 sample treatments discussed in Section 2.2.2 and the CSU-CFDC heat treatments of single
1034 particles discussed in Section 2.2.1. In relation to these latter investigations, we also introduce
1035 diagnostic tests of the arable soil dust INP parameterizations of Tobo et al. (2014).

1036 Each of the above-noted deterministic parameterizations was used to predict N_{INP} at -30
1037 $^{\circ}\text{C}$, -25 $^{\circ}\text{C}$, -20 $^{\circ}\text{C}$, and -15 $^{\circ}\text{C}$ using the equations and inputs described in Table 4 and
1038 summarized below. We do not attempt an analysis using stochastic parameterizations.

1039 1) DeMott 2015 is based on CSU-CFDC laboratory measurements of ice nucleation on
1040 mineral dust soil samples as well as field data from situations dominated by mineral dusts
1041 (i.e., dust plumes from major deserts), collected for CFDC operational conditions
1042 essentially the same as for this study (i.e., simulated immersion freezing conditions at
1043 105% RH) (DeMott et al., 2015). For FIN-03, aerosol concentrations measured by the LAS
1044 (> 0.5 μm dry diameter) and converted to STP concentrations were used as the input for
1045 this parameterization for comparison to INP data that is also reported at STP
1046 concentrations. Predictions also depend on temperature (Table 4). Since PALMS data
1047 indicates that dust particles dominated the coarse mode only at sizes above 1 μm in
1048 diameter (Figure 4), we first adjust LAS data accordingly for the percentage of dust
1049 particles with diameters > 0.5 μm as input to this parameterization, which we have already
1050 stated is 23%. A correction factor (CF) of 3 was also applied (as indicated in Table 4)
1051 according to the results in DeMott et al. (2015) which showed that when applying the
1052 parameterization to represent immersion freezing dust INP concentrations in a model or in
1053 comparison to other immersion freezing methods, this CF is needed to account for CFDC
1054 underestimates of immersion freezing INPs (see Methods). The CF is applied in this case
1055 because calculations will be compared to the average N_{INP} from all measurements.

1056 2) The Niemand 2012 parameterization (Table 4) for mineral dust INPs is based entirely from
1057 laboratory measurements and incorporates measurements of temperature and particle
1058 surface area as the basis for prediction of INPs. It is especially important to limit the size

1059 range of aerosols for which this parameterization is applied, because total surface area was
 1060 dominated by small particles in FIN-03. Therefore, with reference to Figure 4, we will
 1061 assume that all dust surface area occurs at sizes larger than 0.5 μm and represents 50% of
 1062 that surface area.

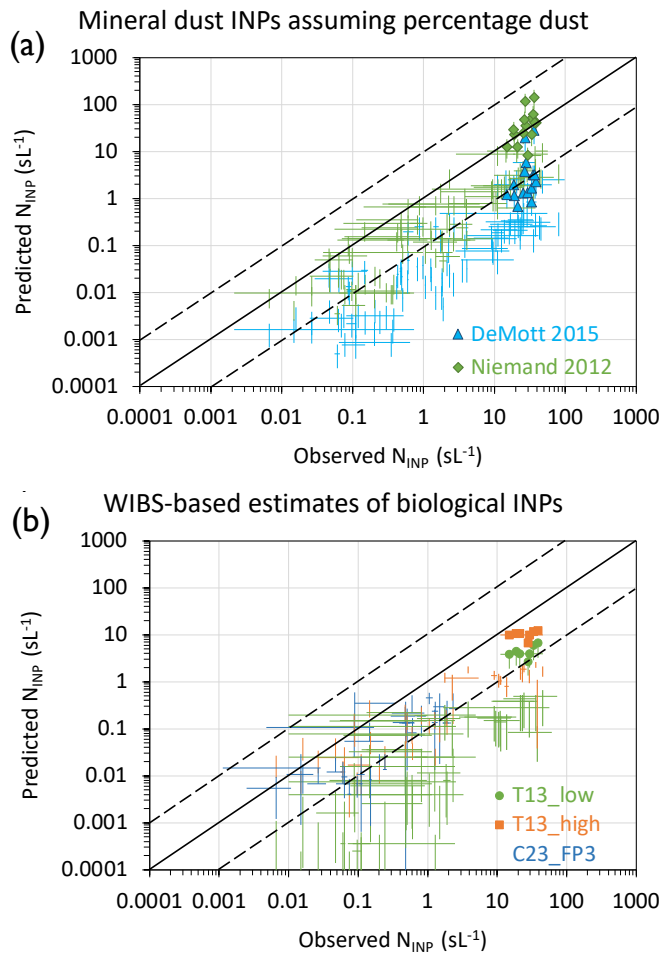
1063 **Table 4.** Summary of INP parameterizations.

Param.	Equation	Constants
Mineral dust INPs: Niemand et al. (2012)	$N_{INP}(T_C) \approx n_s(T_C)S_{tot} = (a \exp(b(T_C) + c))(S_{tot})$ $N_{INP}(T_C) = \text{INP concentration (sL}^{-1}\text{) at T (Celcius)}$ $S_{tot} \text{ in units } \mu\text{m}^2\text{cm}^{-3} \text{ and } n_s \text{ in units } \text{m}^{-2}$	$a = 1 \times 10^{-9}$ $b = -0.517$ $c = 8.934$
Mineral dust: DeMott et al. (2015)	$N_{INP}(T_K) = (cf)(n_{a>0.5\mu\text{m}})^{(\alpha(273.16-T_K)+\beta)}$ $\exp(\gamma(273.16 - T_K) + \delta)$ $N_{INP}(T_K) = \text{INP concentration (sL}^{-1}\text{) at T (Kelvin)}$ $n_{a>0.5\mu\text{m}} = \text{mineral particle number concentration } > 0.5 \mu\text{m (scm}^{-3}\text{)}$ $cf = 1 \text{ (CFDC data comparison) or } 3 \text{ (other immersion freezing)}$	$\alpha = -0.074$ $\beta = 3.8$ $\gamma = 0.414$ $\delta = -9.671$
Fluorescing biological aerosol particle INPs: Tobo et al. (2013)	$N_{INP}(T_k) = (N_{FBAP>0.5\mu\text{m}})^{(\alpha'(273.16-T_k)+\beta')}$ $\exp(\gamma'(273.16 - T_k) + \delta')$ $N_{INP} = \text{INP concentration (sL}^{-1}\text{)}$ $N_{FBAP} = \text{FBAP concentration (scm}^{-3}\text{)}$	$\alpha' = -0.108$ $\beta' = 3.8$ $\gamma' = 0$ $\delta' = 4.605$
Fluorescing biological aerosol particle INPs: Cornwell et al. (2023)	$N_{INP}(T_C) = f(T_C)1000N_{FBAP>0.5\mu\text{m}}$ $f(T_C = -20 \text{ }^\circ\text{C}) = 0.318$ $f(T_C = -15 \text{ }^\circ\text{C}) = 0.016$	N/A
Arable soil dust INPs: Tobo et al. (2014)	$N_{INP}(T_C) \approx n_s(T_C)S_{tot} = (a \exp(b(T_C) + c))(S_{tot})$ $N_{INP}(T_C) = \text{INP concentration (sL}^{-1}\text{) at T (Celcius)}$ $S_{tot} \text{ in units } \mu\text{m}^2\text{cm}^{-3} \text{ and } n_s \text{ in units } \text{cm}^{-2}$	Total soil: $a = 1 \times 10^{-5}$ $b = -0.4736$ $c = 0.3644$ Inorganics: $a = 1 \times 10^{-5}$ $b = -0.6773$ $c = 7.8436$

1064
 1065 3) As discussed earlier, we use two definitions of FBAP at sizes larger than 0.5 μm to and
 1066 temperature to predict biological INP concentrations based on Tobo 2013 as defined in

1067 Section 2.1, presuming to bracket low and high estimates of their links to INPs. We also
1068 explore links of higher temperature freezing data (> -20 °C) to FP3 particles, using the
1069 same scalings of the relation between FP3 concentrations and INP concentrations as a
1070 function of temperature that were established by Cornwell et al. (2023) for a coastal
1071 California environment. While we have no reason to expect that these scaling factors
1072 listed in Table 4 are valid for the high altitude, continental environment of FIN-03, they
1073 are starting points to explore this additional link of certain FBAP particles to INPs.

1074 To compare these parameterized values with observations, an overall mean observed
1075 immersion freezing N_{INP} was calculated for each three-hour period based on all the available data
1076 from all the instruments. This was considered as a reasonable approach since it factors in the
1077 inherent variability found between methods. Immersion freezing N_{INP} was predicted for each
1078 parameterization using mean WIBS-4A, and LAS data, both at STP concentrations, collected in
1079 the coincident 3-hour periods of time as the INP data. The observed and predicted immersion
1080 freezing N_{INP} are plotted against each other in Figure 9. Four temperatures of comparison (-15 , $-$
1081 20 , -25 and -30 °C) are presented in Figure 9 for DeMott 2015, Niemand 2012, and Tobo 2013,
1082 while two temperatures of comparison (-15 , -20 °C) are used for links to FP3-based prediction of
1083 biological INPs. Temperatures are indicated via levels of shading of the data points.

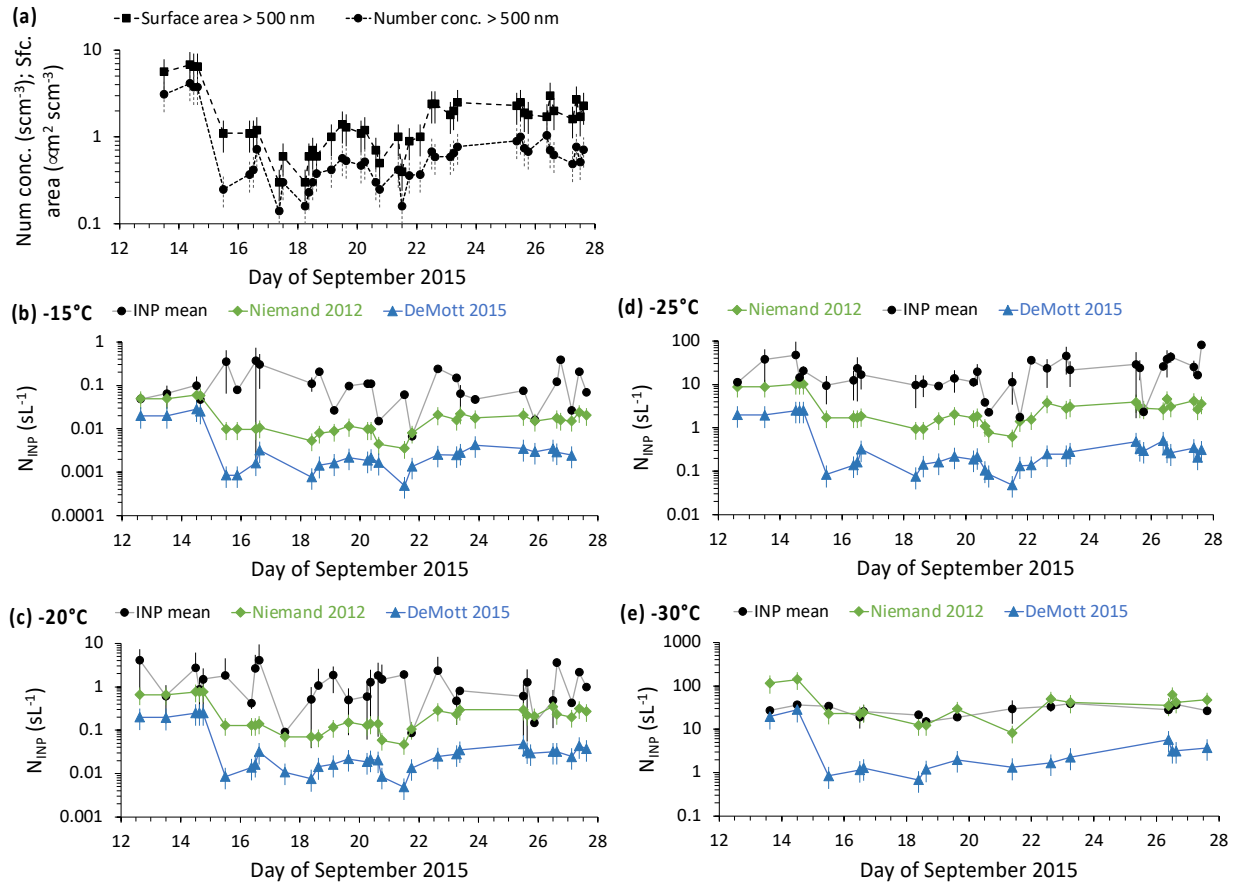


1084

1085 **Figure 9.** a) Comparison of mean observed N_{INP} (all instrument average) and predicted N_{INP} calculated
 1086 from DeMott et al. (2015) (DeMott 2015) and Niemand et al. (2012) (Niemand 2012) mineral dust INP
 1087 parameterizations at temperatures -30 °C, -25 °C, -20 °C, and -15 °C (gradations in shading from dark to
 1088 light) for the PALMS estimated percentages of dust particle number and surface area at sizes above 0.5
 1089 μm . Mean N_{INP} are averaged over three-hour periods and plotted uncertainties are standard deviations.

1090 Predicted N_{INP} uncertainties are propagated based on 25 % uncertainty in aerosol number and surface area
 1091 concentrations. b) Comparison of mean observed N_{INP} and predicted N_{INP} calculated from
 1092 parameterizations linking to FBAP concentrations from *Tobo et al.* (2013) (T13_low and T13_high; see
 1093 text for description) and from *Cornwell et al.* (2023) (C23_FP3) following the FP3 particle definition of
 1094 *Wright et al.* (2014). Only -15 and -20 °C comparisons are shown for the FP3 prediction. The solid line in
 1095 each plot is the 1:1 line and the dashed lines represent an order of magnitude in both directions.

1096 Using the constraint on mineral particles from the combination of PALMS and LAS data
1097 for the campaign average, predictions underestimate the mean N_{INP} at all temperatures (Figure 9a).
1098 The Niemand 2012 surface-area-based INP estimates come modestly closer to observations,
1099 averaging 25% of the total INP concentrations for all times and all temperatures, while the DeMott
1100 2015 predictions average 4% of INP concentrations, with large variability apparent. These results
1101 can be expected to be highly sensitive to the assessed average mineral particle fraction at sizes
1102 above 0.5 μm (varied over the study) and on whether particles that have a source from regional
1103 soils will be represented only by those with mineral content. Therefore, for comparison,
1104 parameterization results in Figure S5 use the assumption that all particles at diameters exceeding
1105 0.5 μm were dust particles. In this case, a somewhat unrealistic maximum assumption on soil dust
1106 numbers and surface area that considers all particles and compositions in this size range as
1107 emanating from dust, Niemand 2012 estimates a dust source for 50% and DeMott 2015 estimates
1108 25% of observed INPs on average. Thus, the predictions of the two parameterizations become
1109 more closely aligned for assumption of more overall mineral dust particles in the size range larger
1110 than 0.5 μm . Discrepancy has been noted previously in applying these parameterizations to link to
1111 the aerosol model in an Earth System model for the Southern Ocean region (McCluskey et al.,
1112 2023). In that case, calculations were based on aerosol model derived dust distributions and
1113 occurred under very low dust loading scenarios where neither parameterization has been firmly
1114 tested in the laboratory or field. Under both assumptions on mineral particle number, since DeMott
1115 2015 was developed based on CFDC measurements for particles $< 2.5 \mu\text{m}$ in the field and
1116 laboratory, a low bias compared to Niemand 2012 might be expected in comparison to average
1117 immersion freezing data that includes larger particles.
1118



1119

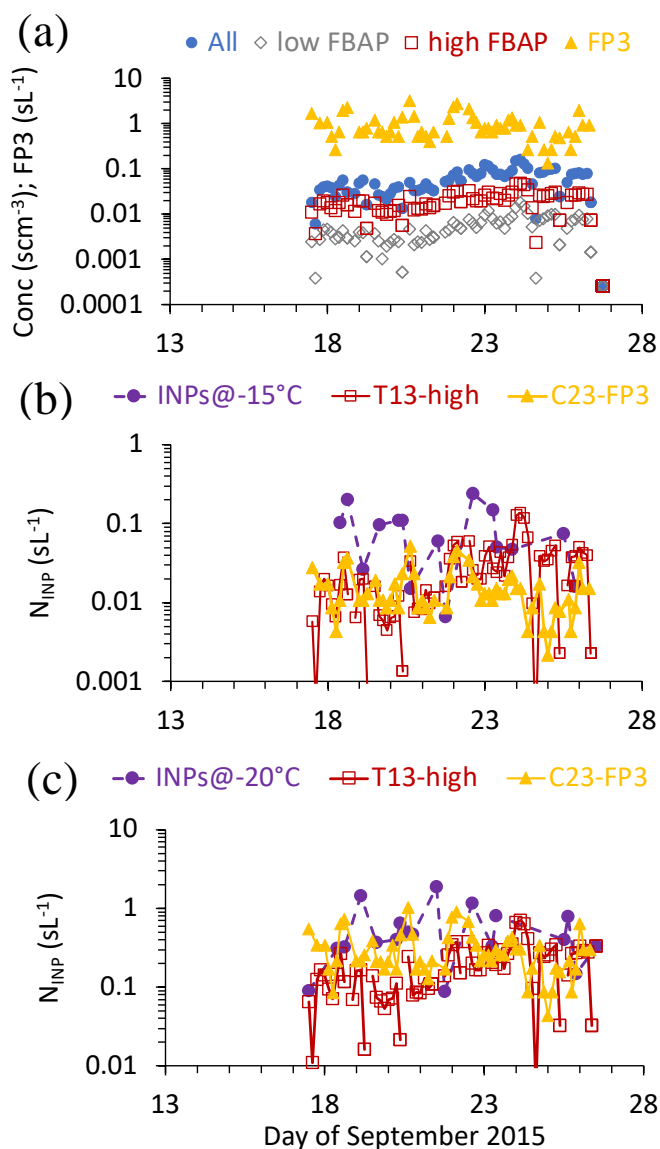
1120 **Figure 10.** Time series of aerosol number concentration and surface area (3-h averages at STP) in a), and
 1121 observed mean measured immersion freezing N_{INP} (INP mean) plotted with predicted N_{INP} from the mineral
 1122 dust parameterizations of Niemand 2012 and DeMott 2015 as described in the main text (all three-hour
 1123 averages at STP) at temperatures of -15, -20, -25, and -30 °C in b) to e), respectively. Lines are intended
 1124 only to connect data points and do not imply knowledge of intermediate values. Uncertainties mark one
 1125 standard deviation above and below the mean values of all parameters.

1126

1127 The timeline of predicted N_{INP} for the two dust parameterizations in comparison to mean
 1128 observed N_{INP} is shown in Figure 10 for the same temperatures used in Figure 9. These analyses
 1129 emphasize that 1) INP observations do not show a special enhancement during the biomass burning
 1130 event at the start of FIN-03, and hence closer agreement of the dust parameterizations with

1131 observations at that time is likely an artifact of attributing dust-like INP activation properties to
1132 the dominant biomass burning compositions at that time; 2) the structure of the timeline of
1133 predicted N_{INP} resembles that of the observed N_{INP} only below $-20\text{ }^{\circ}\text{C}$, as expected for a dominance
1134 of dust-like INPs; and 3) the predictions fare less well in describing the observed INP populations
1135 at $> -20\text{ }^{\circ}\text{C}$ where biological INPs may be expected to have greater influence. Thus, these analyses
1136 overall suggest the presence of a dust-like immersion freezing INP type active at lower
1137 temperatures during FIN-03, but that the typical INP efficiency (INP as a function of dust
1138 concentration and temperature) attributed to mineral dust underestimates the freezing behavior of
1139 INPs overall during the period of study.

1140 For FIN-03, the Tobo 2013 parameterization of biological INPs consistently
1141 underpredicted N_{INP} , independent of the WIBS FBAP definition used, denoted as T13_low and
1142 T13_high in the scatterplot comparison of measured versus predicted values (at all times and
1143 temperatures) in Figure 9b and the timeline comparisons at -15 and $-20\text{ }^{\circ}\text{C}$ shown in Figure 11.
1144 Figure 11 also shows the timeline of WIBS total fluorescent particle concentrations, the high and
1145 low FBAP concentrations, and FP3 concentrations. The higher FBAP prediction of INPs falls
1146 much closer to the observations than the low FBAP prediction in Figure 9b and shares some
1147 proximal equivalence to observations at -15 to $-20\text{ }^{\circ}\text{C}$ at times. This result is like that found by
1148 Twohy et al. (2016) for air over the site where Tobo et al. (2013) collected their data, with the
1149 higher FBAP estimate bounding the upper end of measured immersion freezing INP
1150 concentrations at temperatures $> -20\text{ }^{\circ}\text{C}$. Also notable in Figure 9b and Figure 11 is that the C13-
1151 FP3 INP concentration predictions filled a similar space as the T13_high estimates, coming closest
1152 together at $-20\text{ }^{\circ}\text{C}$. While these results suggest that biological INP parameterizations can explain
1153 the higher temperature INP concentrations observed during FIN-03, with caveats on the large and



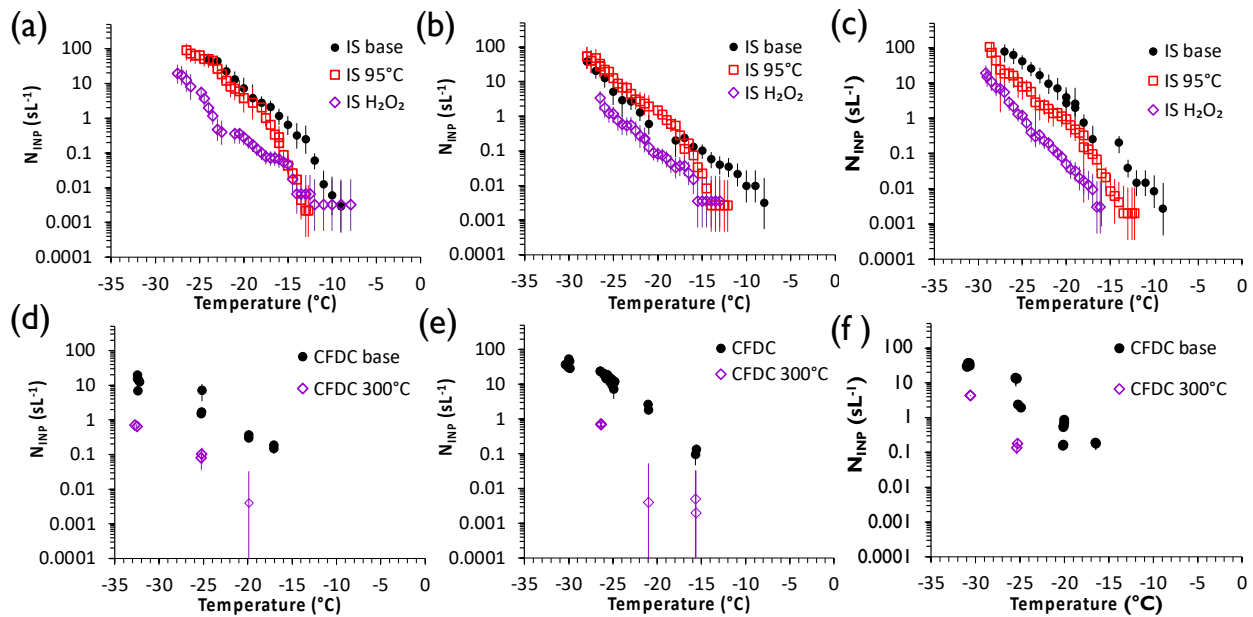
1154

1155 **Figure 11.** a) Timelines of WIBS-based fluorescent particles assignments (all fluorescing in any channel,
 1156 low and high FBAP, and FP3 particles), as defined in the text, during FIN-03. b) INP observed mean
 1157 concentrations, and biological INP parameterization predictions linked to high FBAP following Tobo et al.
 1158 (2013) (T13-high) and FP3 particles following Cornwell et al. (2023) at -15 °C in b) and -20 °C in c).

1159

1160 likely not fully quantifiable uncertainty in such predictions, the temporal analysis indicates that
 1161 there is no consistent temporal agreement between predicted and measured INPs, even if different

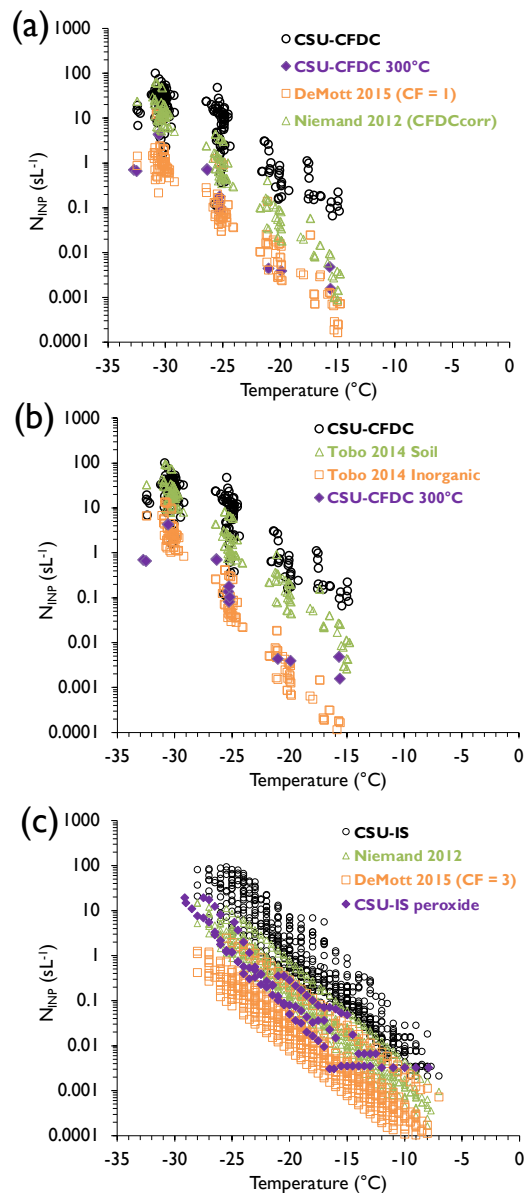
1162 scaling factors were applied to the predictions. Predictions at $-20\text{ }^{\circ}\text{C}$ show better overall
 1163 agreement, while those at $-15\text{ }^{\circ}\text{C}$ suggest that the Cornwell et al. (2023) scaling factor should be
 1164 higher for the SPL site at the time of FIN-03 to better describe mean values of biological INP
 1165 concentrations using the FP3 particle signal.
 1166



1167
 1168 **Figure 12.** Summary of treated IS filter suspensions using heat and peroxide (a, b, c) and dry heat-treated
 1169 CSU CFDC single particle data (d, e, f), for September 15, 23 and 25 (a-c, d-f, respectively). Error bars
 1170 represent 95% confidence intervals for individual experimental spectra for the CSU-IS and for individual
 1171 CSU CFDC measurements.

1172 The results of CSU-IS and CSU-CFDC treatments on INP concentrations measured for
 1173 three (of 21 overall) intercomparison time periods are shown in Figure 12, for examination of
 1174 consistency with the results of the diagnostic parameterization analysis just discussed. In Figure
 1175 12a-c, it is seen that thermal treatments indicated the strong contribution of inferred biological
 1176 INPs primarily at temperatures higher than about $-20\text{ }^{\circ}\text{C}$, but that peroxide digestion of organic

1177 compounds lowered INP activity at all tested temperatures by an order of magnitude on average.
1178 Similar reductions of INPs measured for single particles by the CSU-CFDC following dry heating
1179 (Figure 12d-e) demonstrate strong consistency with the IS results for bulk immersion freezing on
1180 the dominance of organic INP compositions, even though CSU-CFDC measured unamended INP
1181 concentrations were always lower. The CSU-IS heat treatment results (Figure 12a-c) suggest that
1182 biological INPs may have been ubiquitous during FIN-03 at temperatures above $-20\text{ }^{\circ}\text{C}$, and
1183 extended to lower temperatures at times, as indicated by the results from September 25. This is
1184 broadly consistent with the parameterization results based on FBAP measurements, although the
1185 Tobo 2013 and FP3 parameterizations did not capture all the influence of apparent biological INPs
1186 during the study. Whether for size-limited ($< 2.5\text{ }\mu\text{m}$) as in CSU-CFDC measurements, or bulk
1187 aerosol collected for CSU-IS immersion freezing measurements, the inferred INP compositions
1188 that were typically dominated by organics at temperatures $< -20\text{ }^{\circ}\text{C}$ could reflect origins from
1189 arable soil dusts (Testa et al., 2021) that surround the region of study. Biomass burning aerosols
1190 also have influence as organic INPs (Schill et al, 2020; Barry et al., 2021a). However, while
1191 biomass burning type particles were noted as a prevalent composition in FIN-03, these types of
1192 potential INPs likely cannot explain INP concentrations in FIN-03 because Barry et al. (2021a)
1193 showed that Western U.S. biomass burning INPs have active site densities about 3 orders of
1194 magnitude lower than those attributed to dust particles that also were ubiquitous at modest number
1195 concentrations during FIN-03. Furthermore, the strong biomass burning event noted on September
1196 14 had only modest, if any, apparent impacts on INP concentrations despite greatly elevated
1197 aerosol concentrations and surface areas, as already mentioned above (Figure 10).



1198

1199 **Figure 13.** a) Comparison of all untreated CSU CFDC data (black circles), cases after passing through the
 1200 upstream 300 °C tube heater (purple diamonds), and calculations from the DeMott 2015 dust
 1201 parameterization in (orange squares) and with CF = 1 as appropriate for a direct comparison to CSU CFDC
 1202 data (see text). b) The same exercise as in a) but using predictions of total soil organic INP concentrations
 1203 and inorganic INP concentrations within soil INPs, both from Tobo et al. (2014). c) The same exercise but
 1204 for all CSU-IS data and the cases with peroxide digestion. In this case, CF = 3 must be used in DeMott
 1205 2015 and the mineral dust INP prediction of Niemand 2012 is also shown.

1206 Finally, in Figure 13 we address whether the treatment results support the conclusion of
1207 the diagnostic parameterization analysis suggesting that inorganic INPs (mineral particles in
1208 particular) were of minor influence during FIN-03. For this purpose, we introduce results for the
1209 parameterization of Tobo et al. (2014) (hereafter, Tobo 2014) for arable soil dust INPs listed in
1210 Table 4. Tobo et al. (2014) parameterized the ice nucleation behavior of soil dusts from Wyoming,
1211 regionally proximal to the FIN-03 site at SPL, specifically using the and the CSU-CFDC dry heat
1212 method at 300 °C to indicate organic versus inorganic INP contributions from such soil particles.
1213 A caveat is that their results were for dusts generated in the laboratory and size-selected at 600 nm.
1214 This parameterization, like Niemand 2012, is based on the surface area of dust particles and so we
1215 apply the same assumptions as before to restrict to the proportion of dust larger than 0.5 μm . Since
1216 the CSU-CFDC is also restricted to measuring INPs at diameters below 2.5 μm , we apply a
1217 correction factor to the surface area to account for the fact that the surface area at below this size
1218 was 90% of the project average total surface area. No significant impact of the treatments is
1219 assumed on aerosol concentrations or surface area at sizes above 0.5 μm in Figure 13.

1220 Figures 13a and 13b focus on specific comparisons to CSU-CFDC data. In Figure 13a, it
1221 is seen that INP concentrations predicted by the DeMott 2015 parameterization for sampling
1222 periods during the entire campaign show remarkable agreement with the 300 °C CSU-CFDC data
1223 on selected days when applying $\text{CF} = 1$ in the parameterization, as is appropriate for a direct
1224 comparison to CSU-CFDC instrument data that is uncorrected for the underestimates that led to
1225 selecting $\text{CF} = 3$ for atmospheric modeling studies. In Figure 13b, it is shown that the Tobo 2014
1226 parameterizations for untreated total soil dust and its inorganic remnants also give very good
1227 agreement with CFDC untreated and treated N_{INP} data, supporting the likely important influence
1228 of such arable soil dusts during FIN-03. Predictions for untreated soils do not quite reach the level

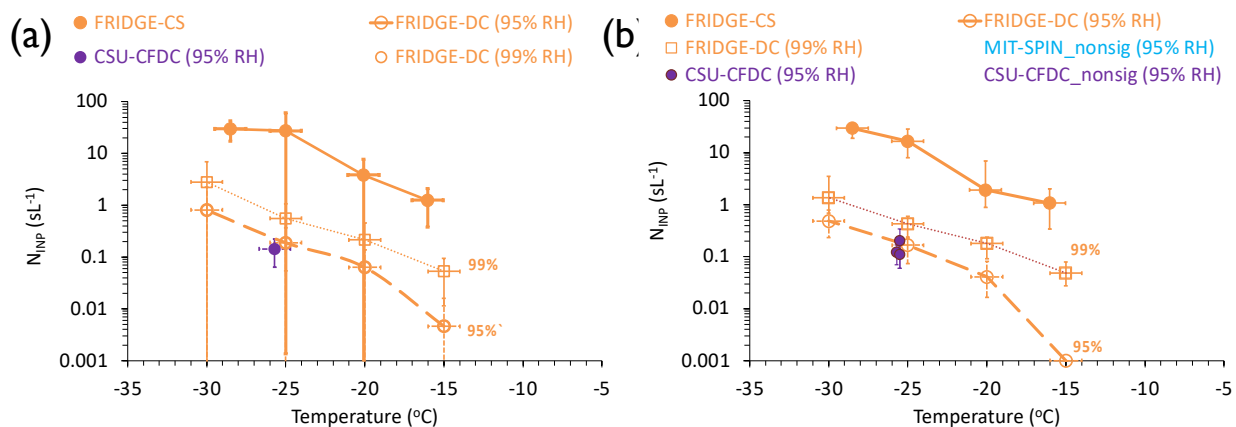
1229 of the observed INPs, but this could be explained by the additional contribution of biological INPs
1230 that has already been discussed.

1231 In Figure 13c, direct comparisons of the Niemand 2012 and DeMott 2015 predictions for
1232 mineral dust INPs for the entire project are shown in comparison to the CSU-IS untreated and
1233 H₂O₂ treated data on selected days. The DeMott 2015 prediction of INP concentrations uses CF =
1234 3 in this case, as appropriate. The same discrepancy between the DeMott 2015 and Niemand 2012
1235 predictions as discussed already regarding Figure 9a appears in this comparison. Nevertheless, it
1236 is seen that both parameterizations grossly underestimate untreated CSU-IS INP concentrations
1237 and the treated CSU-IS results fall between the predicted values, agreeing better with the Niemand
1238 2012 parameterization. While one might wish to allude to the fact that the IS filters sample particle
1239 sizes, to 10 μm and possible larger that may have higher ice nucleation efficiencies, while the
1240 CSU-CFDC was restricted to sampling particles <2.5 μm as a source for the lower DeMott 2015
1241 estimate in comparison to CSU-IS data, we have already addressed that there was no general
1242 consistency in INP concentrations for methods that sampled similar size particles overall. The best
1243 that can be stated is that the parameterization exercises and treatment data strongly support that
1244 inorganic INPs were of weak influence during FIN-03 and that arable soil dusts and biological
1245 INPs accounted for the strongest influences during sampling, akin to the findings of Testa et al.
1246 (2021).

1247 **3.6 Observations of INPs in the deposition nucleation regime**

1248 Measurements of deposition nucleation N_{INP} are summarized in Figures 14 and 15.
1249 FRIDGE-DC nucleation substrates were collected for 1 to 5 periods on many days during FIN-03
1250 and processed at 5-degree interval temperatures from -15 to -30 °C, and for setpoint humidity of
1251 95% and 99% RH (uncertainties to 2%). Data collected at 102% via the standard FRIDGE methods

1252 are not included herein. CSU-CFDC and MIT-SPIN deposition data were collected nominally at
 1253 95% RH with an uncertainty of about 2.5% RH, and at a range of temperatures on different days.
 1254 Mean values and standard deviation error bars of the FRIDGE-DC data are shown in Figure 14a
 1255 and median values of FRIDGE-DC N_{INP} (with interquartile values as error bars) are shown in
 1256 Figure 14b. Standard deviations were large over the course of the study for comprehensive
 1257 FRIDGE-DC data when binned at 5-degree interval temperatures. Nevertheless, average
 1258 concentrations of deposition INPs measured by the FRIDGE-DC indicated a consistent 3-5 factor

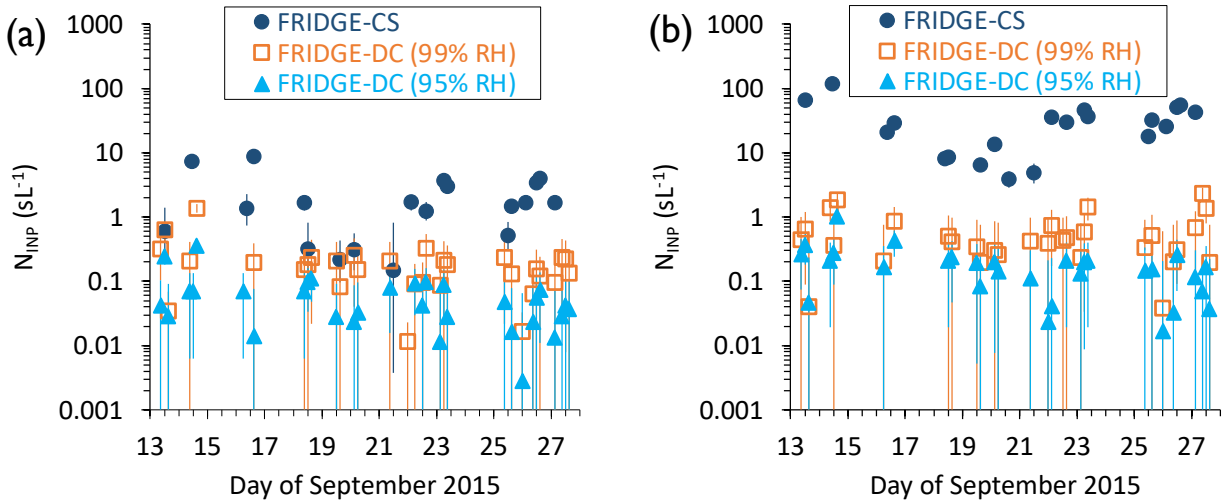


1259
 1260 **Figure 14.** Summary of deposition-mode N_{INP} (sL^{-1}) as a function of temperature. In a), mean FRIDGE-
 1261 DC data at 95% (open orange circles) and 99% (open orange squares) RH are shown along with mean
 1262 immersion freezing data from the FRIDGE-CS (filled orange circles) and the mean for the few cases of
 1263 statistically significant CSU-CFDC data (filled purple circle) at 95% RH. Error bars are one standard
 1264 deviation of the means. In b), median FRIDGE-DC data are shown and error bars for these are the 95%
 1265 confidence intervals. The significant CSU-CFDC measurement points at 95% RH are also shown with
 1266 their 95% confidence intervals. Data measured at 95% RH from the CSU-CFDC and MIT-SPIN that were
 1267 positively valued, but failed significance testing are shown without errors as open purple and open blue
 1268 circles, respectively.

1269

1270 increase between 95 and 99% RH over the range of temperatures investigated. N_{INP} differences at
1271 the two RH values were slightly smaller for median values (Figure 14b), and the median values
1272 are slightly lower than the means. Finally, FRIDGE-CS values are plotted in each panel of Figure
1273 14, indicating that FRIDGE-DC N_{INP} concentrations averaged for 99% RH are factors 10 to 30
1274 lower than average immersion freezing N_{INP} concentrations, depending on temperature.

1275 One day of significant data was obtained for the CSU-CFDC deposition measurements
1276 while using the aerosol concentrator, on September 14, containing three different time periods.
1277 These are averaged to create the only online data point represented as a mean in Figure 14a. The
1278 individual period measurements from this day, with confidence intervals as errors, are shown for
1279 the CSU-CFDC in Figure 14b. Thereby it is seen that these measurements at close to -25 °C agree
1280 very well with the mean FRIDGE deposition N_{INP} at -25 °C and 95% RH. No measurements of
1281 significance were achieved with the MIT-SPIN when operating in the deposition regime. In fact,
1282 the most common CSU-CFDC and MIT-SPIN deposition nucleation N_{INP} results were below
1283 instrument detection limits, not meeting the test for significance despite being positively valued,
1284 as shown for all periods from 6 common days of such observations represented in Figure 14b.
1285 Understanding that these data represent a failure to collect statistically-defensible data, the non-
1286 significant data generally scatter about the significant CSU-CFDC data and the FRIDGE-DC data
1287 at 95% RH, with a higher bias for the MIT-SPIN data. This indicates the difficulty for online
1288 continuous flow instruments to capture low deposition N_{INP} concentration data that fall below 1
1289 sL^{-1} at most times, considering the FRIDGE-DC data as the standard. Higher sample volumes and
1290 limited background frost conditions are needed to sense these low atmospheric INP concentrations.



1291
 1292 **Figure 15.** Time series of FRIDGE-CS (immersion freezing) and FRIDGE-DC (deposition) N_{INP} measured
 1293 at a) $-20\text{ }^{\circ}\text{C}$, and b) $-25\text{ }^{\circ}\text{C}$. Data are from individual filters or wafer collections and error bars are 95%
 1294 confidence intervals.

1295 Time series of the FRIDGE-DC measurements at $-20\text{ }^{\circ}\text{C}$ and $-25\text{ }^{\circ}\text{C}$ are shown in Figure
 1296 15. Deposition-mode N_{INP} has been averaged over three-hour periods for this analysis. The
 1297 FRIDGE immersion freezing data is included in this figure to allow for direct comparison
 1298 temporally. Immersion freezing N_{INP} generally exceeded deposition-mode N_{INP} when both types
 1299 of measurements were collected by the two FRIDGE operational methods within the same period
 1300 (or during adjacent time periods). This difference ranged from 0 to 2 orders of magnitude, with
 1301 the largest differences seen at $-25\text{ }^{\circ}\text{C}$ and a period of insignificant differences between the
 1302 operational mode results seen only from the 18th to the 22nd of September at $-20\text{ }^{\circ}\text{C}$ (Figure 15a).

1303 Based on these FRIDGE-CS and FRIDGE-DC results, immersion-mode ice nucleation
 1304 dominates at most times at mixed-phase cloud temperatures. Nevertheless, deposition-mode ice
 1305 nucleation contributes modestly to the pool of INP at mixed-phase cloud temperatures in the
 1306 atmosphere, and thus may bear consideration for parameterization in atmospheric models. The
 1307 ability of online ice nucleation instruments to measure N_{INP} in the deposition mode in

1308 correspondence to offline measurements has not been confirmed due to the mentioned inability of
1309 the online instruments used in FIN-03 to capture the low deposition nucleation N_{INP} concentrations.
1310 More work should be carried out on measurements of INPs in the deposition mode to understand
1311 variabilities in time and their relation to INP size and composition, as well as to resolve if online
1312 measurements can be improved. For the time being, the substrate methods appear to be
1313 recommended for ambient atmospheric measurements in the realm below water saturation at
1314 mixed-phase cloud temperatures.

1315

1316 **4. Summary and conclusions**

1317 FIN-03 was an ice nucleation instrument intercomparison conducted in the challenging
1318 environment of the high-altitude mountaintop field setting. Two online systems (CSU-CFDC,
1319 MIT-SPIN) and three offline systems (FRIDGE, CSU-IS, NCSU-CS) were represented in FIN-03.
1320 The immersion freezing INP concentrations measured in FIN-03 by one or more instruments
1321 spanned a dynamic range of over five orders of magnitude (10^{-3} to $\approx 10^2$ L⁻¹) over the temperature
1322 range -34 °C to -7 °C. Intercomparisons for two or more measurements were made from -30 to $-$
1323 15 °C. Agreement within one order of magnitude in immersion freezing N_{INP} was generally
1324 observed between all ice nucleation instruments measuring immersion INP concentrations at any
1325 given temperature if measurement and sampling times were matched to within 3 hours. Better than
1326 one order of magnitude agreement was found at temperatures lower than -25 °C and higher than $-$
1327 18 °C, with occasional deviations larger than an order of magnitude in the temperature range -25
1328 °C to -18 °C. Always better than an approximate 5x factor agreement was found between average
1329 ratios of the N_{INP} measured by pairs of instruments for all times of sampling. We do not have a full
1330 understanding of what controls better or worse agreement at different times or different

1331 temperatures, though some factors have been previously discussed in documenting FIN-02
1332 laboratory studies (DeMott et al., 2018). In this study, there was some inference that the different
1333 filters and impinger used did not equally capture particles in all size ranges, which is something to
1334 improve on in future studies. A review of handling and storage protocols for consistency amongst
1335 groups could also help isolate the role of such factors. Given the constant changes in the
1336 concentration, size distribution and composition of the ambient aerosol population, inevitable with
1337 any field campaign, the level of agreement found represents state-of-the-art, at least as judged
1338 based on recent laboratory and other field comparisons using similar instrumentation that appear
1339 to show 5x factor agreements (e.g., Knopf et al., 2021; Brasseur et al., 2022; Lacher et al., 2024).

1340 Although FIN-03 was not conducted as an aerosol/INP closure study per se, ancillary data
1341 on aerosol sizes and compositions as recommended in more recent discussions of needs for true
1342 closure exercises (Knopf et al., 2021; Burrows et al., 2022) were purposefully collected for
1343 integration into analyses. This included explicit measurements of the aerosol size distribution, and
1344 single particle measurements of aerosol chemical and biological composition. These
1345 measurements allowed inferences to be made about INP compositions that provided context for
1346 the period of study and establish an example for future intercomparison and long-term
1347 measurement efforts. Through comparing INP data to some current parameterizations describing
1348 biological, mineral and soil dust INPs, and additional direct investigations of INP composition via
1349 certain pre-treatments to remove biological and organic immersion-freezing INPs, these
1350 investigations revealed ubiquitous biological and organic-influenced soil-dust-like INP influences
1351 that mimic those found over other continental regions (Knopf et al., 2021; Testa et al., 2021; Lacher
1352 et al., 2024). Biological INPs were indicated via selected immersion freezing heat treatments to be
1353 dominant at > -20 °C, although of potential influence at all mixed-phase temperatures. Prediction

1354 of these based on parameterizations that utilize single particle fluorescence data (Tobo et al., 2013;
1355 Wright et al., 2014; Cornwell et al., 2023) suggest the average utility of such parameterizations
1356 but these were unable to predict the full temporal variation of biological INPs. This suggests that
1357 local variations of these INPs, which may in fact represent multiple biological particle types, is an
1358 area that requires more effort. Based on relatively good consistency between predicted and
1359 measured mineral influences on immersion-freezing N_{INP} concentrations, strictly mineral or other
1360 inorganic components of INPs were suggested to have a modest contribution to total INP
1361 concentrations at most times and at the freezing temperatures probed during this study. As in most
1362 prior studies, the mineral influence became stronger at the lowest temperatures assessed. In
1363 contrast, it was found by comparison to a parameterization based on proximally regional soil
1364 particles that arable soil INPs likely explained the second most important contribution (behind
1365 biological INPs) of INPs during FIN-03, those emanating from other organic particle components
1366 that may have been internally mixed with minerals. Biomass burning influences were possible but
1367 appear to have not contributed greatly to the climatology of INPs during the study. It was critically
1368 important in arriving at these conclusions to have single particle aerosol composition data, from a
1369 mass spectrometer that could discern the sizes and fractional contribution of minerals and from a
1370 laser-based single particle fluorescence measurement to estimate the biological character of
1371 particles. Nevertheless, there is a limit beyond the instrumentation complex here utilized in that
1372 INPs may always constitute a subset of the aerosol different in composition and size than the
1373 predominant aerosol. Knowledge advance may require improvement in methods that link INP and
1374 compositional measurements on single particles to specifically isolate these factors. Hence, a great
1375 amount of work is still needed to generally parameterize the mixed INP populations that may occur
1376 temporally in the atmosphere at higher altitude sites like SPL, or anywhere for that matter.

1377 Importantly, FIN-03 included an assessment of the separate relative contributions of
1378 deposition and immersion freezing INP concentrations, one of the few existing data sets of this
1379 kind. The offline FRIDGE-DC method was used to acquire comprehensive deposition N_{INP}
1380 measurements in dependence on RH (95 and 99%), while the CSU-CFDC and MIT-SPIN
1381 instruments attempted focused deposition nucleation measurements at (nominally) 95% RH on
1382 several days. The deposition INP concentration obtained by FRIDGE-DC increased from 95% RH
1383 to 99% RH on average by a factor of 3.3. Also, deposition N_{INP} were nearly always lower than
1384 immersion freezing N_{INP} for the temperatures assessed. Deposition INP concentrations at most
1385 times at 99% RH (always at 95% RH) were lower by an order of magnitude than immersion
1386 freezing INP concentrations at -20 °C and by more than an order of magnitude at -25 °C. For the
1387 online instruments, only limited periods of deposition INP measurements with the CSU-CFDC
1388 achieved statistical significance. While these data were in good agreement with FRIDGE-DC data
1389 at -25 °C and 95% RH, the most striking result was that all other measurement periods for the
1390 CSU-CFDC and MIT-SPIN gave measurements that were not significant at the 95% confidence
1391 level. Thus, currently, offline methods for measuring deposition INPs appear to offer the best
1392 chance for success in measuring the lower concentrations of INPs that activate below water
1393 saturation in the mixed-phase temperature regime. It would be useful to make such assessments at
1394 a variety of sites to confirm measurements made during FIN-03 on the relative contributions and
1395 variability of INPs active in these conditions toward ice formation in clouds. Additional instrument
1396 developments for online measurements of these, and future intercomparisons, will be useful.

1397 In summary, the agreements amongst instruments during FIN-03, within factors ranging
1398 from nearly 1 to up to 5 times on average between individual measurements and rarely exceeding
1399 one order of magnitude in short time periods, match those found in the FIN-02 laboratory studies.

1400 These represented state-of-the-art for measurements at the time of FIN-03 and taken together with
1401 further improvements since this time as reflected in recent studies (Knopf et al., 2021; Brasseur et
1402 al., 2022; Lacher et al., 2024) demonstrate steady improvement in the community’s collective
1403 ability to detect and quantify atmospheric ice nucleation. There was not a clear divide between the
1404 ability of online and offline systems to measure immersion freezing INP concentrations from the
1405 data collected in this study, although the need to carefully consider aerosol sampling efficiencies
1406 for different instruments was highlighted as a potential issue, one requiring close attention in future
1407 studies. In principle, both types of instruments show excellent promise for future field studies. For
1408 full closure studies of ice nucleation by atmospheric aerosols, methods for identifying INP
1409 composition as demonstrated herein and recommended by other recent discussions in Knopf et al.
1410 (2021) and Burrows et al. (2022) are critical for understanding and improving INP measurements
1411 overall.

1412 There is a clear need in the future to extend measurement comparisons to the
1413 atmospherically-relevant and critically important temperature range higher than $-15\text{ }^{\circ}\text{C}$. The low
1414 atmospheric number concentrations of INPs existing at times at these temperatures is a significant
1415 challenge for such, reflected in this study by the inability to measure INP concentrations above
1416 detection limits at the SPL site even for 3-to-4-hour filter collections at temperatures higher than
1417 $-7\text{ }^{\circ}\text{C}$. Longer sample times and higher volume collections can improve this situation, but
1418 introduce other technical challenges and do not appear possible for online instruments.

1419 We also herein do not address the relevance of INP measurements overall for
1420 understanding ice formation in clouds, where secondary processes may come into play. This is an
1421 additional topic for critical investigation, given a degree of confidence now established in
1422 measuring INPs. However, the fact that 5-factor to order of magnitude correspondence between

1423 measurements equate to 3.5 to 5 °C temperature uncertainties in assessment of INPs is something
1424 that also deserves scrutiny from the cloud modeling community concerning if this is satisfactory,
1425 and if not, what level of correspondence should the INP research community be seeking.

1426

1427 **Data availability**

1428 All data used for the figures in this paper can be accessed at

1429 <https://radar.kit.edu/radar/en/dataset/eGhfvcOhsOyADZXN> (persistent

1430 doi:10.35097/eGhfvcOhsOyADZXN). Original workshop data are available from the

1431 corresponding author on request.

1432 **Author contributions**

1433 Paul J. DeMott, Jessica A. Mirrielees and Sarah D. Brooks wrote the paper with assistance from

1434 all teams and authors contributing information on instrument descriptions and comments on all

1435 results and conclusions, with contributions from Jake Zenker on some data analysis. Paul J.

1436 DeMott, Ezra J.T. Levin, Thea Schiebel, Kaitlyn Suski, and Tom Hill provided data and analyses

1437 from the CSU-CFDC and IS instruments. Daniel J. Cziczo, Martin J. Wolfe, Sarvesh Garimella,

1438 and Maria Zawadowicz provided MIT-SPIN team measurements and analyses. Markus D. Petters

1439 and Sarah S. Petters provided data and analysis for the NCSU-CS instrument. Heinz G. Bingemer,

1440 Jann Schrod, and Daniel Weber provided data and analyses for the FRIDGE instrument. Anne

1441 Perring provided data and analyses for the WIBS-4A. Karl Froyd provided data and analyses for

1442 the LAS and PALMS. Anna Gannet Hallar and Ian McCubbin oversaw field operations,

1443 coordinated with visiting teams at Storm Peak Laboratory, and provided nephelometer and

1444 meteorological measurements. Paul J. DeMott, Daniel J. Cziczo, Ottmar Möhler contributed to

1445 organize the campaign in connection with the other FIN activities.

1446

1447 **Competing interests**

1448 The contact author has declared that none of the authors has any competing interests.

1449

1450

1451 **Acknowledgements**

1452 Partial financial support for this project was provided by the U.S. National Science
1453 Foundation, Grant No. AGS-1339264 and U.S. Department of Energy's Atmospheric System
1454 Research, an Office of Science, Office of Biological and Environmental Research program, under
1455 grant no. DE-SC0014487. Paul J. DeMott, Ezra J.T. Levin, Thea Schiebel, Kaitlyn Suski, and Tom
1456 Hill acknowledge partial and in-kind research support during FIN-03 from NSF grant no. AGS-
1457 1358495. Markus Petters acknowledges partial and in-kind support during FIN-03 from NSF grant
1458 no. AGS-1450690. Jann Schrod acknowledges research support from the European Union's
1459 Seventh Framework Programme (FP7/2007-2013) project BACCHUS under grant agreement no.
1460 603445. Heinz G. Bingemer and Daniel Weber acknowledge research support under DFG grant
1461 BI 462/3-2. Thea Schiebel and Ottmar Möhler received support through the German Science
1462 Foundation Projects INUIT and INUIT-2 (MO 668/4-1 and MO 668/4-2). Anne Perring
1463 acknowledges support from the NOAA Health of the Atmosphere Program and the NOAA
1464 Atmospheric Composition and Climate Program. Special thanks to Romy Fösig (Ullrich) for
1465 assistance with data archival.

1466

1467

1468 **References**

- 1469 Alsante, A. N., Thornton, D. C. O., & Brooks, S. D.: Ice nucleation catalyzed by the
 1470 photosynthesis enzyme RuBisCO and other abundant biomolecules. *Communications*
 1471 *Earth & Environment*, 4(1). doi:10.1038/s43247-023-00707-7, 2023.
- 1472 Agresti, A. and Coull, B. A.: Approximate is better than "exact" for interval estimation of
 1473 binomial proportions, *The American Statistician*, 52, 119-126,
 1474 <https://doi.org/10.1080/00031305.1998.10480550>, 1998.
- 1475 Andreae, M. O., & Rosenfeld, D.: Aerosol-cloud-precipitation interactions. Part 1. The nature
 1476 and sources of cloud-active aerosols. *Earth-Science Reviews*, 89(1-2), 13-41.
 1477 <https://doi.org/10.1016/j.earscirev.2008.03.001>, 2008.
- 1478 Andrews, E., and Coauthors, 2019: Overview of the NOAA/ESRL Federated Aerosol
 1479 Network. *Bull. Amer. Meteor. Soc.*, 100, 123–135, <https://doi.org/10.1175/BAMS-D-17-0175.1>.
- 1481 Ardon-Dryer, K., & Levin, Z.: Ground-based measurements of immersion freezing in the eastern
 1482 Mediterranean. *Atmospheric Chemistry and Physics*, 14(10), 5217-5231.
 1483 <https://doi.org/10.5194/acp-14-5217-2014>, 2014.
- 1484 Barry, K. R., Hill, T. C. J., Levin, E. J. T., Twohy, C. H., Moore, K. A., Weller, Z. D., Toohey, D. W., Reeves,
 1485 M., Campos, T., Geiss, R., Fischer, E. V., Kreidenweis, S. M., and DeMott, P. J.: Observations of ice
 1486 nucleating particles in the free troposphere from western US wildfires. *Journal of Geophysical*
 1487 *Research: Atmospheres*, 126, e2020JD033752. <https://doi.org/10.1029/2020JD033752>, 2021a.
- 1488 Barry, K. R., Hill, T. C. J., Jentsch, C., Moffett, B. E., Stratmann, F., and DeMott, P.J.: Pragmatic protocols
 1489 for working cleanly when measuring ice nucleating particles, *Atmospheric Research*, 250, 105419,
 1490 <https://doi.org/10.1016/j.atmosres.2020.105419>, 2021b.
- 1491 Beall, C. M., Lucero, D., Hill, T. C. J., DeMott, P. J., Stokes, M. D., and Prather, K. A.: Best
 1492 practices for precipitation sample storage for offline studies of ice nucleation in marine
 1493 and coastal environments, *Atmos. Meas. Tech.*, 13, 6473–6486,
 1494 <https://doi.org/10.5194/amt-13-6473-2020>, 2020.
- 1495 Boose, Y., Sierau, B., Isabel García, M., Rodríguez, S., Alastuey, A., Linke, C., Schnaiter, M.,
 1496 Kupiszewski, P., Kanji, Z. A., and Lohmann, U.: Ice nucleating particles in the Saharan
 1497 Air Layer. *Atmospheric Chemistry and Physics*, 16(14), 9067-9087.
 1498 <https://doi.org/10.5194/acp-16-9067-2016>, 2016.
- 1499 Boucher, O., Randall, D., Artaxo, P., Bretherton, C., Feingold, G., Forster, P., Kerminen, V.-M.,
 1500 Kondo, Y., Liao, H., Lohmann, U., Rasch, P., Satheesh, S. K., Sherwood, S., Stevens, B.,
 1501 and Zhang, X. Y.: *Clouds and Aerosols. In: Climate Change 2013: The Physical Science*
 1502 *Basis. Contribution of Working Group I to the Fifth Assessment Report of the*
 1503 *Intergovernmental Panel on Climate Change*. Retrieved from Cambridge, United
 1504 Kingdom and New York, NY, USA, 2013.
- 1505 Brasseur, Z., Castarède, D., Thomson, E. S., Adams, M. P., Drossaert van Dusseldorp, S.,
 1506 Heikkilä, P., Korhonen, K., Lampilahti, J., Paramonov, M., Schneider, J., Vogel, F., Wu,
 1507 Y., Abbatt, J. P. D., Atanasova, N. S., Bamford, D. H., Bertozzi, B., Boyer, M., Brus, D.,
 1508 Daily, M. I., Fösig, R., Gute, E., Harrison, A. D., Hietala, P., Höhler, K., Kanji, Z. A.,
 1509 Keskinen, J., Lacher, L., Lampimäki, M., Levula, J., Manninen, A., Nadolny, J., Peltola,
 1510 M., Porter, G. C. E., Poutanen, P., Proske, U., Schorr, T., Silas Umo, N., Stenszky, J.,
 1511 Virtanen, A., Moisseev, D., Kulmala, M., Murray, B. J., Petäjä, T., Möhler, O., and

1512 Duplissy, J.: Measurement report: Introduction to the HyICE-2018 campaign for
 1513 measurements of ice-nucleating particles and instrument inter-comparison in the Hyytiälä
 1514 boreal forest. *Atmospheric Chemistry and Physics*, 22(8), 5117–5145.
 1515 <https://doi.org/10.5194/acp-22-5117-2022>, 2022.

1516 Burrows, S. M., McCluskey, C. S., Cornwell, G., Steinke, I., Zhang, K., Zhao, B., Zawadowicz,
 1517 M., Raman, A., Kulkarni, G., China, S., Zelenyuk, A. and DeMott, P. J.: Ice-nucleating
 1518 particles that impact clouds and climate: Observational and modeling research needs,
 1519 *Reviews of Geophysics*, **60**, e2021RG000745. <https://doi.org/10.1029/2021RG000745>,
 1520 2022.

1521 Collaud Coen, M., Andrews, E., Aliaga, D., Andrade, M., Angelov, H., Bukowiecki, N., Ealo,
 1522 M., Fialho, P., Flentje, H., Hallar, A. G., Hooda, R., Kalapov, I., Krejci, R., Lin, N.-H.,
 1523 Marinoni, A., Ming, J., Nguyen, N. A., Pandolfi, M., Pont, V., Ries, L., Rodríguez, S.,
 1524 Schauer, G., Sellegri, K., Sharma, S., Sun, J., Tunved, P., Velasquez, P., and Ruffieux,
 1525 D.: Identification of topographic features influencing aerosol observations at high altitude
 1526 stations: Identification of topographic features influencing aerosol observations at high
 1527 altitude stations. *Atmospheric Chemistry and Physics*, 18(16), 12289-12313.
 1528 <https://doi.org/10.5194/acp-18-12289-2018>, 2018.

1529 Coluzza, I., Creamean, J., Rossi, M. J., Wex, H., Alpert, P. A., Bianco, V., Boose, Y., Dellago,
 1530 C., Felgitsch, L., Fröhlich-Nowoisky, J., Herrmann, H., Jungblut, S., Kanji, Z. A., Menzl,
 1531 G., Moffett, B., Moritz, C., Mutzel, A., Pöschl, U., Schauperl, M., Scheel, J., Stopelli, E.,
 1532 Stratmann, F., Grothe, H., and Schmale, D. G.: Perspectives on the Future of Ice
 1533 Nucleation Research: Research Needs and Unanswered Questions Identified from Two
 1534 International Workshops. *Atmosphere*, 8(8). <https://doi.org/10.3390/atmos8080138>, 2017.

1535 Cornwell, G. C., McCluskey, C. S., Hill, T. C. J., Levin, E. J. T., Rothfuss, N. E., Taia, S.-L.,
 1536 Petters, M. D., DeMott, P. J., Martin, A., Kreidenweis, S. M., Prather, K. A. and
 1537 Burrows, S. M.: Bioaerosols are the dominant source of warm-temperature immersion-
 1538 mode INPs and drive uncertainties in INP predictability in the ambient atmosphere.
 1539 *Science Advances*, **9**, eadg3715, <https://doi.org/10.1126/sciadv.adg3715>, 2023.

1540 Cornwell, G. C., McCluskey, C. S., Levin, E. J. T., Suski, K. J., DeMott, P. J., Kreidenweis, S.
 1541 M., & Prather, K. A.: Direct online mass spectrometry measurements of ice nucleating
 1542 particles at a California coastal site. *Journal of Geophysical Research: Atmospheres*, 124,
 1543 12,157–12,172. <https://doi.org/10.1029/2019JD030466>, 2019.

1544 Creamean, J. M., Suski, K. J., Rosenfeld, D., Cazorla, A., DeMott, P. J., Sullivan, R. C., White,
 1545 A. B., Ralph, F. M., Minnis, P., Comstock, J. M., Tomlinson, J. M., and Prather, K. A.:
 1546 Dust and biological aerosols from the Sahara and Asia influence precipitation in the
 1547 western U.S. *Science*, 339(6127), 1572-1578. <https://doi.org/10.1126/science.1227279>,
 1548 2013.

1549 David, R. O., Fahrni, J., Marcolli, C., Mahrt, F., Brühwiler, D., and Kanji, Z. A.: The role of
 1550 contact angle and pore width on pore condensation and freezing, *Atmos. Chem. Phys.*, **20**,
 1551 9419–9440, <https://doi.org/10.5194/acp-20-9419-2020>, 2020.

1552 David, R. O., Cascajo-Castresana, M., Brennan, K. P., Rösch, M., Els, N., Werz, J., Weichlinger,
 1553 V., Boynton, L. S., Bogler, S., Borduas-Dedekind, N., Marcolli, C., and Kanji, Z. A.:
 1554 Development of the DRoplet Ice Nuclei Counter Zurich (DRINCZ): validation and
 1555 application to field-collected snow samples, *Atmos. Meas. Tech.*, **12**, 6865–6888,
 1556 <https://doi.org/10.5194/amt-12-6865-2019>, 2019.

1557 DeMott, P. J., Mohler, O., Cziczo, D. J., Hiranuma, N., Petters, M. D., Petters, S. S., Belosi, F.,
1558 Bingemer, H. G., Brooks, S. D., Budke, C., Burkert-Kohn, M., Collier, K. N.,
1559 Danielczok, A., Eppers, O., Felgitsch, L., Garimella, S., Grothe, H., Herenz, P., Hill, T.
1560 C. J., Höhler, K., Kanji, Z. A., Kiselev, A., Koop, T., Kristensen, T. B., Krüger, K.,
1561 Kulkarni, G., Levin, E. J. T., Murray, B. J., Nicosia, A., O'Sullivan, D., Peckhaus, A.,
1562 Polen, M. J., Price, H. C., Reicher, N., Rothenberg, D. A., Rudich, Y., Santachiara, G.,
1563 Schiebel, T., Schrod, J., Seifried, T. M., Stratmann, F., Sullivan, R. C., Suski, K. J.,
1564 Szakáll, M., Taylor, H. P., Ullrich, R., Vergara-Temprado, J., Wagner, R., Whale, T. F.,
1565 Weber, D., Welti, A., Wilson, T. W., Wolf, M. J., Zenker, J.: The Fifth International
1566 Workshop on Ice Nucleation phase 2 (FIN-02): laboratory intercomparison of ice
1567 nucleation measurements. *Atmospheric Measurement Techniques*, 11(11), 6231-6257.
1568 <https://doi.org/10.5194/amt-11-6231-2018>, 2018.

1569 DeMott, P. J., Hill, T. C. J., Petters, M. D., Bertram, A. K., Tobo, Y., Mason, R. H., Suski, K. J.,
1570 McCluskey, C. S., Levin, E. J. T., Schill, G. P., Boose, Y., Rauker, A. M., Miller, A. J.,
1571 Zaragoza, J., Rocci, K., Rothfuss, N. E., Taylor, H. P., Hader, J. D., Chou, C., Huffman,
1572 J. A., Pöschl, U., Prenni, A. J., and Kreidenweis, S. M.: Comparative measurements of
1573 ambient atmospheric concentrations of ice nucleating particles using multiple immersion
1574 freezing methods and a continuous flow diffusion chamber, *Atmos. Chem. Phys.*, 17,
1575 11227–11245, <https://doi.org/10.5194/acp-17-11227-2017>, 2017.

1576 DeMott, P. J., Prenni, A. J., McMeeking, G. R., Sullivan, R. C., Petters, M. D., Tobo, Y.,
1577 Niemand, M., Möhler, O., Snider, J. R., Wang, Z., and Kreidenweis, S. M: Integrating
1578 laboratory and field data to quantify the immersion freezing ice nucleation activity of
1579 mineral dust particles. *Atmospheric Chemistry and Physics*, 15(1), 393-409.
1580 <https://doi.org/10.5194/acp-15-393-2015>, 2015.

1581 DeMott, P. J., Mohler, O., Stetzer, O., Vali, G., Levin, Z., Petters, M. D., Murakami, M., Leisner,
1582 T., Bundke, U., Klein, H., Kanji, Z. A., Cotton, R. Jones, H., Petters, M. D., Prenni, A.,
1583 Benz, S. Brinkmann, M., Rzesanke, D., Saathoff, H. Nicolet, M., Gallavardin, S., Saito,
1584 A., Nillius, B., Bingemer, H., Abbatt, J., Ardon, K., Ganor, E., Georgakopoulos, D. G.,
1585 and Saunders, C.: Resurgence in ice nuclei measurement research. *Bulletin of the*
1586 *American Meteorological Society*, 92(12), 1623-+. [https://doi.org/10.1175/bams-d-10-](https://doi.org/10.1175/bams-d-10-3119.1)
1587 [3119.1](https://doi.org/10.1175/bams-d-10-3119.1), 2011

1588 DeMott, P. J., Prenni, A. J., Liu, X., Kreidenweis, S. M., Petters, M. D., Twohy, C. H.,
1589 Richardson, M. S., Eidhammer, T., Kreidenweis, S. M., and Rogers, D. C.: Predicting
1590 global atmospheric ice nuclei distributions and their impacts on climate. *Proceedings of*
1591 *the National Academy of Sciences of the United States of America*, 107(25), 11217-
1592 11222. <https://doi.org/10.1073/pnas.0910818107>,

1593 Durant, A. J., and Shaw, R. A.: Evaporation freezing by contact nucleation inside-out.
1594 *Geophysical Research Letters*, 32(20). <https://doi.org/10.1029/2005gl024175>, 2005.

1595 Eidhammer, T., DeMott, P. J., Prenni, A. J., Petters, M. D., Twohy, C. H., Rogers, D. C., Stith,
1596 J., Heymsfield, A., Wang, Z., Haimov, S., French, J., Pratt, K., Prather, K., Murphy, S.,
1597 Seinfeld, J., Subramanian, R. and Kreidenweis, S. M.: Ice initiation by aerosol particles:
1598 Measured and predicted ice nuclei concentrations versus measured ice crystal
1599 concentrations in an orographic wave cloud. *J. Atmos. Sci.*, 67, 2417–2436.
1600 <https://doi.org/10.1175/2010JAS3266.1>, 2010.

1601 Fornea, A. P., Brooks, S. D., Dooley, J. B., and Saha, A.: Heterogeneous freezing of ice on
1602 atmospheric aerosols containing ash, soot, and soil. *Journal of Geophysical Research:*
1603 *Atmospheres*, 114(D13). <https://doi.org/10.1029/2009jd011958>, 2009.

1604 Froyd, K.D., Yu, P., Schill, G.P. *et al.* Dominant role of mineral dust in cirrus cloud formation
1605 revealed by global-scale measurements. *Nat. Geosci.* **15**, 177–183.
1606 <https://doi.org/10.1038/s41561-022-00901-w>, 2022.

1607 Froyd, K. D., Murphy, D. M., Brock, C. A., Campuzano-Jost, P., Dibb, J. E., Jimenez, J.-L.,
1608 Kupc, A., Middlebrook, A. M., Schill, G. P., Thornhill, K. L., Williamson, C. J., Wilson,
1609 J. C., and Ziemba, L. D.: A new method to quantify mineral dust and other aerosol
1610 species from aircraft platforms using single-particle mass spectrometry. *Atmospheric*
1611 *Measurement Techniques*, 12(11), 6209–6239. <https://doi.org/10.5194/amt-12-6209-2019>,
1612 2019.

1613 Gabey, A. M., Gallagher, M. W., Whitehead, J., Dorsey, J. R., Kaye, P. H., and Stanley, W. R.:
1614 Measurements and comparison of primary biological aerosol above and below a tropical
1615 forest canopy using a dual channel fluorescence spectrometer. *Atmospheric Chemistry*
1616 *and Physics*, 10(10), 4453–4466. <https://doi.org/10.5194/acp-10-4453-2010>, 2010.

1617 Garimella, S., Kristensen, T. B., Ignatius, K., Welti, A., Voigtländer, J., Kulkarni, G. R., Sagan,
1618 F., Kok, G. L., Dorsey, J., Nichman, L., Rothenberg, D. A., Rösch, M., Kirchgäßner, A.
1619 C. R., Ladkin, R., Wex, H., Wilson, T. W., Ladino, L. A., Abbatt, J. P. D., Stetzer, O.,
1620 Lohmann, U., Stratmann, F., and Cziczo, D. J.: The SPectrometer for Ice Nuclei (SPIN):
1621 an instrument to investigate ice nucleation. *Atmospheric Measurement Techniques*, 9(7),
1622 2781–2795. <https://doi.org/10.5194/amt-9-2781-2016>, 2016.

1623 Garimella, S., Rothenberg, D. A., Wolf, M. J., David, R. O., Kanji, Z. A., Wang, C., Rösch, M.,
1624 and Cziczo, D. J.: Uncertainty in counting ice nucleating particles with continuous flow
1625 diffusion chambers. *Atmospheric Chemistry and Physics*, 17(17), 10855–10864.
1626 <https://doi.org/10.5194/acp-17-10855-2017>, 2017.

1627 Hader, J. D., Wright, T. P., & Petters, M. D.: Contribution of pollen to atmospheric ice nuclei
1628 concentrations. *Atmospheric Chemistry and Physics*, 14(11), 5433–
1629 5449. <https://doi.org/10.5194/acp-14-5433-2014>, 2014.

1630 Healy, D. A., Huffman, J. A., O'Connor, D. J., Pöhlker, C., Pöschl, U., & Sodeau, J. R.: Ambient
1631 measurements of biological aerosol particles near Killarney, Ireland: a comparison
1632 between real-time fluorescence and microscopy techniques. *Atmospheric Chemistry and*
1633 *Physics*, 14(15), 8055–8069. <https://doi.org/10.5194/acp-14-8055-2014>, 2014.

1634 Hallar, A. G., G. Chirokova, I. McCubbin, T. H. Painter, C. Wiedinmyer, and C.
1635 Dodson: Atmospheric bioaerosols transported via dust storms in the western United
1636 States, *Geophys. Res. Lett.*, 38, L17801, <https://doi.org/10.1029/2011GL048166>, 2011.

1637 Healy, D. A., Huffman, J. A., O'Connor, D. J., Pöhlker, C., Pöschl, U., & Sodeau, J. R.: Ambient
1638 measurements of biological aerosol particles near Killarney, Ireland: a comparison
1639 between real-time fluorescence and microscopy techniques. *Atmospheric Chemistry and*
1640 *Physics*, 14(15), 8055–8069. <https://doi.org/10.5194/acp-14-8055-2014>, 2014.

1641 Hiranuma, N., Augustin-Bauditz, S., Bingemer, H., Budke, C., Curtius, J., Danielczok, A., Diehl,
1642 K., Dreischmeier, K., Ebert, M., Frank, F., Hoffmann, N., Kandler, K., Kiselev, A.,
1643 Koop, T., Leisner, T., Möhler, O., Nillius, B., Peckhaus, A., Rose, D., Weinbruch, S.,
1644 Wex, H., Boose, Y., DeMott, P. J., Hader, J. D., Hill, T. C. J., Kanji, Z. A., Kulkarni, G.,
1645 Levin, E. J. T., McCluskey, C. S., Murakami, M., Murray, B. J., Niedermeier, D., Petters,
1646 M. D., O'Sullivan, D., Saito, A., Schill, G. P., Tajiri, T., Tolbert, M. A., Welti, A., Whale,

1647 T. F., Wright, T. P., and Yamashita, K.: A comprehensive laboratory study on the
1648 immersion freezing behavior of illite NX particles: a comparison of 17 ice nucleation
1649 measurement techniques, *Atmospheric Chemistry and Physics*, 15(5), 2489-2518.
1650 <https://doi.org/10.5194/acp-15-2489-2015>, 2015.

1651 Huffman, J. A., Prenni, A. J., DeMott, P. J., Pöhlker, C., Mason, R. H., Robinson, N. H.,
1652 Fröhlich-Nowoisky, J., Tobo, Y., Després, V. R., Garcia, E., Gochis, D. J., Harris, E.,
1653 Müller-Germann, I., Ruzene, C., Schmer, B., Sinha, B., Day, D. A., Andreae, M. O.,
1654 Jimenez, J. L., Gallagher, M., Kreidenweis, S. M., Bertram, A. K., and Pöschl, U.: High
1655 concentrations of biological aerosol particles and ice nuclei during and after rain.
1656 *Atmospheric Chemistry and Physics*, 13(13), 6151-6164. [https://doi.org/10.5194/acp-13-](https://doi.org/10.5194/acp-13-6151-2013)
1657 [6151-2013](https://doi.org/10.5194/acp-13-6151-2013), 2013.

1658 Jones, H. M., Flynn, M. J., DeMott, P. J., and Mohler, O.: Manchester Ice Nucleus Counter
1659 (MINC) measurements from the 2007 International workshop on Comparing Ice
1660 nucleation Measuring Systems (ICIS-2007). *Atmospheric Chemistry and Physics*, 11(1),
1661 53-65. <https://doi.org/10.5194/acp-11-53-2011>, 2011.

1662 Kanji, Z. A., DeMott, P. J., Mohler, O., and Abbatt, J. P. D.: Results from the University of
1663 Toronto continuous flow diffusion chamber at ICIS 2007: instrument intercomparison
1664 and ice onsets for different aerosol types. *Atmospheric Chemistry and Physics*, 11(1), 31-
1665 41. <https://doi.org/10.5194/acp-11-31-2011>, 2011.

1666 Kanji, Z. A., Ladino, L. A., Wex, H., Boose, Y., Burkert-Kohn, M., Cziczo, D. J., & Krämer, M.:
1667 Overview of Ice Nucleating Particles. In D. Baumgardner, G. M. McFarquhar, & A. J.
1668 Heymsfield (Eds.), *Ice Formation and Evolution in Clouds and Precipitation:
1669 Measurement and Modeling Challenges*, *Meteorological Monographs*, 58, 1.1-1.33.
1670 <https://doi.org/10.1175/amsmonographs-d-16-0006.1>, 2017.

1671 Kaye, P. H., Stanley, W. R., Hirst, E., Foot, E. V., Baxter, K. L., and Barrington, S. J.: Single
1672 particle multichannel bio-aerosol fluorescence sensor. *Optics Express*, 13(10), 3583-
1673 3593. <https://doi.org/10.1364/OPEX.13.003583>, 2005.

1674 Knopf, D. A., Barry, K. R., Brubaker, T. A., Jahl, L. G., Jankowski, K. A. L., Li, J., Lu, Y.,
1675 Monroe, L. W., Moore, K. A., Rivera-Adorno, F. A., Saucedo, K. A., Shi, Y., Tomlin, J.
1676 M., Vepuri, H. S. K., Wang, P., Lata, N. N., Levin, E. J. T., Creamean, J. M., Hill, T. C.
1677 J., China, S., Alpert, P. A., Moffet, R. C., Hiranuma, N., Sullivan, R. C., Fridlind, A. M.,
1678 West, M., Riemer, N., Laskin, A., DeMott, P. J., & Liu, X. (2021). Aerosol–Ice
1679 Formation Closure: A Southern Great Plains Field Campaign, *Bulletin of the American
1680 Meteorological Society*, 102(10), E1952-E197, [https://doi.org/10.1175/BAMS-D-20-](https://doi.org/10.1175/BAMS-D-20-0151.1)
1681 [0151.1](https://doi.org/10.1175/BAMS-D-20-0151.1)

1682 Kulkarni, G. and Kok, G (2012).: Mobile Ice Nucleus Spectrometer, Pacific Northwest National
1683 Laboratory, Richland, WA, 13 pg.

1684 Lacher, L., Adams, M. P., Barry, K., Bertozzi, B., Bingemer, H., Boffo, C., Bras, Y., Büttner, N.,
1685 Castarede, D., Cziczo, D. J., DeMott, P. J., Fösig, R., Goodell, M., Höhler, K., Hill, T. C.
1686 J., Jentsch, C., Ladino, L. A., Levin, E. J. T., Mertes, S., Möhler, O., Moore, K. A.,
1687 Murray, B. J., Nadolny, J., Pfeuffer, T., Picard, D., Ramírez-Romero, C., Ribeiro, M.,
1688 Richter, S., Schrod, J., Sellegri, K., Stratmann, F., Swanson, B. E., Thomson, E., Wex,
1689 H., Wolf, M., and Freney, E.: The Puy de Dôme ICe Nucleation Intercomparison
1690 Campaign (PICNIC): Comparison between online and offline methods in ambient air,
1691 *Atmos. Chem. Phys.*, 24, 2651–2678, <https://doi.org/10.5194/acp-24-2651-2024>, 2024.

1692 Levin, E. J. T., DeMott, P. J., Suski, K. J., Boose, Y., Hill, T. C. J., McCluskey, C. S., Schill, G.
1693 P., Rocci, K., Al-Mashat, H., Kristensen, L. J., Cornwell, G. C., Prather, K. A.,
1694 Tomlinson, J. M., Mei, F., Hubbe, J., Pekour, M. S., Sullivan, R. J., Leung L. R., and
1695 Kreidenweis, S. M.: Characteristics of ice nucleating particles in and around California
1696 winter storms, *Journal of Geophysical Research: Atmospheres*, **124**, 11,530-11,551,
1697 <https://doi.org/10.1029/2019JD030831>, 2019.

1698 Lohmann, U., and Feichter, J.: Global indirect aerosol effects: a review. *Atmospheric Chemistry
1699 and Physics*, **5**, 715-737. <https://doi.org/10.5194/acp-5-715-2005>, 2005.

1700 Marcolli, C., Deposition nucleation viewed as homogeneous or immersion freezing in pores and
1701 cavities. *Atmospheric Chemistry and Physics*, **14**(4), 2071-2104.
1702 <https://doi.org/10.5194/acp-14-2071-2014>, 2014.

1703 Mason, R. H., Si, M., Chou, C., Irish, V. E., Dickie, R., Elizondo, P., Wong, R., Brintnell, M.,
1704 Elsasser, M., Lassar, W. M., Pierce, K. M., Leitch, W. R., MacDonald, A. M., Platt, A.,
1705 Toom-Saunty, D., Sarda-Estève, R., Schiller, C. L., Suski, K. J., Hill, T. C. J., Abbatt, J.
1706 P. D., Huffman, J. A., DeMott, P. J., and Bertram, A. K.: Size-resolved measurements of
1707 ice-nucleating particles at six locations in North America and one in Europe, *Atmos.
1708 Chem. Phys.*, **16**, 1637–1651, <https://doi.org/10.5194/acp-16-1637-2016>, 2016.

1709 McCluskey, C. S., Gettelman, A., Bardeen, C. G., DeMott, P. J., Moore, K. A., Kreidenweis, S.
1710 M., Hill, T. C. J., Barry, K. R., Twohy, C. H., Toohey, D. W., Rainwater, B., Jensen, J.
1711 B., Reeves, J. M., Alexander, S. P. and McFarquhar, G. M.: Simulating Southern Ocean
1712 aerosol and ice nucleating particles in the Community Earth System Model version 2.
1713 *Journal of Geophysical Research: Atmospheres*, **128**, e2022JD036955, 2023.
1714 <https://doi.org/10.1029/2022JD036955>, 2023.

1715 McCluskey, C. S., Hill, T. C. J., Humphries, R. S., Rauker, A. M., Moreau, S., Stratton, P. G.,
1716 Chambers, S. D., Williams, A. G., McRobert, I., Ward, J., Keywood, M. D., Harnwell,
1717 J., Ponsonby, W., Loh, Z.M., Krummel, P. B., Protat, A., Kreidenweis, S.M., and
1718 DeMott, P. J.: Observations of ice nucleating particles over Southern Ocean waters.
1719 *Geophysical Research Letters*, **45**, 11,989–11,997,
1720 <https://doi.org/10.1029/2018GL079981>, 2018.

1721 Möhler, O., Adams, M., Lacher, L., Vogel, F., Nadolny, J., Ullrich, R., Boffo, C., Pfeuffer, T.,
1722 Hobl, A., Weiß, M., Vepuri, H. S. K., Hiranuma, N., and Murray, B. J.: The Portable Ice
1723 Nucleation Experiment (PINE): a new online instrument for laboratory studies and
1724 automated long-term field observations of ice-nucleating particles. *Atmospheric
1725 Measurement Techniques*, **14**(2), 1143-1166. <https://doi.org/10.5194/amt-14-1143-2021>,
1726 2021.

1727 Morris, C. E., Sands, D. C., Bardin, M., Jaenicke, R., Vogel, B., Leyronas, C., Ariya, P. A., and
1728 Psenner, R.: Microbiology and atmospheric processes: research challenges concerning
1729 the impact of airborne micro-organisms on the atmosphere and climate. *Biogeosciences*,
1730 **8**, 17. <https://doi.org/10.5194/bg-8-17-2011>, 2011.

1731 Murray, B. J., O'Sullivan, D., Atkinson, J. D., & Webb, M. E: Ice nucleation by particles
1732 immersed in supercooled cloud droplets. *Chemical Society Reviews*, **41**(19), 6519-6554.
1733 <https://doi.org/10.1039/C2CS35200A>, 2012.

1734 Niemand, M., Mohler, O., Vogel, B., Vogel, H., Hoose, C., Connolly, P., Klein, H. Bingemer,
1735 H., DeMott, P. J., Skrotzki, J., and Leisner, T.: A Particle-Surface-Area-Based
1736 Parameterization of Immersion Freezing on Desert Dust Particles. *Journal of the
1737 Atmospheric Sciences*, **69**(10), 3077-3092. <https://doi.org/10.1175/jas-d-11-0249.1>, 2012.

1738 Perring, A. E., Schwarz, J. P., Baumgardner, D., Hernandez, M. T., Spracklen, D. V., Heald, C.
1739 L., Gao, R. S., Kok, G., McMeeking, G. R., McQuaid, J. B., and Fahey, D. W.:
1740 Airborne observations of regional variation in fluorescent aerosol across the United
1741 States. *Journal of Geophysical Research-Atmospheres*, 120(3), 1153-1170.
1742 <https://doi.org/10.1002/2014jd022495>, 2015.

1743 Petersen, R. C., Hallar, A. G., McCubbin, I. B., Ogren, J. A., Andrews, E., Lowenthal, D.,
1744 Gorder, R., Purcell, R., Sleeth, D., and Novosselov, I.: Numerical, wind-tunnel, and
1745 atmospheric evaluation of a turbulent ground-based inlet sampling system, *Aerosol*
1746 *Science and Technology*, 53 (6), 712-727,
1747 <https://doi.org/10.1080/02786826.2019.1602718>, 2019.

1748 Petters, M. D., and Wright, T. P.: Revisiting ice nucleation from precipitation samples.
1749 *Geophysical Research Letters*, 42(20), 8758-8766. doi:10.1002/2015gl065733, 2015.

1750 Pöhlker, C., Huffman, J. A., and Pöschl, U.: Autofluorescence of atmospheric bioaerosols –
1751 fluorescent biomolecules and potential interferences. *Atmospheric Measurement*
1752 *Techniques*, 5(1), 37-71. <https://doi.org/10.5194/amt-5-37-2012>, 2012.

1753 Rogers, D.C.: Development of a continuous flow thermal gradient diffusion chamber for ice
1754 nucleation studies. *Atmos. Res.*, 22, 149-181, [https://doi.org/10.1016/0169-](https://doi.org/10.1016/0169-8095(88)90005-1)
1755 [8095\(88\)90005-1](https://doi.org/10.1016/0169-8095(88)90005-1), 1988.

1756 Rogers, D. C., DeMott, P. J., Kreidenweis S. M., and Chen, Y.: A continuous flow diffusion
1757 chamber for airborne measurements of ice nuclei, *J. Atmos. Oceanic Technol.*, 18, 725-
1758 741, [https://doi.org/10.1175/1520-0426\(2001\)018<0725:ACFDCE>2.0.CO;2](https://doi.org/10.1175/1520-0426(2001)018<0725:ACFDCE>2.0.CO;2), 2001.

1759 Schill, G. P., DeMott, P. J., Emerson, E. W., Rauker, A. M. C., Kodros, J. K., Suski, K. J., Hill,
1760 T. C. J., Levin, E. J. T., Pierce, J. R., Farmer, D. K., and Kreidenweis, S. M.: The
1761 contribution of black carbon to global ice nucleating particle concentrations relevant to
1762 mixed-phase clouds. *Proceedings of the National Academy of Sciences*, 117 (37), 22705–
1763 22711, <https://doi.org/10.1073/pnas.2001674117>, 2020.

1764 Schrod, J., Danielczok, A., Weber, D., Ebert, M., Thomson, E. S., and Bingemer, H. G.: Re-
1765 evaluating the Frankfurt isothermal static diffusion chamber for ice nucleation, *Atmos.*
1766 *Meas. Tech.*, 9, 1313–1324, <https://doi.org/10.5194/amt-9-1313-2016>, 2016.

1767 Schrod, J., Thomson, E. S., Weber, D., Kossmann, J., Pöhlker, C., Saturno, J., Ditas, F., Artaxo,
1768 P., Clouard, V., Saurel, J.-M., Ebert, M., Curtius, J., and Bingemer, H. G.: Long-term
1769 deposition and condensation ice-nucleating particle measurements from four stations
1770 across the globe, *Atmos. Chem. Phys.*, 20, 15983–16006, [https://doi.org/10.5194/acp-20-](https://doi.org/10.5194/acp-20-15983-2020)
1771 [15983-2020](https://doi.org/10.5194/acp-20-15983-2020), 2020.

1772 Seifert, P., Ansmann, A., Groß, S., Freudenthaler, V., Heinold, B., Hiebsch, A., Mattis, I.,
1773 Schmidt, J., Schnell, F., Tesche, M., Wandinger, U., and Wiegner, M.: Ice formation in
1774 ash-influenced clouds after the eruption of the Eyjafjallajökull volcano in April 2010.
1775 *Journal of Geophysical Research: Atmospheres*, 116(D20).
1776 <https://doi.org/10.1029/2011jd015702>, 2011.

1777 Shen, X., Bell, D. M., Coe, H., Hiranuma, N., Mahrt, F., Marsden, N. A., Mohr, C., Murphy, D.
1778 M., Saathoff, H., Schneider, J., Wilson, J., Zawadowicz, M. A., Zelenyuk, A., DeMott, P.
1779 J., Möhler, O., and Cziczo, D. J.: Measurement report: The Fifth International Workshop
1780 on Ice Nucleation phase 1 (FIN-01): intercomparison of single-particle mass
1781 spectrometers, *Atmos. Chem. Phys.*, 24, 10869–10891, [https://doi.org/10.5194/acp-24-](https://doi.org/10.5194/acp-24-10869-2024)
1782 [10869-2024](https://doi.org/10.5194/acp-24-10869-2024), 2024..

1783 Suski, K. J., Hill, T. C. J., Levin, E. J. T., Miller, A., DeMott, P. J., and Kreidenweis, S. M.: Agricultural
1784 harvesting emissions of ice-nucleating particles, *Atmos. Chem. Phys.*, 18, 13755-13771,
1785 <https://doi.org/10.5194/acp-18-13755-2018>.

1786 Testa, B., Hill, T. C. J., Marsden, N. A., Barry, K. R., Hume, C. C., Bian, Q., Uetake, J., Hare,
1787 H., Perkins, R. J., Möhler, O., Kreidenweis, S. M. and DeMott, P. J.: Ice nucleating
1788 particles in the boundary layer of the Sierras de Córdoba, Argentina, during the Cloud,
1789 Aerosol, and Complex Terrain Interactions experiment, *Journal of Geophysical
1790 Research: Atmospheres* 126, e2021JD03518, <https://doi.org/10.1029/2021JD035186>,
1791 2021.

1792 Thomson, D. S., Schein, M. E., and Murphy, D. M.: Particle analysis by laser mass spectrometry
1793 WB-57 instrument overview, *Aerosol Sci. Technol.*, 33, 153–169,
1794 <https://doi.org/10.1080/027868200410903>, 2000.

1795 Tobo, Y., DeMott, P. J., Hill, T. C. J., Prenni, A. J., Swoboda-Colberg, N. G., Franc, G. C., and
1796 Kreidenweis, S. M.: Organic matter matters for ice nuclei of agricultural soil origin.
1797 *Atmos. Chem. Phys.*, 14, 8521–8531, <https://doi.org/10.5194/acp-14-8521-2014>, 2014.

1798 Tobo, Y., Prenni, A. J., DeMott, P. J., Huffman, J. A., McCluskey, C. S., Tian, G. X., Pöhlker,
1799 C., Pöschl, U., and Kreidenweis, S. M.: Biological aerosol particles as a key determinant
1800 of ice nuclei populations in a forest ecosystem. *Journal of Geophysical Research-
1801 Atmospheres*, 118(17), 10100-10110. <https://doi.org/10.1002/jgrd.50801>, 2013.

1802 Ullrich, R., Hoose, C., Möhler, O., Niemand, M., Wagner, R., Höhler, K., Hiranuma, N.,
1803 Saathoff, H., and Leisner, T.: A New Ice Nucleation Active Site Parameterization for
1804 Desert Dust and Soot. *Journal of the Atmospheric Sciences*, 74(3), 699-717.
1805 <https://doi.org/10.1175/jas-d-16-0074.1>, 2017.

1806 Willeke, K., Lin, X., and Grinshpun, S. A.: Improved Aerosol Collection by Combined
1807 Impaction and Centrifugal Motion, *Aerosol. Sci. Tech.*, 28(5), 439–456.
1808 <https://doi.org/10.1080/02786829808965536>, 1998.

1809 Wright, T. P., & Petters, M. D.: The role of time in heterogeneous freezing nucleation. *Journal of
1810 Geophysical Research: Atmospheres*, 118, 3731–3743.
1811 <https://doi.org/10.1002/jgrd.503652013>, 2013.

1812 Wright, T. P., Hader, J. D., McMeeking, G. R., and Petters, M.D.: High Relative Humidity as a
1813 Trigger for Widespread Release of Ice Nuclei, *Aerosol Science and Technology*, 48 (11),
1814 i-v. <https://doi.org/10.1080/02786826.2014.968244>, 2014.

1815 Wright, T. P., Petters, M. D., Hader, J. D., Morton, T., & Holder, A. L.: Minimal cooling rate
1816 dependence of ice nuclei activity in the immersion mode. *Journal of Geophysical
1817 Research: Atmospheres*, 118, 10,535–10,543. <https://doi.org/10.1002/jgrd.50810>, 2013.

1818 Vali, G., DeMott, P. J., Möhler, O. and Whale, T. F.: Technical Note: A proposal for ice nucleation
1819 terminology, *Atmos. Chem. Phys.*, 15, 10263–10270, <https://doi.org/10.5194/acp-15-10263-2015>,
1820 2015.

1821 Vali, G.: Nucleation terminology. *Journal of Aerosol Science*, 16(6), 575-576,
1822 [https://doi.org/10.1016/0021-8502\(85\)90009-6](https://doi.org/10.1016/0021-8502(85)90009-6), 1985.

1823 Vali, G.: Quantitative evaluation of experimental results on the heterogeneous freezing
1824 nucleation of supercooled liquids. *J. Atmos. Sci.*, 28, 402–409,
1825 [https://doi.org/10.1175/1520-0469\(1971\)028<0402:QEOERA>2.0.CO;2](https://doi.org/10.1175/1520-0469(1971)028<0402:QEOERA>2.0.CO;2), 1971.

1826 Wagner, R., Kiselev, A., Mohler, O., Saathoff, H., & Steinke, I.: Pre-activation of ice-nucleating
1827 particles by the pore condensation and freezing mechanism. *Atmospheric Chemistry and
1828 Physics*, 16(4), 2025-2042. <https://doi.org/10.5194/acp-16-2025-2016>, 2016.

- 1829 Wex, H., Augustin-Bauditz, S., Boose, Y., Budke, C., Curtius, J., Diehl, K., Dreyer, A., Frank,
1830 F., Hartmann, S., Hiranuma, N., Jantsch, E., Kanji, Z. A., Kiselev, A., Koop, T., Möhler,
1831 O., Niedermeier, D., Nillius, B., Rösch, M., Rose, D., Schmidt, C., Steinke, I., and
1832 Stratmann, F.: Intercomparing different devices for the investigation of ice nucleating
1833 particles using Snomax (R) as test substance. *Atmospheric Chemistry and Physics*, 15(3),
1834 1463-1485. <https://doi.org/10.5194/acp-15-1463-2015>, 2015.
- 1835 Willeke, K., Lin, X., and Grinshpun, S. A.: Improved Aerosol Collection by Combined
1836 Impaction and Centrifugal Motion, *Aerosol. Sci. Tech.*, 28(5), 439–456.
1837 <https://doi.org/10.1080/02786829808965536>, 1998.
- 1838 Wright, T. P., & Petters, M. D.: The role of time in heterogeneous freezing nucleation. *Journal of*
1839 *Geophysical Research: Atmospheres*, 118, 3731–3743.
1840 <https://doi.org/10.1002/jgrd.503652013>, 2013.
- 1841 Wright, T. P., Hader, J. D., McMeeking, G. R., and Petters, M.D.: High Relative Humidity as a
1842 Trigger for Widespread Release of Ice Nuclei, *Aerosol Science and Technology*, 48 (11),
1843 i-v. <https://doi.org/10.1080/02786826.2014.968244>, 2014.
- 1844 Wright, T. P., Petters, M. D., Hader, J. D., Morton, T., & Holder, A. L.: Minimal cooling rate
1845 dependence of ice nuclei activity in the immersion mode. *Journal of Geophysical*
1846 *Research: Atmospheres*, 118, 10,535–10,543. <https://doi.org/10.1002/jgrd.50810>, 2013.
- 1847 Yadav, S., Venezia, R. E., Paerl, R. W., & Petters, M. D.: Characterization of ice-nucleating
1848 particles over Northern India. *Journal of Geophysical Research:*
1849 *Atmospheres*, 124, 10467–10482. <https://doi.org/10.1029/2019JD030702>, 2019.
- 1850 Zawadowicz, M. A., Froyd, K. D., Murphy, D. M., and Cziczo, D. J.: Improved identification of
1851 primary biological aerosol particles using single-particle mass spectrometry. *Atmospheric*
1852 *Chemistry and Physics*, 17(11), 7193-7212. <https://doi.org/10.5194/acp-17-7193-2017>,
1853 2017.
- 1854 Zawadowicz, M. A., Froyd, K. D., Perring, A. E., Murphy, D. M., Spracklen, D. V., Heald, C.
1855 L., Buseck, P. R., and Cziczo, D. J.: Model-measurement consistency and limits of
1856 bioaerosol abundance over the continental United States. *Atmospheric Chemistry and*
1857 *Physics*, 19(22), 13859-13870. <https://doi.org/10.5194/acp-19-13859-2019>, 2019.
- 1858 Zenker, J., Collier, K. N., Xu, G., Yang, P., Levin, E. J. T., Suski, K. J., DeMott, P. J., and
1859 Brooks, S. D.: Using depolarization to quantify ice nucleating particle concentrations: a
1860 new method, *Atmos. Meas. Tech.*, 10, 4639–4657, [https://doi.org/10.5194/amt-10-4639-](https://doi.org/10.5194/amt-10-4639-2017)
1861 [2017](https://doi.org/10.5194/amt-10-4639-2017), 2017.

1862

1863